Potential impacts of climate change and land-use change on hydrological drought in the Western Cape (South Africa)

Myra Naik

Dissertation Presented for the Degree of
Doctor of Philosophy
in Environmental & Geographical Science
University of Cape Town (2021)

Supervisor: Associate Professor B. J. Abiodun

Declaration I

I know the meaning of plagiarism and declare that all the work in the dissertation, save for that which is properly acknowledged, is my own.

Signed by candidate

Signature: Myra Naik

Declaration II

Parts of the materials in this doctoral degree dissertation have been submitted for publication before the submission of the dissertation for examination. Hence, the text of this dissertation includes material from the manuscripts entitled:

- **Naik, M**. and Abiodun, B.J. (2020). Projected changes in drought characteristics over the Western Cape, South Africa. Meteorological Applications: The Royal Meteorological Society (published).
- **Naik, M**., Abiodun, B.J. (2021). Influence of bias-correction of climate datasets on hydrological simulations in the Western Cape (South Africa). Advances in Drought Analytical Tools for Better Understanding of Current and Future Climate Change (submitted).
- **Naik, M**. and Abiodun, B.J. (2021). Can land-use change mitigate future impacts of climate change on hydrological droughts in the Western Cape (South Africa)? International Journal of Theoretical & Applied Climatology (submitted).

The co-author of these manuscript publications supervised the dissertation.

The research findings from this dissertation have also provided materials for the deliverables, book chapter, and final report for a project that funded this dissertation. The project, titled “Using land-use changes to mitigate impacts of future droughts on water yields in South Africa”, was submitted to the Water Research Commission of South Africa (Project number: K5/2835).

Abstract

The Western Cape (South Africa) recently witnessed the most severe drought on record. The meteorological drought, which was characterised by below-normal rainfall for three consecutive years (2015 – 2017), cascaded to agricultural and then hydrological drought, resulting in devastating socio-economic consequences. While some studies indicate that climate change may increase the severity and frequency of droughts in the Western Cape in the future, there is a lack of information on how to mitigate the effects of future climate change on hydrological drought. This dissertation therefore investigated the extent to which land-use changes could be applied to reduce climate change impacts on future hydrological drought in this region. For the study, the revised Soil Water Assessment Tool (SWAT+) was calibrated and evaluated over four river basins in the Western Cape, and the climate simulation dataset from the COordinated Regional Downscaling EXperiment (CORDEX) was bias-corrected. Using the bias-corrected climate data as a forcing, the SWAT+ was used to project the impacts of future climate change on water yield and hydrological drought in the four basins and to quantify the sensitivity of the projection to four feasible land-use change scenarios in these basins. The relevant land-use scenarios are the expansion of mixed forests (FrLand), the restoration of grassland (GrLand), the restoration of shrubland (SrLand), and the expansion of cropland (CrLand).

The model evaluation shows good agreement between the simulated and observed monthly streamflow at hydrological stations, and the bias correction of the CORDEX datasets improved the quality of the SWAT+ hydrological simulations in the four basins. The climate change projection depicts an increase in temperature and potential evapotranspiration but a decrease in precipitation and all the hydrological variables. Drying is projected across the Western Cape, and the magnitude of such drying increases with higher global warming levels (GWLs). The land-use changes alter the impacts of climate change by influencing the hydrological balance. While FrLand mitigates the impacts of climate change on the frequency of hydrological drought by increasing streamflow, soil water and percolation, CrLand mitigates the impacts by increasing surface runoff. However, the magnitudes of these land-use change impacts are very small compared to the climate change impacts. Hence, the results suggest that land-use changes may not be an efficient strategy for mitigating the climate change impacts on hydrological drought over the region. The findings obtained from this research provide relevant information towards mitigating the severity of future droughts and improving water security in Western Cape River Basins.

Keywords: climate change, drought, evapotranspiration, land use change, water yield, river basins, Western Cape, South Africa

Acknowledgements

As my dissertation journey concludes, I realise that what has felt like a solitary task, has in truth been facilitated greatly by the support of many organisations and individuals. I would like to take this opportunity to offer my sincere appreciation to everyone who may have directly or indirectly contributed towards making my dream of a doctoral dissertation a reality.

First and foremost, I wish to express my gratitude to a wonderful supervisor, Professor B. J. Abiodun, for providing me with the counsel I needed to succeed in this doctoral program. I am truly fortunate to be your student. Your knowledge, experience, innovative ideas, and leadership have inspired me and steered this research project over many years. I will be forever grateful for the encouragement, motivation, and guidance that you have so selflessly provided. Thank you for constantly challenging me - to think deeper about scientific problems, to work smarter, and to aim higher as a fledgling researcher.

This research would not have been possible without generous financial support from the following scholarships: the Water Research Commission of South Africa (2018–2021), the University of Cape Town's Vice-Chancellor's Exceptional Academic Merit Award for Doctoral Research (2019–2021), and the University of Cape Town's International Student's Doctoral Scholarship (2018–2021). My appreciation extends to S. Adams, S. Kalam, C. Swartz and C. Millward for their administrative assistance that supported the many queries, renewal applications, and processing of awards therein.

I am also indebted to R. Hoskins and the team at Roscommon Respublica House, for accommodation in 2019. As an international student it offered me my "home away from home", one that was safe and conveniently close to university, which allowed me to work productively many late nights on the campus toward this dissertation. The accommodation offer came at a critical time when I required it the most, and this allowed me to focus fully on my studies, and to make my academic year a success. For this, I am extremely grateful.

I would also like to thank P. Mukwenha, for hours of invaluable advice on Linux (and Windows) software installations, SWAT+ monitoring and model optimisation tools. N. Lindenberg and T. Slingsby are also thanked for their eager facilitation with GIS on an ad-hoc basis. Thank you to R.

Lord for several hours of proofreading review and invaluable feedback that have helped to improve the quality of this dissertation.

My colleagues, friends, and mentors are also warmly acknowledged. Special thanks to members in the Climate System Analysis Group for their camaraderie, including members of the CORDEX Group (2017), the Paper-Write-Shop Group (2018), the Publication Hub (2019), and the SWAT+ Group (2020), for many comments and useful suggestions during our peer review sessions. I am also grateful to my mentors in health and fitness, M. Cannon and R. Schmidt, for their exemplary leadership (in 2017–2018); you have both inspired me and steered my life trajectory in a positive direction.

Finally, to my father and my mother, thank you for your unconditional and unwavering love. Your support and encouragement have been invaluable, not only in this dissertation journey, but in my every life endeavour, every single day. Thank you for being the anchors that keep my boat steady in the tumultuous sea of life.

Dedication

To my father,

for giving me my passion for science,

and for willingly sacrificing so much for my education.

List of Figures

List of Tables

Table of Contents

List of Acronyms

AAO	Antarctic Oscillation
ACRU	Agricultural Catchments Research Unit (model)
AL	Angola Low
ANNs	Artificial neural networks
AWC	Available water storage capacity in soil
BSVG	Fallow (Barren or sparsely vegetated)
CChange	Climate Change experiments
CGIAR–CSI	Consortium for Spatial Information of The Consultative Group Of International Agricultural Research
CMIP5	Coupled Model Intercomparison Project Phase 5
CMIP6	Coupled Model Intercomparison Project Phase 6
CN2	The Soil Conservation Service-Curve Number (SCS CN)
CORDEX	Coordinated Regional Downscaling Experiment
CORDEX_ORG	CORDEX Original
CORDEX_MBCr	CORDEX using MBCr
CORDEX_MBCn	CORDEX using MBCn
CORDEX_QDM	CORDEX using QDM
COSMO-CLM	Consortium for Small-scale Modeling Regional Climate Model
CRDY	Dry cropland and pasture
CrLand	the expansion of cropland experiment
CRGR	Cropland/grassland mosaic
CRU	Climate Research Unit
CRWO	Cropland/Woodland mosaic
CWB	climate water balance
DELAY	Groundwater delay
DEM	Digital Elevation Model
DWS	Department of Water and Sanitation
ET	Evaporation
ENSO	El Niño Southern Oscillation
EPCO	Plant evaporation compensation factor

ESCO	Soil evaporation compensation factor
FAO	Food and Agriculture Organization
FLO_MIN	Water table depth for return flow
FODB	Deciduous broadleaf forest
FOEB	Evergreen broadleaf forest
FOMI	Mixed (broadleaf and evergreen) forest
FrLand	the expansion of forest experiment
GCMs	Global climate models
GDP	Gross Domestic Product
GLCC	Global Land Cover Characterization (USGS)
GMFD	Global Meteorological Forcing Dataset
GrLand	the restoration of grassland experiment
GRAS	Pasture-grassland
GPCC	Global Precipitation Climatology Centre
GWLs	Global Warming Levels
HG	Hargreaves Method
HSG	Hydrologic Soil Group
KHL	Kalahari Heat Low
HRUs	Hydrological Response Units
IPCC	Intergovernmental Panel on Climate Change
ITCZ	Inter-Tropical Convergence Zone
IPEAT+	Integrated Parameter Estimation and Uncertainty Analysis Tool+ framework
JJA	June-July-August
K	Saturated hydraulic conductivity
LS	Linear scaling
LSUs	Landscape Units
LULC	Land-use/land-cover
MAR	Mean annual run-off
MIKE-SHE	Mike System Hydrology European
MBC	Multivariate bias correction
MBCn	Multivariate bias correction using N-dimensional probability density function transform

MBCr	Multivariate bias correction using Spearman rank correlation
MSE	Mean Square Error
NCEP/NCAR	National Centres for Environmental Prediction
	– National Centre for Atmospheric Research
NSE	Nash-Sutcliffe model efficiency coefficient
OBJBEST	Objective Best Function
PBIAS	Percentage bias
PERC	Percolation
PERCI	Percolation Index
PDSI	Palmer Drought Severity Index
PHDI	Palmer Hydrological Drought Severity Index
PERCI	Percolation Index
PET	Potential evapotranspiration
PM	Penman–Monteith
QDM	Quantile delta mapping
QGIS	Quantum Geographical Information System
QSWAT	Quantum Soil Water Assessment Tool (GIS)
RCA	The Rossby Centre Regional Climate Model 4
REVAP_CO	Groundwater “revap” coefficient
R^2	Coefficient of determination
REVAP_MIN	Threshold water depth in shallow aquifer
RCMs	Regional Climate Models
RCP 8.5	Representative Concentration Pathway 8.5
RFI	Runoff Index
RMSE	Root mean square error
SADC	Southern African Development Community
SAH	South Atlantic High
SAM	Southern Annular Mode
SASD	South Atlantic Subtropical Atlantic Dipole
SAVA	Savanna
SFI	Streamflow Index
SHRB	Shrubland

SIH	South Indian High
SIOD	Subtropical Indian Ocean Dipole
SOM	Self-Organizing Map
SPI	Standardized Precipitation Index
SPEI	Standardized Precipitation Evapotranspiration Index
SRI	Surface Run-Off Index
SRM	Solar Radiation Management
SRTM	Shuttle Radar Topography Mission Digital Elevation Model
SSMI	Standardized Soil Moisture Index
SSFI	Standardized Streamflow Index
SrLand	the restoration of shrubland experiment
SW	Soil Water
SWI	Soil Water Index
SRM	Solar radiation management
SURLAG	Surface lag coefficient
SWAT	Soil and Water Assessment Tool
SWAT+	Soil Water Assessment Tool Plus
SWM	Stanford Watershed Model IV
SWSI	Surface Water Supply Index
TWT	Theewaterskloof dam
TRMM	Tropical Rainfall Measuring Mission
UNESCO	United Nations Educational, Scientific and Cultural Organization
URMD	Urban residential medium density
USDA-ARS	United States Department of Agriculture—Agricultural Research Service
USGS	United States Geological Survey
UTM	Universal Transverse Mercator
WATR	Water
WASMO-DE	Water And Snow balance MODelling
WATLAC	A Water Flow Model for Lake Catchments
WCRP	World Climate Research Programmes
WCWSS	Western Cape Water Supply System

WMO	World Meteorological Organization
WMAs	Water Management Areas
WRB	Western Cape River Basins
WYLDI	Water Yield Drought Index

Chapter 1:
Introduction

1.1 Background

The Western Cape, one of the most populous provinces and the most popular province in South Africa, is drenched in natural beauty. Nestled at the southernmost point of the African continent, where the warmer Indian Ocean, along the southern coastline, meets the cold Atlantic Ocean, along the western coastline (Figure 1.1), the Western Cape is a unique world in one province. Encompassing a unique assortment of vast oceans and pristine beaches, rugged mountains and fruit-filled valleys, the province is also home to Cape Town, South Africa's 'Mother City' and a world-famous tourist destination. The Western Cape is world-renowned for its breath-taking scenery, a wealth of endemic species and rich biodiversity. For example, the Cape Floristic Region World Heritage Site (a unique floral kingdom that stretches from the Cape Peninsula to the Eastern Cape) and the Knysna-Tsitsikamma indigenous forest offer travellers the chance to explore untamed wildernesses. The major land cover types include fynbos, renosterveld and succulent karoo ecosystems, and each has high ecological importance. Numerous nature reserves with abundant coastal and mountain hiking trails also offer visitors access to seemingly endless fields of Cape Fynbos, the prolific native scrub, and seas of endemic wildflowers. These natural attractions of the province are complemented by a rich variety of cultures, historical landmarks, world-class restaurants, and entertainment hotspots. Cape Point, iconic Table Mountain, the Cape Winelands, and Robben Island are only a few of the province's greatest tourist attractions, and all are popular with local and international visitors alike. Travelling inland from Cape Town, visitors can experience the farming country with its undulating fields of rolling wheat and canola, and its tranquil, fashionable vineyards. While along the West Coast, there are quaint fishing villages and historical towns, the semi-desert landscapes of the Great Karoo provide the perfect contrast to the lush coast. However, all these natural attractions and socio-economic activities in the province are anchored on the river basins of the Western Cape.

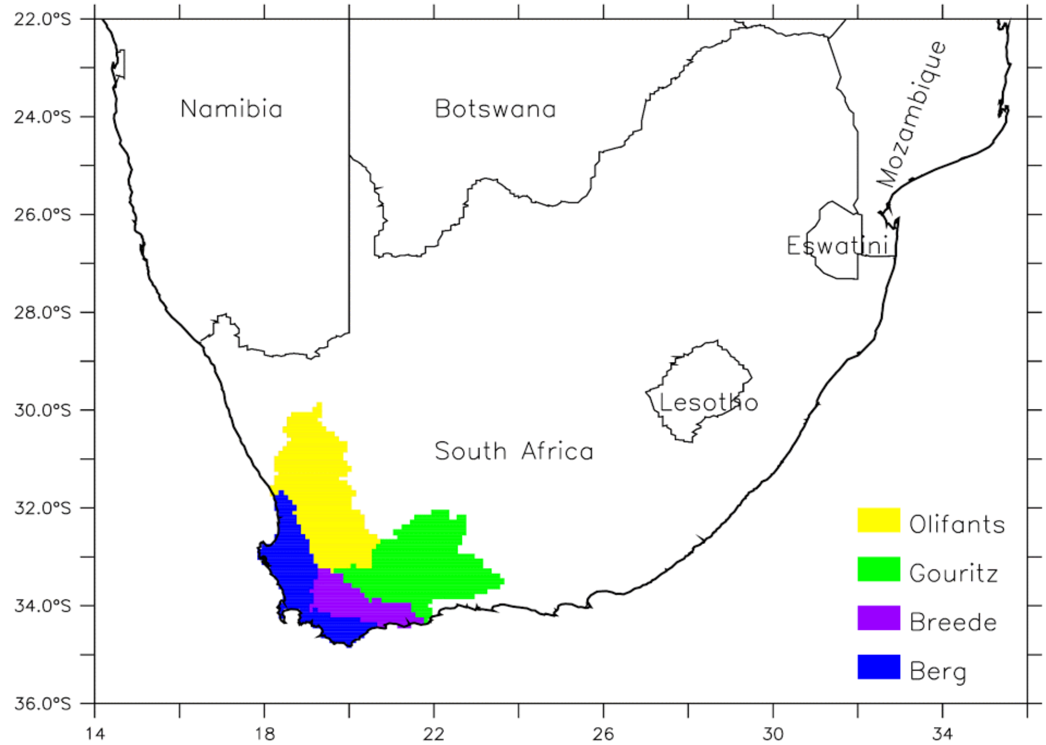

Figure 1.1: The four major Western Cape River Basins (Breede, Berg, Olifants, and Gouritz) examined in this study.

The four river basins in the Western Cape, namely, the Breede, the Berg, the Olifants, and the Gouritz, (Figure 1.1), play a key role in the region's socio-economic fabric. Apart from comprising more than half of South Africa's strategic water resources, the river basins in the Western Cape provide water for agriculture (to support a wide variety of fruits, grains, vegetables, and livestock), as well as for domestic, urban, industrial (e.g., manufacturing, transportation, construction, mining, and communication) and tourism activities. For example, the Berg River Basin contributes to the regional economy by supporting the cultivation of grapes (viticulture, wine tourism and wineries), wheat and deciduous fruits, as well as sheep farming, dryland grain farming, and commercial pine forests (Statistics South Africa, 2010). The Gouritz River Basin also supports irrigation agriculture (grapes, fruit, fodder, vegetables, grains), livestock production (ostriches, sheep, cattle, and goats), and forestation activities (timber production). The fish and shellfish industry in this basin also contribute significantly to the economy of the province (DEADP, 2011). Similarly, the Olifants River Basin accommodates intensive livestock grazing (predominantly of sheep and goats), irrigation agriculture, and cultivation of citrus, deciduous fruits, grapes, and potatoes (DEADP, 2011), while the Breede River Basin supports intensive irrigation agriculture. These Western Cape agricultural activities, which cover more than 11 million hectares, supply about 20% of the South Africa's agricultural production, and contribute to more than half of national agricultural exports, thus contributing about ZAR 124 billion to the country's Gross Domestic Product (GDP) (Du Plessis & Schloms, 2017; Pegram & Baleta, 2014).

These river basins, which support a rich variety of endemic species (both flora and fauna), also underpin the regional tourism industry. For example, the Berg River Basin (the country's most developed tourism region) is also home to the Berg River Estuary, which is of major conservation importance for birdlife (Green Cape, 2019). The Breede River flows through the Bontebok National Park before it reaches the sea at Witsand, which is an ecological hotspot estuary for fish. Nearby Cape Infanta offers tourist whale-watching and a variety of water sports activities in spring and early summer. Similarly, the Olifants River Basin includes important conservation areas, like the Tankwa-Karoo National Park, the Verlorenvlei wetland in the Sandveld (which has Ramsar status i.e., a wetland site designated to be of international importance), the Cederberg Wilderness Area, and the Groot Winterhoek Wilderness Area, which house several endangered indigenous and endemic fish (DEADP, 2011). These river basins directly underpin the tourism industry, but also indirectly supply tourism-related water use facilities (e.g., hotels, wellness spas, swimming pools, golf estates, and provision of catering goods) and support job creation. The importance of water in the Western Cape economy can be best illustrated when we consider what happens in the absence of it. Reductions in water supply during drought conditions caused water stress in these river basins, which was particularly severe during the extended drought of 2015 – 2017.

Water availability in these river basins is highly erratic already, due to the large variability in the Western Cape climate. The climate variability often induces severe hydrological drought with devastating socio-economic impacts. Hence, to ensure the sustainable future development of socio-economic activities in the region, there is a need for studies on how to reduce the influence of this climate variability on the hydrology of Western Cape River Basins.

1.2 Climate of the Western Cape

The Western Cape has a unique climate relative to the rest of South Africa. The region, which covers an area of 129 370 km^2, has a temperate Mediterranean climate with mild moist winters and warm dry summers. Summer temperatures range from 15 to 27 degrees Celsius, while winter temperatures range from 5 to 22 degrees Celsius (Hurry & Van Heerden, 1982; Kruger, 2004 a&b; Tyson, 1986). Inland temperatures are 3 to 5 degrees Celsius higher. The Western Cape is one of South Africa's driest regions, with only 350 mm of rain per year, far less than the national annual average of 500 mm (Dennis & Dennis, 2012). However, in contrast to much of southern Africa, which experiences summer rains and dry winters, the Western Cape is unique in that it receives its highest precipitation during the austral winter months of June-July-August (JJA). The region's rainfall is, however, highly heterogeneous, varying considerably with the region's complex topography. Mean annual rainfall varies significantly, with mountainous regions receiving up to 3000 mm of rain, while low-lying regions (40 m above sea level) receive less than 200 mm (Lakhraj-Govender & Grab, 2019). The prominent Cape Fold Mountain Belt extends along the length of the province (1300 km), forming an L-shaped mountain range that extends north-south, along the western coast, and east-west along the southern coast. This mountain range acts as an orographic barrier that creates dry interior conditions and augments the rainfall (through orographic rain) in the coastal parts. The Western Cape Province has three major rainfall zones, including the winter, late summer, and all-year seasonality regimes, and each of these extends into at least one adjacent province (i.e., the Free State, Eastern Cape, or Northern Cape). The winter rainfall zone occurs along the southwestern and western parts of the province (West Coast), where annual precipitation ranges from less than 200 mm (in the north) to over 1000 mm (over the mountainous regions). This zone typically receives winter rainfall (May to August) from cyclones originating over the South Atlantic, and it is affected by the combination of the cold Benguela current and the northward displacement of high-pressure systems (Du Plessis & Scholms, 2017). The late summer (February-March) rainfall zone occurs over the north-east part of the province (Great Karoo) and is bound inland by South Africa's interior plateau. The all-year rainfall zone occurs along the southern coastline, stretching eastward from Cape Agulhas (South Coast and Little Karoo), where the lower annual precipitation ranges from between 200 and 400 mm throughout the year, though often with a summer maximum, and often in the form of thunderstorms (Mahlalela et al., 2019; Van Niekerk & Joubert, 2011). The climate of this zone is influenced by the movement of warm, moist air from the Indian Ocean, producing all-year rainfall (Du Plessis and Scholms, 2017). This region's climatic pattern is largely due to the subcontinent's location relative to low-pressure systems between 40° and 50° south (Midgley et al., 2005). Seasonally, when the westerly waves shift northward, these low-pressure systems bring rainfall to the southwestern part of the country in the form of cold fronts (Louw, 2007). Thus, rainfall in the Western Cape is typically caused by cold fronts and associated extratropical cyclones, or by rare westerly disturbances such as cut-off lows, which frequently cause extreme rainfall events in the spring and autumn (Midgley et al., 2005). The Western Cape region is also influenced by coastal low-pressure systems, which generate hot, dry ‘berg' winds that blow from the interior and cause above-average warm conditions in the spring and late winter (Louw, 2007). However, it is the large variability in this dry climate that induces severe droughts in Western Cape.

1.3 What is Drought?

Drought – a slow-onset, naturally occurring phenomenon – generally occurs due to a deficiency in precipitation over a prolonged period (Gillette, 1950). Drought effects frequently accumulate slowly over time and may linger for years after the event has ended (months or years). Drought always starts with a lack of precipitation (Wilhite & Glantz, 1985; Wilhite et al., 2014). Drought is a relative concept, and definitions reflect differences in regions, disciplinary approaches, and needs. That is, different stakeholders have different perceptions of drought, depending on the context considered (e.g., social, economic, agricultural, or environmental) (Rossi et al., 2007). Also, a drought event in one region may represent normal conditions in a different region or even to a different stakeholder in the same region. As such, definitions of drought must realistically be region-, application- or impact-specific (Wilhite, 2005).

1.3.1 Drought Categories

Drought is classified into four types, as illustrated in Figure 1.2: meteorological drought, agricultural drought, hydrological drought, and socio-economic drought (Wilhite & Glantz, 1985). The first three approaches are concerned with methods of measuring drought as a physical phenomenon, whereas the last is concerned with drought in terms of supply and demand, tracking the effects of water scarcity as it ripples through socio-economic systems (NDMC, 2021). This illustrates that drought is not merely a physical phenomenon, but rather an interaction between a natural event and the human system demands for water supply (Wilhite, 2005). Note that, while all four drought categories are discussed in the sections below, the emphasis of this dissertation is specifically on meteorological and hydrological drought.

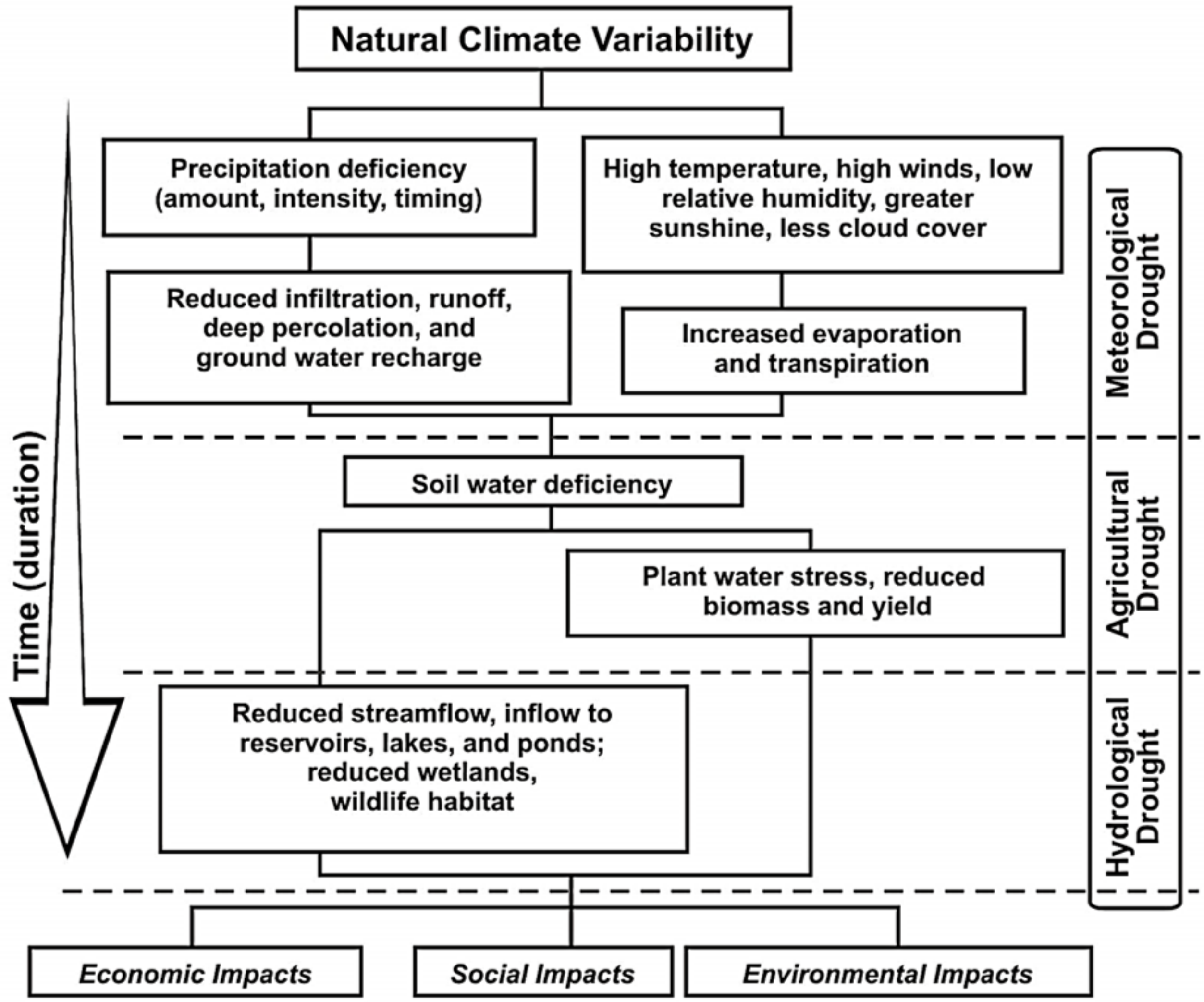

Figure 1.2: Drought types, causal factors, and their usual sequence of occurrence (NDMC; National Drought Mitigation Centre, 2021).

1.3.1.1 Meteorological drought

Meteorological drought is typically defined by the amount of dryness (in comparison to some "normal" or average amount) and the length of the dry period (months or years) (NDMC, 2021). The decrease in precipitation is often compared to the long-term average (Dai, 2011). All droughts begin with a precipitation deficit that lasts for an extended period of time, but other factors such as high temperatures, low relative humidity, and high winds can increase the severity of the drought. Definitions of meteorological drought must be considered region-specific because atmospheric conditions that result in precipitation deficits vary greatly from region to region. Different regions have different rainfall characteristics, and precipitation thresholds should thus be region-specific.

Moreover, the two regions may also have different prevailing large-scale atmospheric patterns that bring about dry conditions (Hoerling et al., 2006; Giannini et al., 2003; Meque & Abiodun, 2015). The latter three types of droughts occur as a result of a prolonged meteorological drought, and they have societal consequences (Lake, 2011).

1.3.1.2 Agricultural drought

Agricultural drought is a period when soil moisture deficits result from below-average precipitation, above-normal evaporation, increased temperature, and persistent wind (Mishra & Singh, 2010). If the soil moisture available to sustain the growth of crops/forage is insufficient during the growing season, this may affect plant growth, and lead to crop failure and lower agricultural productivity. Note, however, that different plants have different water use efficiencies, and hence, the impact may vary among crops. Moreover, local factors (e.g., evapotranspiration, soil type [or water holding capacity], antecedent moisture conditions, and slope) also influence available soil moisture. Agricultural drought is not directly proportional to precipitation (Wilhite & Glantz, 1985). Typically, agricultural drought occurs after meteorological drought and before hydrological drought.

1.3.1.3 Hydrological drought

Hydrological drought is associated with the effects of periods of precipitation deficits on surface and subsurface waters (i.e., streamflow, reservoir and lake levels, and groundwater) (Wilhite, 2005). It is often recognised as the most important type of drought (Shukla & Wood, 2008; Van Loon, 2015), because various sectors, such as agriculture, urban life, industry, and hydropower generation, rely heavily on surface water (Jehanzaib, 2020; Vasiliades et al., 2011). The hydrological system may be affected by a decrease below long-term mean levels in river streamflow and water resource management systems (e.g., aquifers, lakes, or reservoirs), or when percolation and runoff influence the groundwater and reservoirs (Dai, 2011). Hydrological drought typically develops more gradually, lagging after the occurrence of meteorological and agricultural droughts. Land use and land cover change, land degradation and poor water management may all exacerbate these types of droughts. This type of drought affects the availability of water for hydropower (resulting in power outages) and other dam operations (Calzi, 2013), and it may also negatively influence activities like river transportation or agricultural irrigation under conditions of reduced streamflow. Hydrological drought may furthermore affect the tourism sectors, through impacts on water sports, and it may also have an impact on endangered fish species (UNISDR, 2009).

1.3.1.4 Socio-economic drought

Socio-economic drought occurs when the meteorological, agricultural, and hydrological drought types begin to affect the economy of a nation or region, mainly due to the imbalance between supply and demand of goods, i.e., demand exceeds supply (of, for example, water, grazing, hydroelectric power) (Mishra & Singh, 2010; Wilhite, 2005). Socio-economic drought may have a differential impact of drought on different groups within the population, depending on their access to resources. Severe drought may be devastating and even lead to economic collapse, as well as to other factors, such as poverty, strife, war, or the forced migration of people (Boken et al., 2005).

1.3.2 Drought Characteristics

Drought impacts are determined by several important drought characteristics:

- Intensity: the degree of precipitation (or other drought indicator) deficit in each area over a specified period. It is often calculated as the ratio of magnitude divided by the duration of the drought event.
- Frequency: the recurrence interval between drought episodes over a defined region.
- Duration: the length of time (number of consecutive months or weeks) in which the precipitation (or any other drought indicator, e.g., soil moisture or surface runoff) is below a defined threshold (Andreadis et al., 2005). The duration is a function of the threshold declared for the start and end of the drought episode.
- Magnitude: the cumulative precipitation deficit (below the threshold) during the drought event (Santos, 2010).
- Severity: the value of precipitation (or other drought indicator) in each month during the drought event or the minimum of precipitation during the event (Thompson, 1999; Vidal et al., 2010).
- Spatial coverage: the geographical extent affected by a specific drought event.

Drought indices are simply quantitative measures used to characterise the intensity, duration, and frequency of a drought event. A significant number of drought indices have been developed to quantify aspects of meteorological, hydrological, and agricultural droughts (Jiang et al., 2015; Mishra & Singh, 2010; Zargar et al., 2011).

1.4 Impacts of Droughts in the Western Cape

Parts of the Western Cape have recently been affected by a severe multi-year drought, one of the worst in the country's history. The meteorological drought, which was characterized by below-normal rainfall for three consecutive years (2015–2017), had a cascading series of agricultural, hydrological, and socio-economic consequences. Although similar rainfall deficits occurred in previous years, the effects of the recent drought were especially severe and had a negative impact on the regional economy. During this extended drought, the water storage levels of the Western Cape's major dams declined to about 23%, and in addition, the last 12% of the dam water was unusable (Botai et al., 2017). The province was declared a disaster region, and the crisis triggered the local government to impose severe water restrictions on agricultural, urban, and industrial consumers. It was the worst water shortage in the province in the last 113 years (Botai et al., 2017). The drought had severe impacts on the Western Cape Water Supply System and on various socio-economic activities. The multi-year crisis reduced the water supply by about 60%. The extreme lack of rainfall reduced water levels in the major reservoirs to critically low levels, resulting in severe water restrictions (50 litres per person per day) for citizens and local businesses as they prepared for what the City of Cape Town called "Day Zero." (i.e., a water crisis event when regional reservoir levels would decline to critically low levels and the city's domestic taps would have to be switched off) (City of Cape Town Day Zero Dashboard; Gibson, 2018). The industrial and urban water use sectors needed to compete with the agricultural sector. The drought had a substantial impact on livestock and agriculture production, as well as on livelihoods, especially among rural communities in the Western Cape's farmlands. There was a significant decline in agricultural output that resulted in an estimated economic loss of ZAR 5.9 billion and led to 30,000 job losses, with a decline in exports of about 13 to 20% (Green Cape, 2019). This had a ripple effect on food security (driven by decreased food production and decreased affordability because supply was curtailed). Furthermore, water restrictions undermined mining, urban activities, and industrial manufacturing. The severity of the recent drought-induced water crisis was exacerbated by human aspects, including poor management, lack of foresight and increased water demand due to population growth (Bohatch, 2017). These socio-economic impacts could be reduced through an improved understanding of how to predict drought impacts over Western Cape River Basins in the future. A good understanding of drought characteristics under both past and future climates may improve drought preparedness and reduce socio-economic and environmental vulnerability. The devastating socio-economic impacts of the recent Western Cape droughts have heightened the search for how to mitigate future droughts.

1.5 Drivers of Hydrological Drought

The two main drivers of the hydrological cycle and hydrological drought are climate variability and human activities.

1.5.1 Climate Variability

Climate variability refers to the way in which climate fluctuates yearly, either above, or below, a long-term average value. Climate variability is not as easily detectable as weather variability, which occurs across a shorter-term timescale (hours or days), and differs from climate change, which occurs across continuous, longer-term (multi-decadal or even multi-century) timescales. Climate variability is measured by anomalies, or deviations, compared to long-term statistics for the same calendar period, across temporal (typically intraseasonal to interdecadal timescales, over a month, season, or year) and spatial scales. Climate variability affects hydrological drought through changes in large-scale atmospheric features that alter temperature and precipitation patterns. These changes in climate alter associated variables in the hydrological cycle (e.g., evaporation, soil moisture, surface runoff, groundwater). More specifically, negative variations (or deviations) from normal hydrologic conditions, either through increased evapotranspiration, due to increases in temperature, and/or decreases in precipitation may heighten the intensity and frequency of hydrological drought and associated water resource availability (Dai, 2013; Sheffield et al., 2012).

The climate variability over the Western Cape (and more broadly across Southern Africa) is controlled by a complex interplay of many large-scale atmospheric patterns. Climate variability, both in terms of temperature and rainfall, is controlled by the complex interaction of the region's subtropical location, the oceans, the height of the mountainous interior plateau, and the influence of the dominant atmospheric circulations on the subcontinent (Van der Walt & Fitchett, 2020). The influence of tropical and temperate pressure regimes, as well as the intra-annual migration of the inter-tropical convergence zone (ITCZ), result in significant seasonal differences in temperature and rainfall patterns. The ITCZ is a region of cloud band and heavy rainfalls that originates from the convergence between the southeastern and northeastern trade winds. During the austral winter (June to August), the ITCZ is displaced in the Northern Hemisphere, while during the austral summer (December to February), it shifts further south. The ITCZ shifts in response to changes in the sun's maximum insolation and the location of dominant atmospheric high- and low-pressure systems on a monthly and seasonal basis. In the summer, high-pressure systems sit over the subcontinent's southern tip, and in the winter, they sit over the interior. There are two semi-permanent anticyclone cells, one over the Atlantic Ocean, known as the South Atlantic High (SAH), and the other over the Indian Ocean, known as the South Indian High (SIH) (Van Heerden & Taljaard, 1998). The position of these two subtropical highs influences the rainfall over much of the region. These high-pressure systems are broken up by mid-latitude cyclones that bring rain to the southwest. The subtropical high-pressure belt and mid-latitude westerlies, along with their associated fronts, have a significant inter- and intra-annual variation (Van der Walt & Fitchett, 2020). Other important synoptic patterns that modulate temperature and rainfall over the broader region are the Angola Low (AL), the Kalahari Heat Low (KHL) (Macron et al., 2014). These local and regional scale atmospheric circulations greatly influence the characteristics of both meteorological and hydrological drought.

Teleconnections also contribute to local and regional climate variability. Teleconnections are simply the climate variability links between non-contiguous geographic regions (Bridgman & Olivier, 2014; Glantz, 2001; Nigam, 2003). For instance, teleconnections affecting the Southern African climate, include the Subtropical Indian Ocean Dipole (SIOD) (Behera & Yamagata, 2001; Hansingo & Reason, 2009; Reason, 2001), the South Atlantic Subtropical Atlantic Dipole (SASD, e.g., Rodriguez et al., 2015), and the Benguela Niño (Florenchie et al., 2003; Shanon, 1996). However, the most significant teleconnection in Southern Africa is the El Niño Southern Oscillation (ENSO). The different phases of ENSO, El Niño and La Niña events drive changes in circulation, winds, rainfall, and ocean surface temperatures over this region. Generally, dryer than normal conditions or droughts may occur during El Niño, and wetter than normal conditions, with frost or floods, may occur during La Niña events (e.g., Kane, 2009; Mason, 2001; Misra, 2003; Reason & Rouault, 2002; Richard et al., 2000). While the summer rainfall regions are known to be influenced by the ENSO (e.g., Dieppois et al., 2015; Hoell et al., 2015; Hoell & Cheng, 2018; Hoell et al., 2021; Pomposi et al., 2018), over the winter rainfall regions (i.e., southwestern tip of Western Cape), the expected El-Niño-rainfall relationship is not evident. Although ENSO may have some influence on the summer climate of Western Cape through regulation of the adjacent sea surface temperature and coastal upwelling (Rouault et al., 2010), there is no clear El-Niño-rainfall relationship (Blamey & Reason, 2007; Reason & Rouault, 2005). In fact, the well-below-average rainfall of 2016 – 2017 occurred during a weak La Niña and a weak El-Niño respectively (Wolski, 2018). Nevertheless, other important teleconnections over the Western Cape include, for example, the Southern Annular Mode (SAM), also known as the Antarctic Oscillation (AAO) (Thompson & Wallace, 2000). SAM has been linked to the dominant variability of the summer mean surface air temperature (Manatsa & Mukwada, 2012), as well as to dry spell frequencies or wet days across the Southern African region (Thoithi et al., 2021), and rainfall variability, specifically over the Western Cape (Ibebuchi, 2021). The AAO is a low-frequency mode that exists in the mid-latitudes and is defined by pressure anomalies between Antarctica and the mid-latitudes of the Southern Hemisphere. It has also been demonstrated that particularly wet winters are associated with a negative phase of the AAO over the south-western Cape, and vice versa (Reason & Rouault, 2005). Antarctic sea ice extent (Reason et al., 2002; Blamey & Reason, 2007) and South Atlantic sea surface temperature (Phillipon et al., 2012; Reason & Jagadheesha, 2005) are also important indicators of climate variability in the Western Cape.

1.5.2 Human Activities and Land Cover Changes

In addition to climate variability, human activities and land cover changes are also dominant drivers of hydrological drought. Human activities describe operations to modify the physical environment, usually to obtain resources from the land. This includes, for instance, the conversion of natural vegetation to agricultural cropland or forest plantations, invasion by alien plant species, the removal of natural vegetation for urbanisation, or agricultural management practices (e.g., application of fertilizer or pesticide, overgrazing, improper crop rotation, poor irrigation practices). Human activities often include land use changes. In contrast, land cover changes refer to the natural shifts in surface vegetation (that are not usually associated with human activity). This includes, for instance, transitions from semiarid grassland to shrubland. Nevertheless, for this dissertation, we consider human activities coupled with land use and land cover (hereafter, comprehensively referred to as LULC) features.

1.5.2.1 Human activities

Human activities have a crucial role in influencing the hydrological drought characteristics. Human activities – such as reservoir regulation, excessive water abstraction, groundwater pumping, agricultural irrigation, urbanisation, or industrialisation – all enhance the risk of hydrological drought, as increasing volumes of water are extracted, diverted, and consumed (AghaKouchak et al., 2015; He et al., 2017; Wada et al., 2013). For example, flow regulation and water storage in dams or reservoirs can effectively alleviate drought by releasing water further downstream during periods of low streamflow. Conversely, water abstraction to meet sectoral demand (such as for irrigation agriculture) could exacerbate an existing streamflow deficit. These activities all undeniably alter the hydrological cycles of river basins, and may also manifest in contrasting geographical differences of hydrological drought within the same river basin.

For instance, human activities associated with reservoir regulation have already affected hydrological drought across China during recent decades (1961 – 2016), alleviating hydrological drought in the southern region (e.g., Yangtze River) but amplifying hydrological drought in the northern parts of China (e.g., along the Yellow River) (Jiao et al., 2020; Yang et al., 2020). Human activities associated with the development of hydropower dams have also affected the occurrence of droughts, low water levels in the dry season, and sediment load in the upper Mekong River Basin (China), with major consequences for biodiversity, fisheries and the economies of the lower Mekong countries (Cambodia, Vietnam, Laos)(Campbell and Barlow, 2020). Similarly, in an attempt to increase agricultural production, human activities associated with already excessive water abstraction for irrigation and groundwater pumping have intensified hydrological drought, such as over river basins in India (Asoka et al., 2017; Rodell & Famiglietti, 2001; Shah, et al., 2021; Tiwari et al., 2009). Similarly, although the rainfall deficit was the main driver of the drought over the Western Cape (2015 – 2017), human activities (such as poor water-management practices and infrastructure deficiencies) certainly worsened the crisis (Bischoff-Mattson et al., 2020; Pascale, 2020), when water resources needed to be carefully allocated between agricultural irrigation, urbanisation, or industrialisation consumers. Overlooking this influence of human activities when assessing hydrological drought hinders our ability to effectively prepare, manage, forecast, and respond (Shah et al., 2021; Van Loon et al., 2016).

1.5.2.2 LULC activities

Land-use and land-cover (LULC) activities can influence atmospheric variables, like temperature and precipitation, which drive hydrological processes (Juang et al., 2007). LULC changes may create both positive and negative feedback on climatological conditions via modification of the atmospheric conditions in the lower planetary boundary layer (Oki et al., 2013). This is where the surface vegetation interacts with the atmosphere. Under a given boundary layer condition (i.e., pressure, temperature, humidity, and wind), surface vegetation receives precipitation, downward shortwave and longwave radiation, and returns fluxes (such as sensible heat, latent heat, and carbon dioxide) to the atmosphere. LULC influences local and regional water balances through processes such as precipitation partitioning (interception, soil moisture, and runoff) and evaporative demand (via changes in cloud cover, air temperature, and humidity) (Ek & Holtslag, 2004; Schubert et al., 2004). As a result, LULC is a key component in climate variability, and it also interacts with the atmosphere at longer timescales, ranging from decadal to centennial. Thus, the biophysical properties of LULC are linked to a variety of hydrological processes. This has serious implications for water resources.

LULC changes have a significant impact on the hydrological drought characteristics of a river basin. LULC changes can have a significant impact on the water cycle and, more importantly, water yield (soil moisture and surface runoff). LULC changes influence various hydrological processes, such as streamflow, evapotranspiration, interception, infiltration groundwater, reservoir levels and underground base flow (DeFries & Eshleman, 2004; Falkenmark et al., 1999; Guo et al., 2014; Joorabian Shooshtari et al., 2017). Depending on the type and degree of LULC changes, the impacts can have both negative and/or positive effects. In general, an increase in vegetated land lowers water yield due to a higher rate of evapotranspiration and water infiltration, while an increase in bare land and built-up areas enhances water yield because of their impermeable surfaces (e.g., Donaldson, 2004; Lerner, 1990). For example, LULC changes involving forestation may decrease runoff and decrease streamflow, while human settlement may increase runoff and increase streamflow (Li et al., 2018). However, LULC changes involving conversion of forest to crops may reduce evaporation or increase river flow, while removal of forests and replacement with agriculture may cool air temperature (Rost et al., 2008; Teuling et al., 2010). In addition, there is some uncertainty, as LULC changes impacts on hydrological processes may be non-linear or exhibit a threshold effect (Abiodun, 2021; Li et al., 2007). Nevertheless, the biophysical characteristics of LULC changes contribute to local climate variability, thereby altering the regional hydrological cycle, and potentially the frequency and severity of hydrological drought in a river basin (e.g., over Australia, see Cai et al., 2009) (Sheffield et al., 2012; Van Loon et al., 2016). To that end, the focus of this dissertation is on how LULC changes may influence the hydrological drought characteristics of river basins in the Western Cape.

1.6 Motivation for the Dissertation

The severe drought of 2015 – 2017 highlighted how vulnerable the socio-economic activities of the Western Cape are to droughts. However, there is a concern that the socio-economic impacts of future droughts may be even more severe than those experienced in 2015 – 2017 for two reasons. Firstly, the natural beauty and popularity of the Cape will continue to attract more people from within and outside South Africa into the province; hence the increased water demand associated with population and economic growth will increase water demand and enhance the socio-economic impacts of any future droughts. Secondly, future projections over the province indicate a warmer and drier climate, which suggests enhanced potential evapotranspiration, leading to more severe droughts, with even more devastating socio-economic impacts. Hence, there is a need for more studies on how to mitigate the potential impacts of climate change on future droughts and on socio-economic activities in the province. However, in order to identify effective mitigation strategies, there is a need to first project and quantify the impacts of the climate change, not only on climatological, but also on agricultural and hydrological drought, because the socio-economic activities of the province are so deeply anchored within these river basins. Such future projections would require hydrological modelling, in which a hydrological model would be calibrated, evaluated and applied to downscale the possible impacts of climate change projections in relation to soil moisture and hydrology over the Western Cape River Basins.

LULC changes may be used to mitigate some of the impacts of climate change on droughts because it plays a crucial role in relation to surface run-off and evaporation in river basins. Given that LULC changes can have both positive and negative influences on the hydrology of a river basin, there is a need to investigate the extent to which the positive influence could offset the impacts of climate change, as well as the extent to which the negative influence can enhance the impact of climate change over the Western Cape. This dissertation thus explores these two directions.

1.7 Research Aim and Objectives

The goal of this dissertation was to investigate the impacts of climate change on the future characteristics of meteorological and hydrological drought in the Western Cape, as well as to assess how LULC changes can help mitigate the effects of climate change on hydrological drought in the region.

The specific objectives of the dissertation were:

- To examine future changes in the characteristics of meteorological drought over the Western Cape.

- To assess the performance and sensitivity of a hydrological model (SWAT+) in simulating the hydrology of the Western Cape.
- To investigate the influence of bias correction of climate datasets on simulation of hydrological drought in the Western Cape.
- To examine the future impacts of climate change on hydrological drought in the Western Cape.
- To explore the extent to which LULC changes could be used to mitigate future climate change impacts on hydrological drought in the Western Cape.

1.8 Dissertation Outline

The remainder of this dissertation is divided into seven chapters (Chapters 2 to 8): Chapter 2 gives a compressive review of relevant literature on topics including, quantification of hydro-meteorological drought, hydro-meteorological modelling frameworks, and the impact of LULC changes on hydrology. Chapter 3 presents the methodology of the study, including a description of the study region, the datasets, the hydrological model used and the experimental design. The results of the study are presented and discussed in Chapters 4 to 8. Chapter 4 focuses on future changes in the characteristics of meteorological drought. Chapter 5 presents results on the sensitivity and performance of the hydrological model in simulating the hydrology. Chapter 6 investigates the influence of bias correction of the climate datasets on simulation of hydrological drought. Chapter 7 examines future impacts of climate change on hydrological drought. Chapter 8 explores the extent to which LULC changes could be used to mitigate such climate change impacts on hydrological drought. Finally, Chapter 9 presents the discussion, conclusion and recommendations for future research work.

Chapter 2:
Literature Review

This chapter begins with a review of relevant literature that is commonly used to quantify drought and highlights two commonly used meteorological indices. It then discusses a hydro-meteorological framework for modelling drought, by reviewing various hydrological models, their structure, sources of uncertainty, and the importance of bias-correcting their input data. The chapter concludes by reviewing some of the potential hydrological impacts linked to land-use/land-cover (LULC) changes.

2.1 Characterising hydro-meteorological drought

Previous studies have used two major approaches to identify and quantify hydro-meteorological drought. While some studies used drought indicators (e.g., Le Goff et al., 1985; Maity and Sunman, 2019; Meko, 1985; Odoulami et al., 2021; Wolksi, 2018), others used drought indices (e.g., Burke & Brown, 2008; Dai, 2013; Joetzjer, 2013; Lloyd-Hughes, 2014; Nalbantis & Tsakiris, 2009; Sheffield, 2012; Shukla & Wood, 2008; Vicente-Serrano et al., 2012; Zhai et al., 2010). With the drought indicator approach, a specific value or anomaly in the hydro-meteorological variables or parameters (typically precipitation, or reservoir storage, ground water levels, or streamflow) is set as a threshold to identify drought conditions. So, any value below the threshold is regarded as a drought condition. For example, Le Goff et al. (1985) and Meko (1985) used a threshold of 10% of the average precipitation, or the last decile, to identify meteorological drought over Morocco. Odoulami et al. (2020) used a threshold of 30%–50% below average rainfall to study a three-year (2015–2017) drought in the Western Cape. Some studies adopted a variant of the drought indicator approach, the return period method, which identifies the inter-arrival time of consecutive critical droughts (e.g., Bonaccorso et al., 2013; Sharma & Panu, 2010, 2012; Otto et al., 2018). Bonaccorso et al. (2013) used return periods to characterise drought lengths over Europe, while Sharma and Panu (2010, 2012) predicted drought lengths at annual, monthly, and weekly timescales over Canada. While all these studies argued that the drought indicator approach (the threshold or return period method) provides a quick and easy way to identify and quantify hydro-meteorological drought, some studies (e.g., Hayes, 2006; Yihdego et al., 2019) have identified some shortcomings in this approach. Yihdego et al. (2016) argued that the normal for an area is a calculation that some users could confuse with mean or average precipitation. Hayes (2006) suggested that, when using the drought indicator approach, it is difficult to compare droughts over different climate regimes. In contrast to the drought indicator approach, the drought index approach combines several indicators (variables) on a quantitative scale to characterise droughts. The WMO (2012) comprehensively reviews several hydro-meteorological indices commonly used, while Hasan et al. (2019) provide a comprehensive review of their various applications. The commonly used meteorological indices include the Palmer Drought Severity Index (PDSI) by Palmer (1965), Deciles by Gibbs and Maher (1967), or the Standardized Precipitation Index (SPI) by McKee et al. (1993), while hydrological indices include the Surface Water Supply Index (SWSI) developed by Shafer and Dezman (1982), and the Palmer Hydrological Drought Severity Index (PHDI) by Karl (1986). There is good consensus in literature that these drought indices approach provide 'value-added' information by comparing current conditions with historical information on drought in a standardised manner (e.g., Azmi et al., 2016; Eslamian, 2014; Hao & Singh, 2015; Yihdego & Eslamian, 2017; Yihdego et al., 2019). Hence, the present study used the drought indices approach to quantify hydro-meteorological drought.

Among the meteorological drought indices in the literature, the Standardized Precipitation Index (developed by McKee, 1993) seems to be the most popular. Although SPI was developed as early as 1993, it remains a powerful tool for characterising meteorological drought to date. This is because its simplicity, modest data requirements, and versatility make it desirable for studying and comparing droughts across diverse climate regions and at multiple timescales. While Kubiak-Wójcicka et al. (2021) used SPI to identify drought over the temperate Laborec river basin (Slovakia) between 1970 and 2019, Mahmud et al. (2021) used SPI to detect a decline in drought conditions over the humid Teesta River basin (Bangladesh) between 2003 and 2019. Similarly, Melgarejo et al. (2021) used SPI to detect severe drought over the arid Balsas River basin (Mexico) between 1980 and 2017, while Al-Quraishi et al. (2021) used SPI to quantify drought over semi-arid areas of Iraq (between 1998 and 2017). Willink (2020) illustrated the value of the SPI for contrasting the climates of Russia and West Africa. Páscoa et al. (2021) used the SPI for short-, medium- and long-term timescales over the mild Mediterranean Iberian Peninsula. Ntale and Gan (2003), Haile et al. (2020) and Guenang et al. (2019) used SPI to identify drought over tropical East and Central Africa, while Mazibuki et al. (2021), Malherbe et al. (2016) and Trambauer et al. (2014) used the SPI to detect drought in more temperate South Africa. Dutra et al. (2013) and Siebert et al. (2017) used SPI to determine droughts across African river basins that span tropical and sub-tropical climate regions. Nevertheless, despite the versatility and growing popularity of SPI, some studies (e.g., Angelidis et al., 2012; Hayes et al., 1999; Mishra & Singh, 2010; Wu et al., 2005) have discussed the limitations of SPI, arguing that its greatest strength (i.e., its simplicity as a precipitation-only index) may also be its weakness. For example, WMO (2012), WIRES (2015) and Teuling et al. (2013) said that SPI may be insufficient to characterise drought, since it does not account for temperature. These studies emphasised the need to use a more comprehensive drought index that can account for water balance in a region. As an alternative for SPI, Vicente-Serrano et al. (2010) thus developed the Standardized Precipitation and Evapotranspiration Index (SPEI), which incorporates both precipitation and evapotranspiration variables in characterising drought. Several studies (Ujeneza and Abiodun, 2015; Araujo et al., 2016; Meque & Abiodun, 2015; Vicente-Serrano et al., 2010) have underscored the superiority of SPEI over SPI for characterising drought. However, to fully appreciate the unique merits of both SPI and SPEI, some studies have used both drought indices in their drought analysis (Botai et al., 2017; Mathivha, 2020; Mtilatila et al., 2020). For the same reason, the present study has also applied both indices to quantify meteorological drought in the Western Cape.

Numerous studies have used both the SPI and SPEI in future projections of drought due to climate change over river basins in Africa. For instance, over the Volta River basins (West Africa), Oguntunde et al. (2006) found that the magnitude of projected droughts was lower when using SPI versus SPEI. Similarly, using Self-Organizing Map (SOM) classifications, Nguvava et al. (2019) found that SPI may underestimate the severity of droughts, and noted that SPEI may enhance the robustness of future drought projections over East Africa. In southern Africa, Ujeneza and Abiodun (2015), Araujo et al. (2016), and Meque & Abiodun, 2015 also underscored the superior value of SPEI over SPI for monitoring and detecting the spatial and temporal characteristics of future drought. Recent analysis by Abiodun et al. (2019) also concluded that using SPI alone for future drought projections may underestimate the magnitude and robustness of the climate projections over this region. Since using the SPI may underestimate the severity of future drought due to climate change, there is a clear benefit in comparing and contrasting both SPEI and SPI drought in future projections of climate change. To account for the potential role of evapotranspiration, this study will also make use of both the SPEI and the SPI in quantifying future droughts for the Western Cape. In addition to these two meteorological indices, however, the present study will also include hydrological drought indices. For instance, Abiodun et al. (2018) applied both indices to study the characteristics of regionally extreme droughts over Southern Africa in past and future climates, and found that, while both drought indices feature an increase in drought intensity and severity, the magnitude of such increase is higher with SPEI than with SPI. A similar result was reported by Nguvava et al. (2019) over East Africa, by Abiodun et al. (2019) over the major river basins in Southern Africa, and by Oguntunde et al. (2006) over the Volta River basins in West Africa. All these studies warned that SPI may underestimate the severity of droughts. They also showed that SPEI may enhance the robustness of future drought projections over East Africa. Nevertheless, Abiodun et al. (2019) advocate for the use of both indices in projecting future drought because, while SPI may underestimate the severity of future drought (because it does not account for evaporation) SPEI may overestimate the impacts (because it assumes that the potential evaporation may be equal to evaporation). Hence, there is a clear benefit in comparing and contrasting future drought projections using both SPEI and SPI. This present study will thus employ both SPI and SPEI in quantifying future droughts in the Western Cape.

2.2 Framework for hydro-meteorological modelling

Many past studies on hydro-meteorological modelling have followed a standard framework (shown in Figure 2.1), especially for studying the potential impacts of climate change on hydrological variables or droughts (e.g., Chokkavarapu & Mandla, 2019; Teutschbein & Seibert, 2010). This framework for hydro-meteorological modelling includes a chain for the transfer of climate information, with large-scale global circulation models to the regional climate models (via downscaling), and eventually the hydrological model (after bias correction).

2.2.1 Global Climate Models

It is generally accepted that Global Climate Models (GCMs) are the primary tool for understanding hydro-meteorological characteristics over any region, albeit with some limitations when applying their results at a catchment scale. Gutowski et al. (1997), Lau et al. (1996), Roads et al. (1994), Betts et al. (1998, 1999), Roads and Betts (2000), Hirschi et al. (2006) and Hagemann et al. (2004, 2005) all used GCMs to understand hydro-meteorological processes over large river basins at different timescales. Lucarini et al. (2007) reviewed all these studies and pointed out some limitations and discrepancies in the representation of large-scale atmospheric circulation patterns in GCMs. These limitations included problems, for instance, in the representation of some parameterised processes in the GCM, occurring in the atmosphere (e.g., precipitation) and at the interface of land and atmosphere (e.g., soil water vapour transport and evaporation). Hakala (2018) recognises that, to better translate the coarse resolution of GCM outputs to the local-scale hydro-meteorological characteristics, it is necessary to apply some form of downscaling (either statistical or dynamical downscaling).

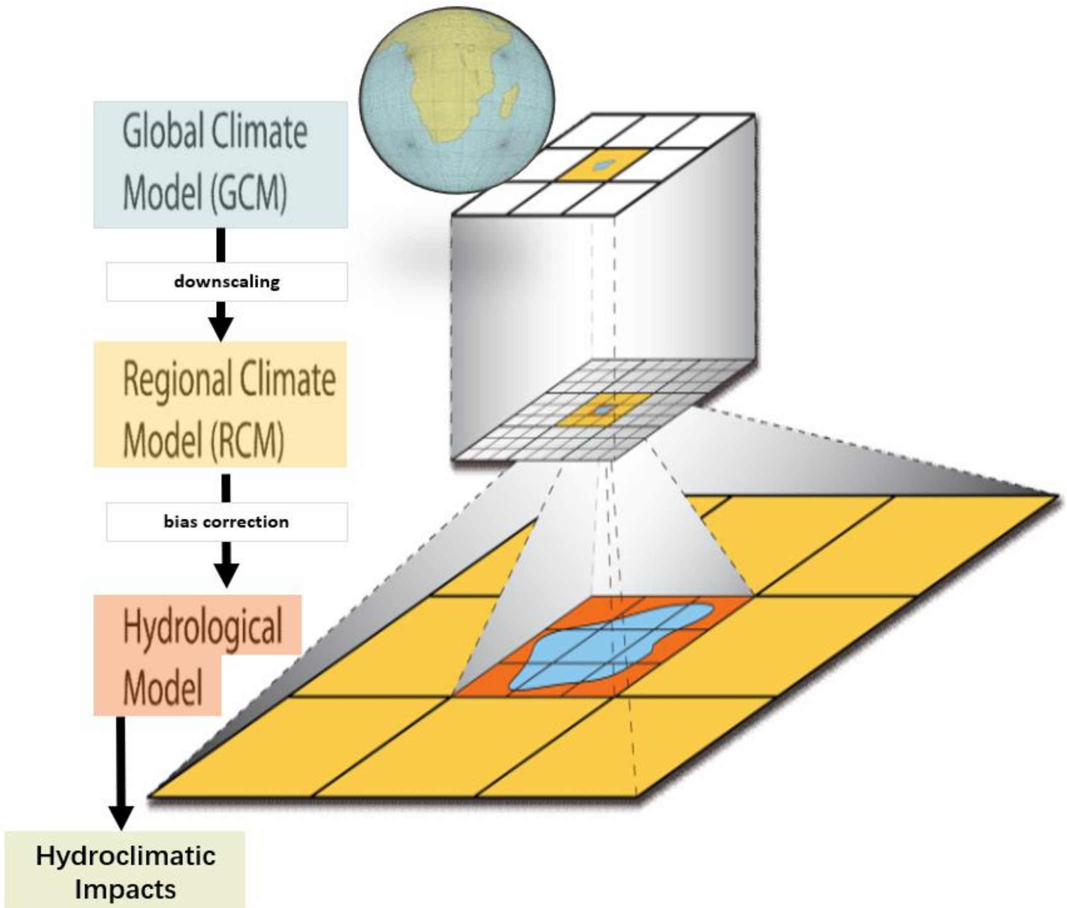

Figure 2.1: Framework for hydro-meteorological modelling describing the climate variable transfer from global climate model (GCM) to the hydrological model at catchment scale (adapted from Chokkavarapu & Mandla, 2019; Teutschbein & Seibert, 2010).

2.2.2 Downscaling of global climate simulations

There are two broad methods in the literature on how to downscale global climate data (GCMs) for use in regional climate models (RCMs). While some studies have used statistical downscaling methods (e.g., Hewitson et al., 2014; Wilby et al., 2004), others use dynamical downscaling methods (e.g., Giorgi, 1990; Giorgi & Mearns, 1999). Popular statistical downscaling techniques that are commonly cited in recent literature, include: linear methods, such as that of Wilks (2010); weather classification methods, including that of Wilby et al. (2004) and Hewitson et al. (2014); and weather generator methods of Wilks (2010) or Semenov and Barrow (2002). These studies all applied various, empirically based techniques to determine the relationships between large-scale climate predictors (e.g., pressure fields) and observed local climate prediction variables (e.g., surface air temperature and precipitation). Zhang et al. (2020) recognise that statistical downscaling is advantageous because of its relatively low computational requirements and fast calculations. Alternatively, dynamical downscaling methods typically involve the use of RCMs. Popular dynamical downscaling techniques that are commonly cited include one-way parasitic nesting (e.g., Jacobson, 2005) or two-way interactive nesting (e.g., Kalnay, 2003), defined depending on how boundary conditions are formulated. Many authors (e.g., Cannistra, 2016 and Flato et al., 2014) recognise that, although RCMs are computationally intensive, they are a particularly useful tool, since they apply sophisticated mathematical equations to provide regional climate information at a local-scale resolution that accounts for physical features (e.g., orography or lakes). As such, RCMs are particularly useful for hydro-meteorological modelling. Many studies have projected the impacts of climate change, used climatic input data generated by a GCM, and downscaled it for input for hydrological modelling at the catchment-scale. For instance, Janža et al. (2013), projected climate change impacts on the hydrological cycle in the Upper Soča River basin (Slovenia), using climatic input data generated by a global climate model and downscaled for local use with the distributed MIKE SHE hydrological model. Gawith et al. (2012), projected climate change impacts on hydrology in the Lindis and Matukituki River Basin (Otago, New Zealand), using 12 different GCMs, downscaled for local use with the TopNet semi-distributed hydrological model. Similarly, hydrological impact assessments using either downscaled output from, either single- or multiple climate models, have been conducted by Mishra et al. (2017), Marchane et al. (2017), and Pandey et al. (2019). Nevertheless, while this is an increasingly common approach, the spatial resolution of the RCMs may be insufficient for hydro-meteorological impact assessment. Ahmed (2011) and others have proposed bias correction to mitigate inherent RCM errors.

2.2.3 Bias correction of downscaled climate model datasets

Several studies have examined the influence of bias-correction methods on climate datasets. Ayugi (2020) highlights the relevance of bias correction particularly for the African subregions, where observation data availability and quality have declined considerably. Previous studies by Cannon et al. (2015), Cannon (2018), Wood et al. (2002), Li et al. (2010) and Teng et al. (2015) recognise the value of bias correction as the transformation of climate model output towards observations (using algorithms) by removing systematic errors (or biases) and illustrate its value in improving the reliability of climate model data by addressing the problem of uncertainty. These biases may be large, since statistical distribution of the climate variables differs from the distribution of the historical observations. Li et al. (2010), Rosenberg et al. (2010) and Xu and Singh (2004) suggest these errors may be attributed to, for example, the limited spatial resolution, simplified physical processes, numerical schemes, or uncertainty of climate system processes inherent in the models. Bias-correction methods range from simple ones, like the delta change technique and linear scaling (LS), to relatively more complex ones, such as power transformation, and the quantile mapping (QM) techniques (Shrestha et al., 2017). There is agreement that distribution-based bias-correction methods (both parametric and non-parametric) give the best performance in terms of reproducing the observed climate, while means-based methods, in particular LS, are almost always ranked as the least skilful (Teng et al., 2015). Nevertheless, while many studies have investigated the impact of bias correction on precipitation and temperature, only few have examined the effect of bias correction of climate variables on the outputs of hydrological models (e.g., Teutschbein & Seibert, 2012, and Chen et al., 2013).

Bias-corrected data is particularly useful in the detection of drought characteristics. For instance, study by Aadhar and Mishra (2017) found the use of bias-corrected satellite-based data (for precipitation and temperature variables) was advantageous for improved estimates of historical and current drought conditions over South Asia; Vernimmen et al. (2012) arrived at similar conclusions with regard to drought monitoring in Indonesia. Other studies also show that bias correcting precipitation simulations prior to calculating drought changes can lead to different conclusions on predicted future drought frequencies. For instance, in order to consider whether bias correcting GCM simulations would improve the representation of historical droughts, Johnson and Sharma (2015) projected the frequencies of future droughts and showed that bias correction reduces the prediction errors when the simulations are compared to drought frequencies calculated from observed data. While a recent study over the Southern African river catchments by Abiodun et al. (2020) examined the impacts of climate change on drought (meteorological and hydrological) under different global warming levels (GWLs) and found a consistent drying signal all over the region, with some variations in magnitude, the drought index used, and the river basin studied, their projections did not use a drought index. Consequently, the results of their study contain systematic biases from the climate model outputs. Thus, there remains limited information on quantifying the uncertainty of these hydrological simulations and the value of bias correction for other regions of Southern Africa, including the Western Cape.

2.2.4 Hydrological models

A review of the literature reveals that over the years, a variety of hydrological models have been developed. Devia et al. (2015) classified all hydrological models into three types: empirical, conceptual, and physically-based models (Table 2.1). The simplest models are empirical, while the most complicated are physical mechanistic models. Physical and conceptual models require a thorough understanding of the physics involved in surface water movement in the hydrological cycle (Srinivasulu, 2008). Conceptual hydrological models, also known as grey-box models, are precipitation-runoff models that are based on observed or assumed empirical relationships among different hydrological variables, according to Liu et al. (2017). They differ from black-box models, which only consider precipitation-runoff relationships statistically. They are also distinct from physical distributed hydrological models, which are based on the solution of differential equations describing the physical laws of mass, energy, and momentum conservation. According to Pechlivanidis et al. (2011), many 'hybrid' models exist that overlap within this classification of model structures. The descriptions of the three structural categories of runoff models, with their respective strengths and weaknesses, and examples of each, are summarised in Table 2.1. In the South African context, for example, Pitman and Bailey developed the Pitman model, which is a lumped or semi-distributed model. This model is often used at the monthly time-step, with fixed conceptual algorithms (Hughes, 2013). It is widely used for water resources assessment in southern Africa and is easy to calibrate against observational data and produces good representation for assessment of past conditions (e.g., Havenga et al., 2007; Herold & Bailey, 2016), though it has also proven more problematic where the data is limited. In contrast, the Agrohydrological model of the Agricultural Catchments Research Unit (ACRU) and the Soil and Water Assessment Tool (SWAT) are both semi-distributed models that use physical based algorithms and are often used at daily time-steps. Although these models are more complex and are more computationally demanding, the spatio-temporal disaggregation of the models' algorithms allows for better representation of actual land use processes, making it easier for the user to simulate vegetation changes. Many studies recognise the growing and international application of SWAT (e.g., Gassman et al., 2007; Kumar et al., 2018; Munoth & Goyal, 2020; Stehr et al., 2008), and thus it has been favoured for this study.

Table 2.1: Characteristics of three types of hydrological models: empirical, conceptual, and physical (Adapted from Devia et al., 2015 and Sitterson et al., 2018).

Models	**Empirical** (Metric model)	**Conceptual** (Parametric model)	**Physical**
Method	non-linear input-output interaction, black-box model	semi-empirical, water balance equations, grey-box model	physical laws and equations based on real-world hydrological responses, white-box model
Advantages	requires few parameters which could be more precise, fast simulation speed/executables	simple mathematical model structure, effortless calibration	includes precise dimensions of spatial-temporal variability
Disadvantages	no link with physical catchment processes, input data distortion	disregards spatial variability within drainage basin	requires numerous site-specific parameters and calibration
Application	in ungauged catchments where runoff is the only required output	when the convergence speed or data is limited	if extensive data is available at high resolution
Examples	Curve Number, Artificial neural networks, fuzzy regression machine learning techniques.	Stanford Watershed Model IV (SWM; Crawford & Linsley, 1966), Hydrologiska Byråns Vattenbalansavdelning (HBV model; Bergström, 1995).	MIKESHE (Abbott et al., 1986), SWAT (Arnold et al., 2012).

2.2.4.1 Model uncertainty

Hydrological models are inherently imperfect and contain sources of uncertainty, since they simplify real processes that are themselves imperfectly understood. Hence, model structure uncertainty arises due to simplification, inadequacy, and ambiguity in the mathematical representation of actual watershed processes. According to Ashrafi et al. (2020), errors may also stem from the input data, including initial conditions from the GCM and the assumptions made in downscaling. Errors may also stem from differences in the model structure itself. Emam et al. (2018) and Vema et al. (2020) suggest that errors may also stem from the model parameter set, since these are estimated through calibration by using the observed records of the watershed response, which in turn contain the measurement errors. However, among these various sources of uncertainty, parameter uncertainty is relatively easy to control through various calibration procedures (viz., the structure and initial conditions of the GCM/RCM), the assumptions made in downscaling, and differences in emission scenarios (Ehret et al., 2012; Singh & Najafi, 2020). Nevertheless, Liu and Gupta (2007) recognise that quantification of uncertainty in hydrological modelling is imperative, and hence different techniques are often necessary to treat such uncertainty, particularly in the input climate dataset.

2.2.5 Application of hydroclimatic modelling for future projections

Many studies have also combined climate and hydrological models to project the hydrological impacts across river catchments in different parts of the world. This is a popular approach, since it allows large-scale climate information (e.g., temperature, precipitation, evapotranspiration), provided by climate models, to be transferred as input to drive the hydrological models and to make predictions at local catchment scales. For instance, Li et al. (2016) used an RCM (COSMO-CLM) and distributed hydrological model (WATLAC) to suggest that future climate change may increase the frequency and severity of droughts and floods in the Poyang River (China). Kienzle et al. (2012) applied GCM scenarios and the ACRU hydrological model to project that future climate change may increase evapotranspiration, groundwater recharge, soil moisture, and streamflow in the Cline River Basin (Canada). Similarly, Chattopadhyay et al. (2017) and Kamali et al. (2017) used a GCM to force the Soil and Water Assessment Tool (SWAT), and thus showed that climate change may alter future drought characteristics over the Karkheh River Basin (Iran) and the Kentucky River Basin (United States). However, studies combining climate and hydrological models in river catchments in Southern Africa remain limited. Li et al. (2015) performed hydrological projections using a single climate and hydrological model (Water And Snow balance MODelling; WASMO-DE coupled with RegCM4) to simulate runoff in Southern Africa. However, Graham et al. (2011) highlighted the advantages of using different downscaling methods, different GCMs and different future emissions scenarios as input to hydrological models when assessing climate change impacts in the Thukela River Basin (South Africa). Their study found considerable variability among the projections, and there was no clear consensus on future runoff impacts. Graham et al. (2011) also underscored the need for additional, well-coordinated regional climate downscaling studies over the region. Nevertheless, previous studies have generally only applied hydrological modelling to examine environmental processes. Such studies include, but are not limited to, Mutema (2016), Ndiritu (2009) as well as Schütte and Schulze (2017), which both examined processes of soil erosion, and assessed urbanisation and dam construction. To date, there is a dearth of studies that have coupled climate and hydrological models to characterise future drought at the catchment scale. Such information would improve our ability to make water resources management decisions and mitigate future drought impacts (Kusangaya et al., 2014). The research conducted in the present study follows this direction, by using climate data to drive a hydrological model to project drought in four Western Cape River Basins.

2.3 Impact of Land-Use/Land-Cover Changes on Hydrology

Several studies illustrate that LULC changes influences various hydrological processes (e.g., surface runoff, streamflow, or soil moisture; Table 2.2). Previous studies, including DeFries and Eshleman (2004), Falkenmark et al. (1999), Guo et al. (2014), Joorabian Shooshtari et al. (2017) and Lumsden et al. (2003), show that the type and extent of the LULC change influences the magnitude and direction of hydrological feedback. For instance, while forestation may reduce soil moisture and surface runoff, urbanisation and human settlement may give rise to higher storm flow and enhanced discharge peaks. Jia et al. (2017) showed that removal of forest reduced the soil moisture across the Loess Plateau (in China). Farley et al. (2005) reported reductions in runoff following the forestation of grassland/shrubland and indicated that the reduction may be higher in drier regions. Youpeng et al. (2010) found that the expansion of urban areas increased surface runoff across the Yangtze River Basin, China. Similarly, Gyamfi (2016a) found that the expansion of urban and agricultural areas also increased surface runoff and water yield over the Olifants River Basin, South Africa. Holder et al. (2019) showed that conversion of temperate grassland to agriculture in the western United Kingdom decreased surface run-off. In contrast, Mango et al. (2011) and Githui et al. (2009) showed that conversion to agriculture along the Mara River (Kenya) and the Chi River (Thailand), respectively, increased surface run-off. Similarly, agricultural activities may reduce storm flows by enhancing the soil's water holding capacity, while livestock grazing may enhance storm flows. Querner and Zanen (2013) showed that simple irrigation and fertiliser application in agricultural lands may increase evapotranspiration. Basin rehabilitation activities may have a positive impact on river flows, while artificial wetlands can minimise the impacts of floods, and a beneficial riparian zone may offer shading and reduce evaporation from the water surfaces. Marais et al. (2021) showed that buffers of natural vegetation around water ecosystems may also mitigate the negative impacts of adjacent land-use practices. These buffers of natural vegetation around water ecosystems may furthermore mitigate the negative impacts of adjacent land-use practices. Baseflow can be defined as streamflow fed from the deep subsurface and shallow subsurface storage between precipitation events, fed to streams by delayed pathways (Tallaksen, 1995; Price, 2011). Land use and land cover (LULC) change may have profound effects on baseflow (Zhang and Schilling, 2006; Wang et al., 2014), including impacts of changing forest and agriculture (Juckem et al., 2008; Zhang et al., 2017) and urbanization (Simmons and Reynolds, 1982; Chang 2007; Dow, 2007; McGrane 2015)(see Bloomfield et al., 2009). Nevertheless, while all these studies have documented how LULC changes may influence the hydrological processes and water yield in a basin, there is still a dearth of information on how and to what extent LULC changes can be used to reduce the impacts of climate change on drought. This information would help to inform appropriate LULC change management and may mitigate the impacts of climate change on water yields and hydrological drought in the future.

LULC changes may also influence the hydrological processes in the Western Cape River catchments. Many studies (e.g., Holden, 2021; Le Maitre et al., 2019; Preston et al., 2018) recognise that LULC changes, such as the spread of invasive alien vegetation, has an impact on water yields and streamflow in the region's river catchments. These studies suggest that the proliferation of 'thirsty' invasive alien vegetation (i.e., trees or plants that are not indigenous to South Africa) consume hundreds of litres of water per day, depleting underground water resources, and reducing runoff into the major dams that supply the Western Cape Water Supply System. Estimates by Ground Up (2018) suggest that more than 100 million litres per day (about 20% of Cape Town's water requirement) are lost due to invasive alien vegetation, such as wattles, eucalypts and hakeas from Australia, and pines from the Mediterranean Basin and California. Such vegetation is often found in old forestry plantations near the Steenbras, Berg and Theewaterskloof catchment areas, where they compete for water (and space) with the Cape's indigenous vegetation. As such, there is some consensus (e.g., Le Maitre et al., 2019; Rostorfer et al., 2015; Turpie, 2018) that the removal of invasive alien vegetation in these river catchments may increase surface water flows, and thereby offer an economically cheap and environmentally low risk option to improve water security for the Greater Cape Town area. Indeed, it may even be that removal of alien vegetation may also reduce the severity of hydrological drought due to future climate change. Hence, an improved understanding of LULC changes, specifically as it relates to the spread of invasive alien vegetation, and future hydrological processes is required. To date, however, only few empirical studies (e.g., Albhaisi et al., 2013; Gyamfi et al., 2016a; Schütte & Schulze, 2017; Warburton et al., 2012) have modelled LULC changes impacts on hydrological processes over South Africa, and there remains a dearth of information on how LULC changes may influence future hydrological drought in the Western Cape.

Table 2.2: Summary of literature illustrating the potential LULC changes impacts on hydrological processes.

LULC changes	**Potential Impacts**	**Regions of interest**	**References**
Urbanisation (increase in impervious, hard surfaces)	Decreased infiltration, increased surface runoff, increased water yield, and/or change in evaporation	Yangtze River, China; Olifants River, South Africa; Jing-Jin-Ji, China; Indian River basin, Upper Brantas, Indonesia	Youpeng et al. (2010); Gyamfi et al. (2016a); Li et al. (2018); Astuti et al. (2019); Wagner et al. (2013); Donaldson (2004); Lerner (1990);
Forestation	decreased surface runoff, decreased water yield, increased evaporation	Jhelum River Basin, Pakistan	Sadiq Khan et al. (2020)
Forest to grassland	increased surface runoff, and/or decreased evaporation	Mara River Basin, Kenya	Mango et al. (2011)
Grassland to agriculture	decreased surface runoff, and/or increased evaporation	United Kingdom; Midwestern United States	Holder et al. (2019); Mao & Cherkauer (2009)
Forest to grassland and agriculture	increased surface runoff, decreased evaporation	Midwestern United States	Mao & Cherkauer (2009)
Evergreen forest to deciduous forest	decreased surface runoff, increased evaporation		
Agricultural expansion	increased surface runoff, increased water yield, and/or decreased evaporation	Chi River, Thailand; Tekeze watershed, Ethiopia; Upper Brantas, Indonesia	Githui et al. (2009); Welde et al. (2017); Astuti et al. (2019)
Clearance/ removal of vegetation	increased surface runoff, and/or decreased evaporation	East Africa	Baker et al. (2013)
Agricultural practices	increased evaporation	Limpopo River Basin, South Africa	Querner and Zanen (2013)

2.4 Summary

The literature review presented in this chapter emphasised the value of two widely applied meteorological indices. A hydro-meteorological framework for modelling drought was also presented. Hydrological models were then discussed, with aim to highlight the value of bias-correcting input data. Thereafter, the potential hydrological impacts of LULC change were presented. The review outcome and the research gaps are summarized below:

- Previous studies have used two major approaches - drought indicators or drought indices - to identify and quantify hydro-meteorological drought. Among the meteorological drought indices in the literature, the Standardized Precipitation Index seems to be the most popular. Nevertheless, numerous studies have used both the SPI and SPEI in future projections of drought due to climate change over river basins in Africa. Furthermore, there is a clear benefit in applying both SPEI and SPI to quantify meteorological drought. As such, the present study has selected both indices to quantify future drought projections in the Western Cape.
- Previous studies on hydro-meteorological modelling have followed a standard framework for studying the potential impacts of climate change on hydrological variables or droughts. This includes a transfer of climate information from large-scale GCMs, to RCMs, and subsequently hydrological models. Bias-corrected data is particularly useful in the detection of drought characteristics. While a recent study over the Southern African river catchments examined the impacts of climate change on drought and found a consistent drying signal (over the region, albeit with some variations in magnitude, the drought index used), their projections did not use a drought index. Consequently, the results of their study contain systematic biases from the climate model outputs. There remains limited information on quantifying the uncertainty of these hydrological simulations and the value of bias correction for other regions of Southern Africa, including the Western Cape.
- Previous studies have also illustrated that LULC changes influences various hydrological processes and water yield in a basin. However, there is still a dearth of information on how, and to what extent, LULC changes can be used to reduce the impacts of climate change on drought. Such information would help to inform appropriate LULC change management and may mitigate the impacts of future climate change on water yields and hydrological drought. To date, however, only few empirical studies have modelled LULC changes impacts on hydrological processes over South Africa, and there remains a dearth of information on how

LULC changes may influence future hydrological drought in river catchments of the Western Cape in particular.

The present study set out to improve knowledge in these areas.

Chapter 3:
Methodology

This chapter presents the methodology of the dissertation as divided in three broad sections. The first section describes the Western Cape study region and the physical features of the Western Cape River Basins. The second section describes the sources of the datasets analysed in the study. The third section discusses the details of the methodology for the experimental design of the simulations performed. These simulation experiments include: (i) the future impacts of climate change on meteorological drought (ii) the Soil Water Assessment Tool Plus (SWAT+) hydrological model performance sensitivity, including the statistical tools used for the model calibration and validation (iii) the influence of bias correction of climate datasets on simulation of hydrological drought, and (iv) the future impacts of land-use change on hydrological drought.

3.1 Study Region

The focus of the study is on river basins in the Western Cape Province of South Africa (Figure 3.1). South Africa has 19 Water Management Areas (WMAs), each containing a large river system. The Western Cape Province, which covers an area of only about 129 462 km^2 (about 30^{o}S – 35^{o}S; 17^{o}E – 25^{o}E), overlaps with four of such river systems: the Breede, the Berg, the Gouritz and the Olifants/Doorn (Figure 3.1) as well as a small section of the Fish to Tsitsikamma (not shown). For the purposes of this study, these four WMAs are hereafter collectively referred to as the Western Cape River Basins (WRB). These basins all have unique physical features (rivers, topography, soils etc), and, as such, the next section will provide a more detailed description of each.

3.1.1 The Berg River Basin

The Berg River Basin is located in the southwest of the Western Cape Province (Figure 3.1). It is named after the Berg River, which has a total length of about 285 km and drains an area of approximately 8 980 km^2 (RHP, 2004). The Berg River source occurs in the Franschhoek and Drakenstein mountains (at an altitude of 1500 m), and flows northwards past Paarl, Wellington, Hermon and Gouda. The river then flows westwards past Porterville, Piketberg and Velddrif, before it finally discharges along the west coast near St. Helena Bay (RHP, 2004). The topography of the Berg River Basin varies considerably along its course. Rainfall ranges from 3000 mm per annum in the southern mountain to less than 300 mm per annum in the inland northwest coastal plain (DEADP, 2011). Mean annual run-off (MAR) is about 1094 million cubic metres per year (Mm^3 per annum) – 2.2% of the national total, although the present-day MAR is 784 Mm^3 per annum (Cole et al., 2018). The geological bedrock of the entire Berg River Basin comprises the rock types of the Klipheuwel and Malmesbury 'Shale' Groups.

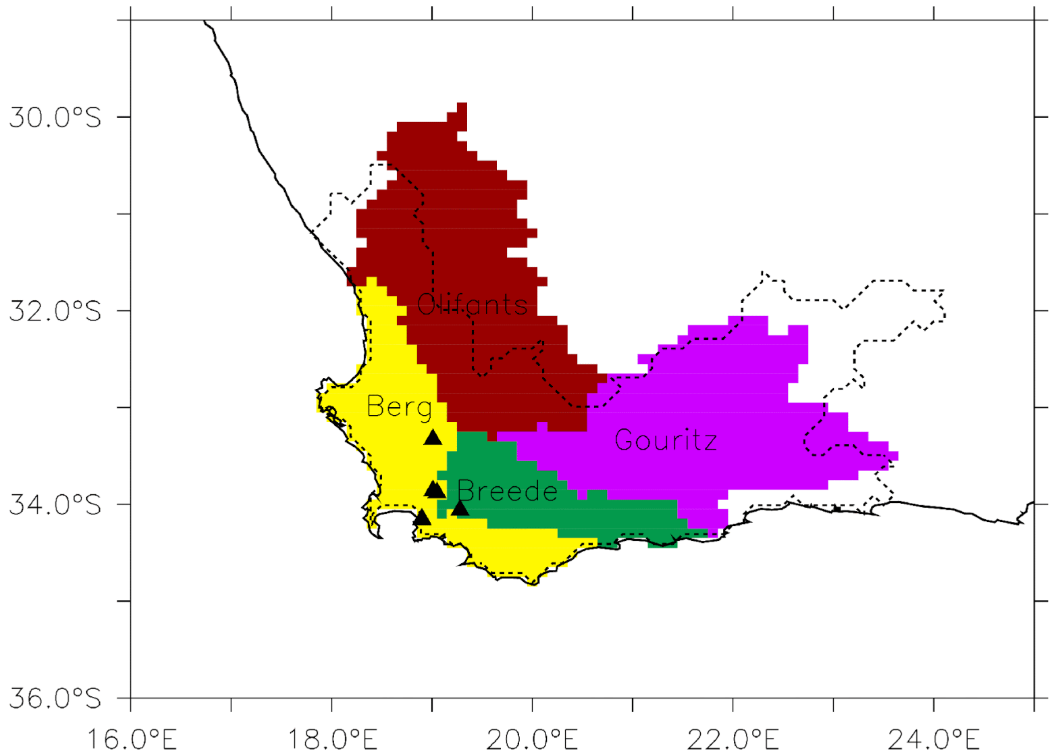

Figure 3.1: The study domain depicting the four main river basins in the Western Cape region (South Africa). The dashed line delineates the Western Cape Province's political boundary, while the triangular peaks represent the location of the major dams in that supply region.

3.1.2 The Breede River Basin

The Breede River Basin is in the south of the Western Cape Province (Figure 3.1). It is named after the Breede (i.e., 'broad') River, which has a total length of about 322 km and drains an area of approximately 12,596 km^2 (Flemming & Martin, 2021). The Breede River rises in the mountains of Ceres in the Cape Fold Belt (Riviersonderend mountains). The river then flows through its self-carved valley before it discharges into San Sebastian Bay just north of Cape Infanta (northeast of Cape Agulhas), and into the Indian Ocean. It is the longest navigable river in the Western Cape and provides irrigation for the farms along the Breede River Valley, flowing past some important agricultural areas of Worcester and Swellendam. The topography across the Breede WMA varies considerably. Rainfall ranges from 3 000 mm per annum in the southwestern mountainous regions to only 250 mm per annum in the north-eastern and central areas (DEADP, 2011). The Cape Fold Belt is the major feature in the river basin, occurring largely as an east-west striking feature and is comprised of metamorphic and sedimentary rocks (DEADP, 2011). The natural geology (consisting of shale) and agricultural land-use activities contribute to the high salinity in the Breede River, which affects the quality of water for irrigation.

3.1.3 The Gouritz River Basin

The Gouritz River Basin is located largely within the Western Cape Province, with small parts in the Northern Cape and the Eastern Cape Provinces (Figure 3.1). It covers an area of approximately 416 km and drains an area of approximately 53,139 km^2 (DEADP, 2011). The Gouritz River is the major river, providing 41% of the surface flow in the basin (DEADP, 2011). The other main rivers, which drain the inland area, are the Buffels, Gamka, Groot, Kammanassie, Olifants, and Touws Rivers. The Gouritz River originates at the confluence of the Gamka and Olifants rivers, where it is joined by the Groot River before flowing through the Langeberg Mountains and across the coastal plain. It finally empties into the Indian Ocean via the Gouritz Estuary in Gouritsmond (34 km south-west of Mossel Bay). Three distinct zones exist in its basin area: the semi-arid Great Karoo, the Olifants River, and the Coastal Belt. A dry and hot Karoo climate dominates in the Olifants and Great Karoo regions, but along the coastline the climate is temperate with higher rainfall, throughout year. While cold fronts approaching from the south-west bring rainfall to the Coastal Beltzone, thunderstorms occur inland over the Karoo and Olifants River zones (from February to April) (DEADP, 2011). Mean annual precipitation decreases from east to west, ranging from 1000 mm per annum in the south-east to as low as 160 mm per annum in the north. MAR is about 674 Mm^3 (Le Maitre et al., 2009). The geological setting of the Gouritz includes rock types of the Kaaiman/Kango and Table Mountain Groups. The geology of the region promotes high evaporation and agricultural impacts, and hence, water quality is better in the headwaters of the tributaries, with water salinity increasing further downstream.

3.1.4 The Olifants River Basin

The Olifants River Basin is not found entirely within the Western Cape Province (Figure 3.1). In fact, this river basin’s boundaries do not correspond with either municipal demarcations or with the provincial boundaries of the Western Cape Province. It is located to the north of the Berg, Breede, and Gouritz WMAs, and the entire basin covers an area of approximately 46,220 km^2. The Olifants River is the major river, while the Doring River (draining the Koue Bokkeveld and Doring areas) and the Sout River (draining the Knersvlakte) are the main tributaries. The Olifants River rises in the mountains in the south-east and flows in a north-westerly direction. It is first joined by the Groot River, before it flows west to its confluence with the Olifants River (DEADP, 2011). Mean annual precipitation is less than about 200 mm across much of this region.

3.2 Datasets

Several types of datasets were used in this study: broadly, they include geographical information system (GIS), climate and hydrological datasets (Table 3.1). The GIS datasets are used to characterise the basin in the hydrological modelling. We used QGIS 3.4 (Madeira) with the QSWAT+ plugin (version 1.2.2) to perform pre-processing of the SWAT+ model input. We obtained global Digital Elevation Model (DEM) data from the Shuttle Radar Topography Mission (SRTM; CGIAR Consortium for Spatial Information of The Consultative Group Of International Agriculture Research) (Jarvis et al., 2008) with a 90 m × 90 m resolution, digital soil data from the Food and Agriculture Organization's (FAO, 2004; UNESCO available from Waterbase.Org) global soil databases (version 3.6), and digital land-use and land cover maps from the USGS Global Land Cover Characterization (GLCC; United States Geological Survey National Centre for Earth Resources; available from the Waterbase.Org) database.

Table 3.1: Main SWAT+ input data.

Input Data	Source	Description	Reference
Digital Elevation Model (DEM)	Shuttle Radar Topography Mission; CGIAR Consortium for Spatial Information	90 m × 90 m resolution	Jarvis et al., 2008.
Weather	Global Meteorological Forcing Dataset	0.5-degree, daily temperature, precipitation, relative humidity, solar radiation, wind	Sheffield et al., 2006.
Stream network (burn in)	Water Resources 2012	(shapefile)	Herold & Bailey, 2016.
Land Use / vegetation cover	USGS Global Land Cover Characterization (v3.6)	Digital land-use and land cover maps (shapefile)	Waterbase.Org
Soil	Food and Agriculture Organization	Digital soil data (shapefile)	Waterbase.Org

The climate datasets include observational, reanalysis and model simulation datasets (see Appendix, Figure A1 for schematic flow diagram overview of the datasets and simulations produced). The observational/reanalysis data for this study includes the Global Meteorological Forcing Dataset (GMFD; version 3.0) (Sheffield et al., 2006) that has been developed by Princeton University to drive models of land surface hydrology. We use the GMFD daily data (precipitation, minimum temperature, maximum temperature, solar radiation, wind speed, and relative humidity) as climate input data in calibrating the hydrological model and in evaluating the climate simulation dataset. The GMFD dataset is constructed by combining a suite of global observation-based datasets and the National Centres for Environmental Prediction – National Centre for Atmospheric Research (NCEP/NCAR) reanalysis dataset (Sheffield et al., 2006). This is a near-surface meteorological dataset developed for global land surface modelling. The dataset provides high resolution (0.5 degree) daily climate data that is available globally for 1901 – 2012. Observational data and model simulations were also used for the Self-Organizing Maps (SOM). Observational data for this was obtained from the University of East Anglia's Climate Research Unit (CRU; Harris et al., 2014; Mitchell & Jones, 2005). CRU data include monthly observations, gridded at horizontal resolution of 0.5∘×0.5∘ for the period 1901 – 2009. Simulation data from the regional climate models (RCMs) in CORDEX were used too (Nikulin et al., 2018). Climate model simulation data from the RCMs in the Coordinated Regional Climate Downscaling Experiment (CORDEX-Africa database website - https://www.cordex.org/; Giorgi et al., 2009; Jones et al., 2011; Nikulin et al. 2018) were used. CORDEX is an international modelling framework, established by the World Climate Research Programmes (WCRP). Its vision is to provide a high-resolution model ensemble of historical climate and future projections, by downscaling the global climate models (GCMs), for all continents, including Africa, to produce regional climate simulations worldwide. Studies have often used the output of either the first phase of the CORDEX RCMs, when ERA-Interim reanalysis was used as a driven run (Akinsanola & Ogunjobi, 2017; Dee et al., 2011), or the second phase when CORDEX RCMs dynamically downscaled CMIP5 GCMs to a lower resolution (Taylor et al., 2012). For this study, we use the latter, i.e., RCM data at a grid spacing of 0.44^{o} X 0.44^{o} (approximately 50 km) over the African continent. The hydrological dataset comprises a daily streamflow dataset provided by the Department of Water Affairs (DWA, 2021). The streamflow data at hydrological stations were utilised to calibrate and validate the hydrological model over the basins. The data sampled include four stations in the Western Cape (one for each river basin, i.e., E2H003, G1H013, H7H006 and J1H019; Table 3.2).

Table 3.2: Description of the Western Cape stations (Herold & Bailey, 2016).

Station	**Gauge Name**	**River**	**Latitude**	**Longitude**	**Area (km^2)**	**Quality Rating (good, average, poor)**
E2H003	Melkoom	Doorn	18.69	–31.86	24044	average
G1H013	Drieheuwels	Berg	18.86	–33.13	2934	good
H7H006	Swellen	Breede	20.41	–34.07	9842	good
J1H019	Buffelsfontein	Groot	21.44	–33.75	12493	average

3.3 Methods

3.3.1 Characterising Droughts

Seven standardised indices were used to characterise droughts (Table 3.4). The use of standardised indices has become increasingly popular in drought assessment. A major advantage of standardised indices is their comparability across time, space, and variables. The calculation procedure used is the same, regardless of the input variable used (i.e., runoff, streamflow, or soil moisture). Meteorological drought is characterised using SPI and SPEI as is detailed in Table 3.3. Both SPI/SPEI indices are similar, in that they are multi-scalar meteorological drought indices, meaning that they can provide drought information at different timescales. This makes them suitable for detecting different types of droughts. However, while SPI requires only rainfall data for computation, SPEI additionally requires a measure of evaporative demand. SPI was calculated by fitting long term precipitation (P) records to a gamma probability density function, which is transformed to a normal distribution. This normalises the data, such that the mean is zero with standard deviation of one. Thus, the values of SPI are expressed in standard deviations by which the observed anomaly deviates from the long-term mean; positive SPI values indicate greater than median precipitation, while negative values indicate less than median precipitation (Edwards and McKee, 1997). The transformed probability gives the SPI values, which mainly vary from –2 to 2 (McKee et al., 1993; Table 3.4). For this study, a drought occurs when the SPI is continuously below zero and reaches a value of −1.0 or below, and it ends when SPI value becomes positive. Details of the equation formulation and calculation for the drought index are specified in previous studies (Edwards and McKee, 1997; Guttman, 1998; McKee et al., 1993). Like SPI, SPEI is a probability-based function calculated using climatic water balance data instead of precipitation data (Vicente-Serrano et al., 2010). For SPEI calculations, climate water balance data (which is rainfall minus potential evapotranspiration, or minus actual evaporative demand) was fitted to a three-parameter log-logistic distribution (Vicente-Serrano et al., 2010). The advantage of using SPEI is the inclusion of the atmospheric water demand, PET, which has been shown to play a crucial role in drought severity. SPEI can be used to identify a drought caused by a decrease in rainfall or higher water demand (i.e., evaporation) or both.

The climate water balance (CWB_i) for the month i is calculated as:

$$CWB_i = P_i - PET_i \qquad \text{Equation 1}$$

The 12-month drought indices (ending in March, which is the end of the rainfall season in the Western Cape) were obtained using the CORDEX and CRU data as input for SPEI/SPI drought algorithms in R statistical software (see Beguera et al., 2013; Vicente-Serrano et al., 2010).

In this dissertation, PET was obtained using the Hargreaves method (HG; Hargreaves & Samani, 1985). Although different methods for calculating PET have been used, such as Thornthwaite (1948), Hargreaves and Samani (1985), and Penman-Monteith (Monteith, 1965), the Penman-Monteith method is often preferred. The Penman-Monteith (PM) method is better suited for the calculation of PET, since it is based on fundamental physical principles and a comprehensive theoretical base. However, the PM method requires extensive data. That is, several climate variables are required (i.e., air temperature, relative humidity, solar radiation, and wind speed), which are available only for a limited number of CORDEX simulations for the study region. As a result, the Hargreaves method is used to calculate the PET because it is generally recommended if the PM method does not have enough data (Hargreaves & Samani, 1985). Beguería et al. (2014) recommended the use of HG for calculating PET, where there is scarce data for the PM method.

In addition, five types of hydrological drought were identified using the SWI, PERCI, RFI, SFI and WYLDI indices over the WRB. Similarly, these indices are essentially based on the methodology for calculating SPI, which involves fitting a distribution to the time series of runoff, streamflow, or soil moisture, and transforming it to a normal distribution. Input data for hydrological drought computation were derived from the SWAT+ model. SWAT+ calculates WYLD as the sum of surface runoff, lateral flow, and groundwater contributions, less transmission losses. This parameter has the advantage of being able to quantify most of the hydrologic components that are important for water resource use systems. WYLD is also calculated for Theewaterskloof dam (TWT). The classification of all the above-mentioned indices is outlined in Table 3.3. All the hydrological indices were calculated following a similar procedure as for SPI, but rainfall data was substituted with the relevant hydrological variable (see e.g., Dutra et al., 2008; Sheffield et al., 2004; Shukla and Wood, 2008).

Table 3.3: Drought indices (for SPI, SPEI, SWI, PERCI, RFI, SFI and WYLD) classification (definitions of the drought indices are in Table 3.4).

Drought indices	**Description**	**Drought type**
SPI	Standardized Precipitation Index, calculated based on precipitation only	Meteorological
SPEI	Standardized Evapotranspiration Index, calculated as the climate water balance, i.e., precipitation minus potential evapotranspiration	Meteorological
SWI	Soil Water Index, calculated based on soil moisture	Hydrological
PERCI	Percolation Index, calculated based on percolation	Hydrological
RFI	Runoff Index, calculated based on surface runoff	Hydrological
SFI	Streamflow Index, calculated based on streamflow	Hydrological
WYLD	Water Yield Index, calculated based on water yield	Hydrological

Table 3.4: The description of drought indices used to characterise meteorological, and hydrological drought in study. All the indices were calculated with monthly data at a 12-month scale.

Drought indices values	**Classification**
≥ 2.00	extremely wet
1.50 to 1.99	very wet
1.00 to 1.49	moderately wet
0.00 to 0.99	near normal
0.00 to –0.99	mild drought
–1.00 to –1.49	moderate drought
–1.50 to –1.99	severe drought
≥ –2.00	extreme drought

3.3.2 Assessing potential impacts of climate change on meteorological drought

The potential impacts of climate change on meteorological drought were assessed by calculating and analysing the SPI and SPEI in CORDEX datasets. The impacts were quantified at four global warming levels (1.5 °C, 2.0 °C, 2.5 °C, and 3.0 °C above the pre-industrial levels) under the Representative Concentration Pathway (RCP) 8.5 future scenario, which is the most realistic scenario of greenhouse gas emissions, considering the current trajectory of greenhouse gas emissions. In the RCP8.5 scenario, the greenhouse gas emissions increase considerably over time, leading to a radiative forcing of 8.5 W m^{-2} at the end of the century (Riahi et al., 2011). The high-emissions scenario is frequently referred to as "business as usual" and represents a likely outcome if society does not make concerted efforts to reduce greenhouse gas emissions. The relevant GCMs and the downscaling RCMs used for these simulations used for the climate change projection simulations are shown in Table 3.5. Following previous study by Nikulin et al. (2018), a GWL climate period is defined as a period of 30-years where the climatology of the mean global temperature is higher than that of the preindustrial (1861 – 1890) baseline period by the targeted global warming value (i.e., 1.5 °C, 2.0 °C, 2.5 °C, and 3.0 °C). Table 3.5 shows the 30-year GWL period differs with the GCM simulations. However, the simulation for the period 1971 – 2000 was used as the present-day climate with which all the GWL climates were compared.

Table 3.5: Global climate models (GCMs) and respective downscaling regional climate models (RCMs) for the simulations used in the study. Corresponding 30-year period for various global warming levels (1.5, 2.0, 2.5 and 3.0°C) are indicated. For more detailed information see Déqué *et al*. (2017). The alphabet letters (a–l) and numbers (1–7) in brackets of the GCMs and RCMs (respectively) are tags to correspond to the simulations (e.g., a5 represents the CanESM2_RCA4 simulation) (modified after Abiodun *et al.*, 2018). All the GCM simulations were downscaled with the RCA4 model in the CORDEX and bias-corrected. [Note: the seven simulations used for the hydrological simulations are underlined (these were selected based on data availability and computational resources)].

GCMs	**Global Warming Levels (GWLs) time period**				**Downscaling RCMs**
	1.5 °C	2.0 °C	2.5 °C	3.0 °C	
CanESM2[a]	1999–2028	2012–2041	2024–2053	2034–2063	RCA4[5]
CNRM-CM5[b]	2015–2044	2029–2058	2041–2070	2052–2081	RCA4[5], CCLM[2], ALADIN[1]
CSIRO-Mk3[c]	2018–2047	2030–2059	2040–2069	2050–2079	RCA4[5]
EC-EARTH-r1[d]	2003–2032	2021–2050	2035–2064	2046–2075	RACMO[4]
EC-EARTH-r3[e]	2006–2035	2023–2052	2036–2065	2047–2076	HIRHAM[3]
EC-EARTH-r12[f]	2005–2034	2021–2050	2034–2063	2047–2076	RCA4[5], CCLM[2]
GFDL-ESM2M[g]	2020–2049	2037–2066	2052–2081	2066–2095	RCA4[5]
HadGEM2-ES[h]	2010–2039	2023–2052	2033–2062	2042–2071	RCA4[5], CCLM[2], RACMO[4]
IPSL-CM5AMR[i]	2002–2031	2016–2045	2027–2056	2036–2065	RCA4[5]
MIROC5[j]	2019–2048	2034–2063	2047–2076	2058–2087	RCA4[5]
MPI-ESM-LR[k]	2004–2033	2021–2050	2034–2063	2046–2075	RCA4[5], CCLM[2], REMO[6],
NorESM1-M[l]	2019–2048	2034–2063	2047–2076	2059–2088	RCA4[5], WRF[7]

The Self-Organizing Maps (SOM) were used to classify and study the patterns of expected change in SPEI and SPI droughts. SOM is a technique for clustering datasets and lowering the dimensionality of a dataset that uses artificial neural networks (ANNs; see Kohonen et al., 1996). Setting the weights in a neural network is done in the hidden layer during training(s). SOM has a large number of input nodes but a small number of output nodes. The data is delivered to the input nodes, which are then processed so that the output nodes are activated based on the weights assigned to each incoming link

(Skupin & Agarwal, 2008). This indicated that the network's input data during training did not correspond to known categorization outcomes (i.e., input-output pairs).

Instead, the output nodes competed for the input vectors, and the input vectors' weights were changed based on the weight of the relevant input nodes. Climate change patterns (drought index and severe drought frequency) related with drought in the Western Cape, South Africa, were classified using the SOM approach. The SOM was thus applied to two datasets separately, using a 12 (4 x 3) node classification: for the first dataset, all the SPI and SPEI projections were considered for four GWLs, for all simulations. For the second dataset, the same were considered, but for projected changes in frequency of SPEI severe droughts (i.e., 12-month SPEI<–1.5) and projected changes in frequency of SPI severe droughts (i.e., 12-month SPI<–1.5). Following Abiodun et al. (2019), the contribution of each drought index, each GWL and each respective simulation to a SOM node was considered. These results are reported in Chapter 4.

3.3.2 Hydrological Modelling: Assessing the sensitivity and performance of SWAT+ for hydrological simulations

The Soil and Water Assessment Tool Plus (SWAT+) was used for all the hydrological modelling in the study. This section provides a description of SWAT+, the model setup (including sensitivity, calibration, and validation), the input datasets, and the statistical tools for performance evaluation.

3.3.2.1 SWAT+ Description and Set-up

The SWAT+ model is an open-source model cooperatively developed by the United States Department of Agriculture—Agricultural Research Service (USDA—ARS) and Texas A&M AgriLife Research. SWAT is a spatially distributed, process-based hydrological model. It is a watershed to river basin-scale model and has been applied to a wide variety of watershed applications (Arnold et al., 2012; Bieger, et al., 2017). As a time-continuous model with multiple components (including, for example, hydrology, soil, plant growth, nutrient transport, land management), it is designed to simulate the quantity and quality of surface- and sub-surface flows (including groundwater), and to simulate the environmental impact of climate change, land-use changes as well as land management. SWAT is extensively used in evaluating prevention and control of soil erosion, non-point source pollution and regional management of watersheds. SWAT is suitable for hydrological modelling streamflow conditions over the South African domain and has been applied and calibrated over South African basins (e.g., Gyamfi et al., 2016b; Ncube, 2005), as well as extensively used for studying the impact of land-use changes (for a review, see Kiros et al., 2015). SWAT+ is the new generation of the SWAT and offers more flexibility, better independent modules (modularisation; Figure 3.2), is more computationally efficient, and generally results in enhanced model performance.

The major differences between SWAT and SWAT+ are presented in Table 3.6. Key strengths of SWAT+ include the advanced aquifers and reservoir functionalities. In SWAT, aquifers used to be regulated entirely in Hydrological Response Units (HRUs), but in SWAT+ the aquifer boundaries can be specified more flexibly without the constraints of the HRUs. Reservoir functions were also one of the major limitations of the SWAT model. Reservoirs with large water releases may have a major contribution to watershed processes. In SWAT+, users now can apply comprehensive operation rules with ease, such that reservoir simulations are better modelled compared to actual operational routines. Other spatial modules with designated functions include: (i) outlets, which add/remove water from the watershed; (ii) canals, which divert water among irrigation channels; (iii) pumps, which extract water aquifers specific objects; and (iv) water rights, which are designated depending on different shares of water demand. Further information is provided in Arnold et al. (2012). The SWAT+ is utilised for this dissertation.

Table 3.6: Major differences between SWAT and SWAT+ functionalities.

Category	SWAT	SWAT+
Calibration Support	not supported	manually calibrated (calibration.cal)
Reservoir Operation	not supported	users can assign operation rules
Coding Flexibility	not supported	easily modify/upgrade modularised coding structure
Aquifer Border	used to be linked with HRUs	flexibly defined without limitations
Connectivity	limited spatial flexibility	definition of individual watershed objects possible

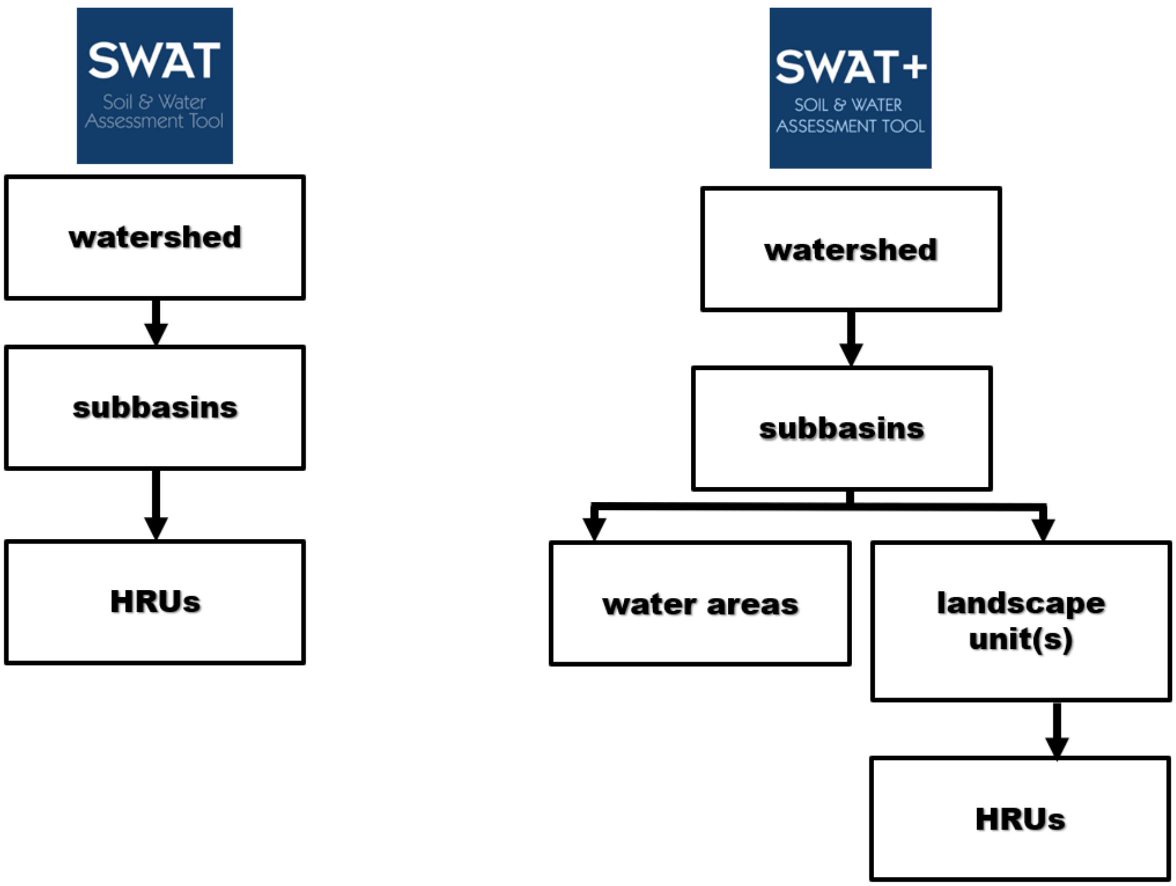

Figure 3.2: Overview of modularisation differences and function between SWAT (old) and SWAT+ (revised).

The SWAT model simulates watershed processes at the sub-basin scale, which is then further divided into HRUs. These are discrete areas of the same land-use, slope, and soil characteristics within a particular sub-basin. SWAT hydrological processes are simulated following the water balance equation of Neitsch et al. (2005):

$$SW_t = SW_0 + \sum_{i=1}^{t} (R_{day} - Q_{surf} - E_a - W_{seep} - Q_{gw}) \qquad \text{Equation 2}$$

where for each day t is time in days, SW_t is the final soil water content, SW_0 is the initial soil water content on day i, and R_{day}, Q_{surf}, E_a, W_{seep} and Q_{gw} daily amounts (mm) of rainfall, surface runoff, evapotranspiration, water in the soil (vadose zone), and the groundwater discharge.

The SWAT+ was set up following the procedure described by Dile et al. (2016). We used the QGIS interface with the QSWAT plugin and default SQLite database (for data management), to delineate the basins, create HRUs and edit the climate inputs before running the model. QSWAT uses TauDEM (Terrain analysis using Digital Elevation Models) for watershed delineation. TauDEM provides a suite of geoprocessing capabilities (e.g., such as pit depression removal using the flooding approach, calculation of flow paths and slopes, calculation of contributing areas using single and multiple flow direction methods, delineation of stream networks using contributing area threshold, delineation of watersheds and subbasins; see Tarboton, 1997). The standard specification library of Message Passing Interface (MPI; Gropp et al., 1996) was used to reduce the processing times of the DEMs. QSWAT was run with MPI installed and 20 processors selected. The delineation of the basins was generated using a burn-in vector file for a predefined stream network to accurately identify stream positions, and default threshold values (or number of DEM cells). TauDEM delineates a given watershed by calculating where streams will flow and subsequently calculating the subbasin region which drains to each reach (i.e., the portion of a stream between two points e.g., stream sources, junctions, inlets, outlets, point sources and reservoirs). Point sources were automatically added to each sub-basin (i.e., snapped to the nearest stream, if within a threshold distance from the stream network). The sub-basins were delineated with a 299 km^2 channel and 299 km^2 stream threshold. No merging of sub-basins was applied.

The four primary basins in the Western Cape were divided into 26 sub-basins and 234 landscape units (LSUs) and 2731 HRUs (Figure 3.3). We inserted a slope band of 10%, and no filtering was used in generating the HRUs. In SWAT+, a landscape unit (LSU) is defined as a collection of HRUs and can be defined as a subbasin, or a flood plain or upland unit, or a grid cell with multiple HRUs. All subbasins were subdivided into upland areas and floodplains. The landscape unit is not routed, it only used for output. The landscape unit output files (e.g., plant weather) are output for HRUs, landscape units, and for the basin. In SWAT+ Editor, all connection objects were populated automatically during project setup. After generating the HRUs, the SWAT+ model assimilated the climate input (i.e., precipitation, air temperature, relative humidity, solar radiation, and wind speed) and used the Penman-Monteith approach to calculate potential evapotranspiration (PET). For the SWAT+, the simulation options and period were set in the SWAT+ Editor.

A map of land-use characteristics (Figure 3.3) shows that the region is dominated by cropland/grassland mosaic (CRGR, 30.74%), shrubland (SHRB, 27.89%), and grassland (GRSL, 23.13%). The remaining area is comprised of dryland cropland and pasture (CDRY; 9.02%), barren or sparsely vegetated (BSVG, 4.95%), savanna (SAVA, 1.69%), cropland/woodland mosaic (CRWO, 1.03%), evergreen broadleaf forest (FOEB, 0.69%), evergreen deciduous forest (FODB, 0.31%), mixed forest (FOMI, 0.43%), urban residential medium density (URMD; 0.09%), or water (WATR; 0.02%). The Soil Conservation Service Curve Number tables (USDA-SCS, 1972) used for SWAT+ simulations accounted for differences in LULC and hydrological soil group, and soil condition (see Appendix, Table A1). Soils in the Western Cape region are variants of loam and sandy loam (Figure 3.3). In the northern and eastern parts of the watershed (Olifants and Gouritz), loam is predominant, while sandy loam is the main soil type in the southern and western parts (Berg and Breede basins) of the Western Cape.

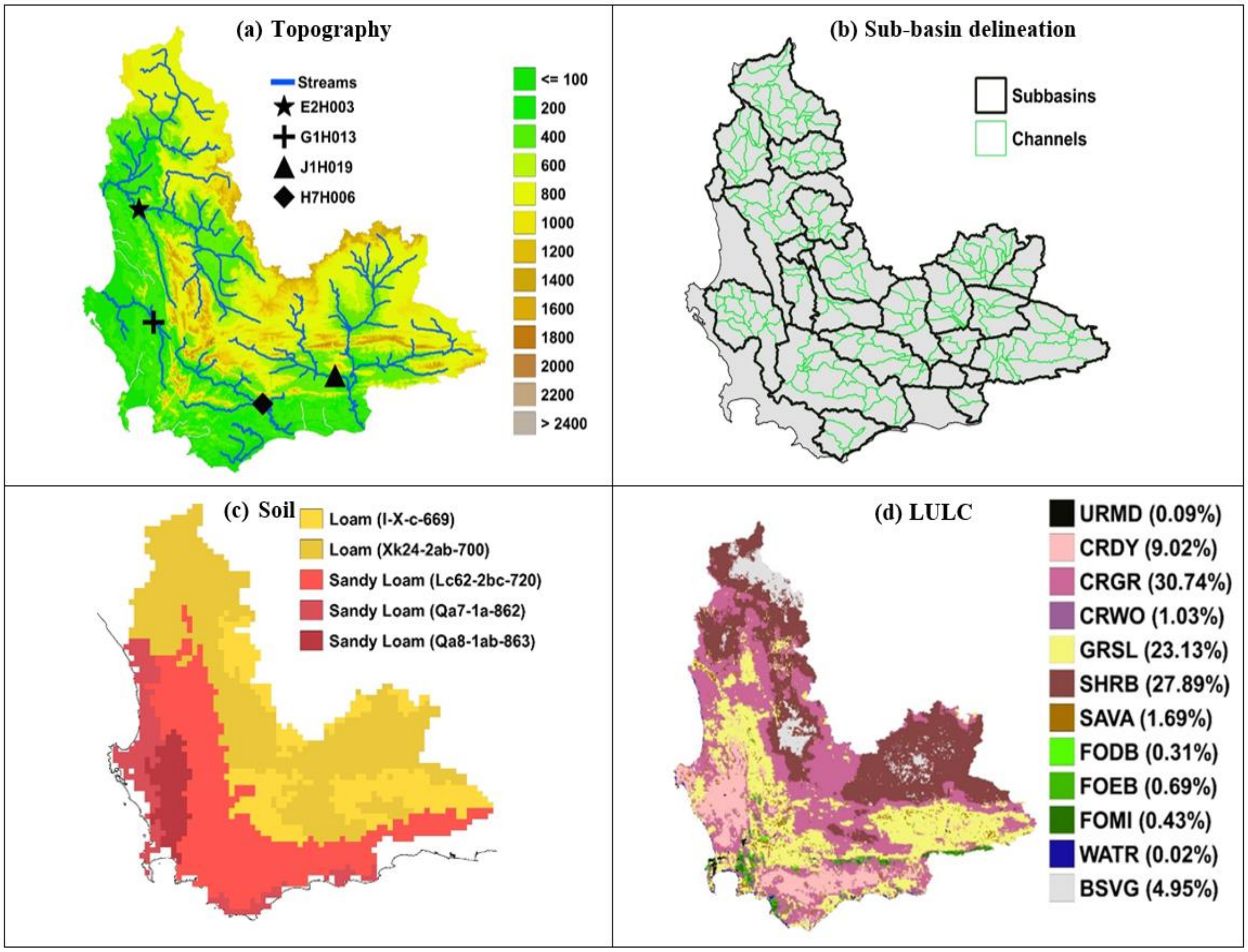

Figure 3.3: The characteristics of the Western Cape River Basins used in the study: (a) the study location indicating the topography of the region (i.e., DEM), streams, streamflow observation stations (i.e., E2H003, G1H013, H7H006, and J1H019); (b) The SWAT+ delineation of the basin into sub-basins and channels; (c) soil types and (d) land-use types: Urban residential medium density (URMD), Shrubland (SHRB), Grassland (GRAS), Cropland/woodland mosaic (CRWO), Cropland/grassland mosaic (CRGR), Dry cropland and pasture (CRDY), Savanna (SAVA), Evergreen broadleaf forest (FOEB), Deciduous broadleaf forest (FODB), Mixed forest (FOMI), Water (WATR), Barren or sparsely vegetated (BSVG). The percentage of each LULC type is indicated in brackets.

3.3.2.2 SWAT+ Calibration and Validation

Model calibration is the process of estimating model parameter values to enable a hydrologic model to match observations, while model validation is the process of demonstrating that a given site-specific model can make sufficiently accurate simulations (Arnold et al., 2012; Refsgaard, 1997).

Validation ensures that the calibrated set of parameters performs reasonably well under an independent dataset, i.e., without any further adjustment at different spatial and temporal scales (Neitsch et al., 2002).

Two experiments were performed for the calibration and validation of SWAT+ model over the basin (Table 3.7). The first experiment was for automatic calibration of SWAT+, while the second experiment was for validation of the calibrated SWAT+. In both experiments, all the simulations used the model set-up and characteristics over the WRB as described in Section 3.3.2.1. The GFMD was used as observed meteorological input data into the simulations. In the calibration experiment, the SWAT+ model was coupled with the Integrated Parameter Estimation and Uncertainty Analysis Tool Plus (IPEAT+; Yen et al., 2019) to perform 300 simulations for the automatic calibration. The IPEAT+ used the 300 simulations to optimally change the model parameters (within ±30% of the default values) and obtained best values for the model parameters over the basin (Table 3.8). The validation experiment consists of one simulation with the best values for the model parameters. The calibration simulations cover a period of 11 years (1980 – 2005) while the validation cover a period of 15 years (1991 – 2005). The calibration and validation simulations used the observed streamflow data from four hydrological stations across the region (E2H003, G1H013, H7H006 and J1H019; Figure 3.3a) as a reference. The stations were chosen by considering the inclusion of representative stations across each of the four river basins (Berg, Breede, Olifants and Gouritz) as well as the data quality and quantity for the calibration and validation periods. The calibration and validation years were chosen because of the completeness of their observed data record. We examined the performance of the SWAT+ model by comparing it with the observed data. Both graphical model evaluation techniques and statistical measures were applied. The statistical metrics used in the evaluations include the Nash-Sutcliffe model efficiency coefficient (NSE), percentage bias (PBIAS), root mean square error (RMSE), and coefficient of determination (R^2). The results of the SWAT+ model calibration and validation are presented in Chapter 5.

Table 3.7: Simulations used in the calibration and validation experiments over the selected river basins (WRB). The indicated simulation periods are after a five-year model spin-up.

Experiment	Simulation periods
Calibration	1980 – 1990
Validation	1991 – 2005

Table 3.8: Selected model parameters for the SWAT+ calibration and their associated best values based on IPEAT+ optimisation using a range of ±30% change in the default values.

Parameter	Description	Unit	Object type	Best value (% change in the default value)
CN2	SCS runoff curve number	unit	HRU	–6.2
ESCO	Soil evaporation compensation factor	unit	HRU	–1.9
EPCO	Plant evaporation compensation factor	unit	HRU	–7.4
AWC	Available water storage capacity in soil	mm_H20/mm	SOL	8.2
K	Saturated hydraulic conductivity	mm/hr	SOL	12.4
DELAY	Groundwater delay, time required for water leaving bottom of the root zone to reach the shallow aquifer	days	GW	1.6
FLO_MIN	Water table depth for return flow	mm	GW	–12.9
REVAP_CO	Groundwater "revap" coefficient	unit	GW	12.4
REVAP_MIN	Threshold water depth in shallow aquifers for return from reach to occur	mm	GW	0.7
SURLAG	Surface lag coefficient, that controls fraction of water entering the reach per day	days	BSN	7.6

3.3.2.3 Statistical tools for Performance Evaluation

Here we provide a brief description of the statistical tools and the interpretations used to evaluate the performance of the SWAT+ hydrological model simulations.

3.3.2.3.1 Nash-Sutcliffe Efficiency (NSE)

We selected the Nash-Sutcliffe Efficiency (NSE) as the major objective functions for the model optimisation. NSE is a normalised statistic that compares the magnitude of the residual variance with the measured data variance (Moriasi et al., 2007; Nash & Sutcliffe, 1970). NSE is widely used and indicates how well the plot of observed versus simulated data fits the 1:1 line. It is reportedly the best objective function for reflecting the overall fit of a hydrograph (Servat & Dezetter, 1991). It is calculated as follows:

$$NSE = 1 - \frac{\sum_{i=1}^{n}(S_i - O_i)^2}{\sum_{i=1}^{n}(O_i - O_{mean})^2} \quad \text{Equation 3}$$

where S_i = model simulated output; O_i = observed hydrologic variable; O_{mean} = mean of the observations that the NSE uses as a benchmark against which performance of the hydrologic model is compared; and N = total number of observations (Golmohammadi et al., 2014).

The value of NSE ranges from negative infinity to 1. If the NSE value < 0, it indicates that the mean observed value is a better predictor than the simulated value (i.e., unacceptable performance). In contrast, if the NSE value is > 0.5, the simulated value is a better predictor than the mean measured value (i.e., acceptable performance)(Santhi et al., 2001) (Table 3.9).

Two other performance indices were also calculated, namely the percentage bias (PBIAS) and the coefficient of determination (R^2).

3.3.2.3.2 Percentage Bias (PBIAS)

PBIAS measures the deviation between variables by comparing the average tendency of the simulated data to the corresponding observed data (Gupta et al., 1999; Moriasi et al., 2007). It is an easy method to quantify water balance errors and indicate model performance.

$$PBIAS = 100 * \frac{\sum_{i=1}^{n} (O_i - S_i)}{\sum_{i=1}^{n} O_i} \quad \text{Equation 4}$$

The optimal value of PBIAS is 0.0, with low-magnitude values showing a correct model simulation. A positive value indicates a model underestimation bias, while a negative value indicates a model overestimation bias (Gupta et al., 1999). PBIAS should range between ± 25% for the model simulation to be considered good (Moriasi et al., 2007; Table 3.9).

3.3.2.3.3 Root mean square error (RMSE)

Root Mean Square Error measures how much error there is between two data sets, i.e., between the simulated and observed values. RMSE is a measure of spread of residuals (i.e., a measure of how far from the regression line data points are). Hence, it indicates how concentrated the data is around the line of best fit.

$$RMSE = \sqrt{\frac{\sum_{i=1}^{n}(O_i - S_i)}{n}} \quad \text{Equation 5}$$

RMSE ranges from zero (ideal model) to positive infinity (worst model). RMSE is biased toward peak flows.

3.3.2.3.4 Coefficient of determination (R^2)

R^2 is used to measure the correlation between variables. The range of R^2 is 0-1 and describes the degree to which the model describes the total variance in the observed data.

$$R^2 = \frac{\sum_{i=1}^{n}(O_i - O)(S_i - O)}{\sqrt{\sum_{i=1}^{n}(O_i - O_{mean})^2 \sum_{i=1}^{n}(S_i - S_{mean})^2}} \quad \text{Equation 6}$$

If $R^2 = 0$, there is no correlation between two variables. If $R^2 = 1$, the two variables are linearly related. R^2 should be greater than 0.60 for the model simulation to be considered good (Santhi et al., 2001; Table 3.9).

3.3.2.3.5 Mean Square Error (MSE)

MSE indicates how close a regression line is to a set of points. Distances from the points to the regression line (i.e., the "errors") are squared to remove any negative signs and finds the average thereof. MSE values of 0 indicate a perfect fit.

$$MSE = \frac{1}{n}\sum_{i=1}^{n}(O_i - S_i)^2 \quad \text{Equation 7}$$

The statistical indicators and visual comparison of the time series plots between observed streamflow and simulated streamflow for calibration and validation are presented in the Chapter 5.

Table 3.9: Values to evaluate model performance for NSE, PBIAS and R^2 (after Moriasi, et al., 2007).

Performance Rating	**NSE**	**PBIAS**	**R^2**
Very good	$0.75 < NSE \leq 1$	$PBIAS \leq \pm 10$	$0.75 < R^2 \leq 1$
Good	$0.6 < NSE \leq 0.75$	$\pm 10 < PBIAS \leq \pm 15$	$0.6 < R^2 \leq 0.75$
Satisfactory	$0.36 < NSE \leq 0.6$	$\pm 15 < PBIAS \leq \pm 25$	$0.36 < R^2 \leq 0.6$
Bad	$0 < NSE \leq 0.36$	$\pm 25 < PBIAS \leq \pm 50$	$0.25 < R^2 \leq 0.5$
Not acceptable	$NSE < 0$	$50 \leq \pm PBIAS$	$R^2 \leq 0$

The results of the sensitivity, calibration and validation experiments are presented and discussed for each basin in Chapter 5.

3.3.3 Assessing influence of bias correction on hydrological simulations

As discussed in Section 2.2.3, RCM simulation datasets like CORDEX do have systematic biases. To minimise the systematic errors in the CORDEX datasets, this study applied three bias-correction methods to the CORDEX datasets. The first method is the Quantile Delta Mapping method (hereafter, QDM; Cannon et al., 2015). QDM, one of the most common bias-correction methods in climate sciences (Cannon, 2018), is a univariate technique that transfers quantiles of a source distribution to quantiles of a target distribution. The main concern with QDM is that, as a univariate technique, it is usually applied to single variables without including the dependence that exists between variables. That is, biases in inter-variable relationships may be disregarded by this univariate technique, and this may affect further analyses that incorporates multiple variables (Wilcke et al., 2013). As an alternate to univariate methods, multivariate bias-correction methods have been suggested for input into hydrological model simulations and calculations of drought indices (Cannon, 2018; Rocheta et al., 2014). Hence, for comparison, the second and third methods used in the present study are multivariate bias-correction methods: a multivariate bias correction that matches marginal distributions using QDM and the Spearman rank correlation dependence structure (hereafter MBCr), and a multivariate bias correction that matches the multivariate distribution using QDM and the N-dimensional probability density function transform (hereafter, MBCn; see Cannon, 2018). While MBCr permits the inter-variable dependence structure of marginal distributions to be measured, MBCn, which operates on the full multivariate distribution, is more flexible and can be considered to be the multivariate analogue of univariate quantile mapping (Cannon, 2018). In either method (MBCr or MBCn), marginal distributions are corrected by the change-preserving QDM algorithm

(Cannon et al., 2015). Bias correction for all three methods was implemented in the QDM R-package (https://rdrr.io/cran/MBC/man/QDM.html; Cannon et al., 2015).

Five experiments were performed with the calibrated SWAT+ model to assess the influence of bias correction on hydrological simulations over the WRB (Table 3.10). The model-set for all the simulations are the same except that they were forced with the different climate datasets. Each experiments carries the name of the climate dataset that forces it. For instance, while the first experiment (GMFD) was forced with the GMFD dataset, the second experiment (CORDEX_ORG) was forced with original CORDEX datasets (CORDEX_ORG), and other experiments were forced with various versions of bias-corrected CORDEX datasets (i.e., CORDEX_QDM, CORDEX_MBCr, and CORDEX_MBCn). In all the experiments, the simulation extends from 1971 – 2000, and the results of the GMFD experiment was used as the reference for validating all the CORDEX forced simulations. These results are reported in Chapter 6.

Table 3.10: Summary of hydrological experiments in the Western Cape River Basins (1970—2000).

Experiments	Description
GMFD	▪ Control ▪ GMFD dataset is coupled to SWAT+
CORDEX_ORG	▪ CORDEX Original dataset is coupled to SWAT+
CORDEX_QDM	▪ CORDEX datasets are corrected using QDM bias correction, then coupled to SWAT+
CORDEX_MBCn	▪ CORDEX datasets are corrected using MBC (N-dimensional probability density function) bias correction, then coupled to SWAT+
CORDEX_MBCr	▪ CORDEX datasets are corrected using MBC (Spearman rank correlation) bias correction, then coupled to SWAT+

3.3.4 Assessing future impacts of climate change on hydrological drought

To assess the future impacts of climate change on hydrological drought, the calibrated SWAT+ was forced with the CORDEX_QDM dataset to simulate the hydrology in the WRB for a period 1971 – 2099 under the RCP8.5 future scenario. The simulation used the default model set-up shown in Figure 3.3. The impacts were considered at 1.5, 2.0, 2.5, and 3.0 °C GWLs. To obtain the impacts of climate change at a given GWL, the simulations of the present-day climate period (1971 – 2000) are subtracted from those of the GWL climate period (also see Appendix, Figure A1). The GWL periods of the simulations are the same as the GWL periods of the CORDEX datasets (described in Table 3.1). The future impacts of climate change on hydrological drought were quantified using four types of hydrological drought indices (SWI, PERCI, RFI, SFI and WYLD). The results of this analysis are reported in Chapter 7.

3.3.5 Assessing future impacts of LULC on hydrological drought

The calibrated SWAT+ was forced with CORDEX_MBCn to perform five LULC change experiments (CtrLand, FrLand, SrLand, CrLand, and GrLand) in studying how various idealized LULC changes can influence the drought projection over the WRB (Table 3.10). The first experiment (CtrLand), which represents the present-day land-use pattern, used SWAT+ default LULC (Figure 3.4a). The second experiment (FrLand), which represents a future land-use scenario with an increase in invasive alien vegetation scenario, used LULC pattern with mixed forest "invades" river basin areas outside their current distributional range (Figure 3.4b). The area of land-use change for this scenario was delineated after consideration of the Working for Water programme that mapped the distribution of alien invasive tree species and identified invaded areas across (riparian and non-riparian) quaternary basins in South Africa (Kotzé et al., 2010; see Appendix, Figure A1). The third experiment (SrLand), which represents shrubland restoration scenario, used the LCLC in which shrubland is introduced to areas currently covered by bare ground/sparse vegetation (i.e., BSVG). The fourth experiment (CrLand), which describes an extensive cropping scenario, used the LULC pattern (Figure 3.4d) in which CRDY replaced CRWO, GRAS, and CRGR. The fifth (GrLand), which describes an expansion of grassland scenario, used the LULC pattern (Figure 3.4e) in which GRAS invasion replaced CRDY, CRGR and CRWO. The LULC changes for the third, fourth, and fifth experiments were chosen after consideration of previous assessment on LULC over Western Cape (see Tizora et al., 2016; see Appendix, Figure A1). Nonetheless, none of these LULC change experiments were designed to simulate specific scenarios of vegetation change, but rather to assess the magnitude and type of regional hydrological impact that could result from a hypothetical, albeit potential, change in future vegetation. While each scenario is based on the scientific literature discussed in previous chapters, all of the experiments represent relatively extreme future changes in comparison to the current LULC change distribution. That is, the LULC experiments were designed to better understand the potential hydroclimatic drought impacts that may occur in the future. The future projection simulations from all the LULC changes experiments (i.e., FrLand, SrLand, CrLand, and GrLand) were compared to those CtrLand experiment. To obtain the impacts of LULC change in an experiment, the simulations of the experiment are subtracted from the corresponding simulations in the CtrLand experiment at the same GWL. The results of this analysis are reported in Chapter 8.

Table 3.11: Summary of LULC change experiments in the Western Cape River Basins.

Experiments	**Description**	**LULC pattern**
CtrLand	▪ Control LULC, which is SWAT+ default land use	Figure 3.4a
FrLand	▪ Increase in mixed forest (e.g., eucalyptus, pine, and black wattle trees in river basin areas) ▪ FOMI occupies 14.45% of the basin	Figure 3.4b
SrLand	▪ Shrubland restoration ▪ SHRB replaces BSVG ▪ SHRB covers 32.74% of the basin	Figure 3.4c
CrLand	▪ Extensive cropping ▪ CRDY replaces GRAS, CRGR and CRWO ▪ CRDY covers 63.98% of the basin	Figure 3.4d
GrLand	▪ Expansion of grassland expansion ▪ GRAS replaces CRDY, CRGR and CRWO ▪ GRAS occupies 63.98% of the basin	Figure 3.4e

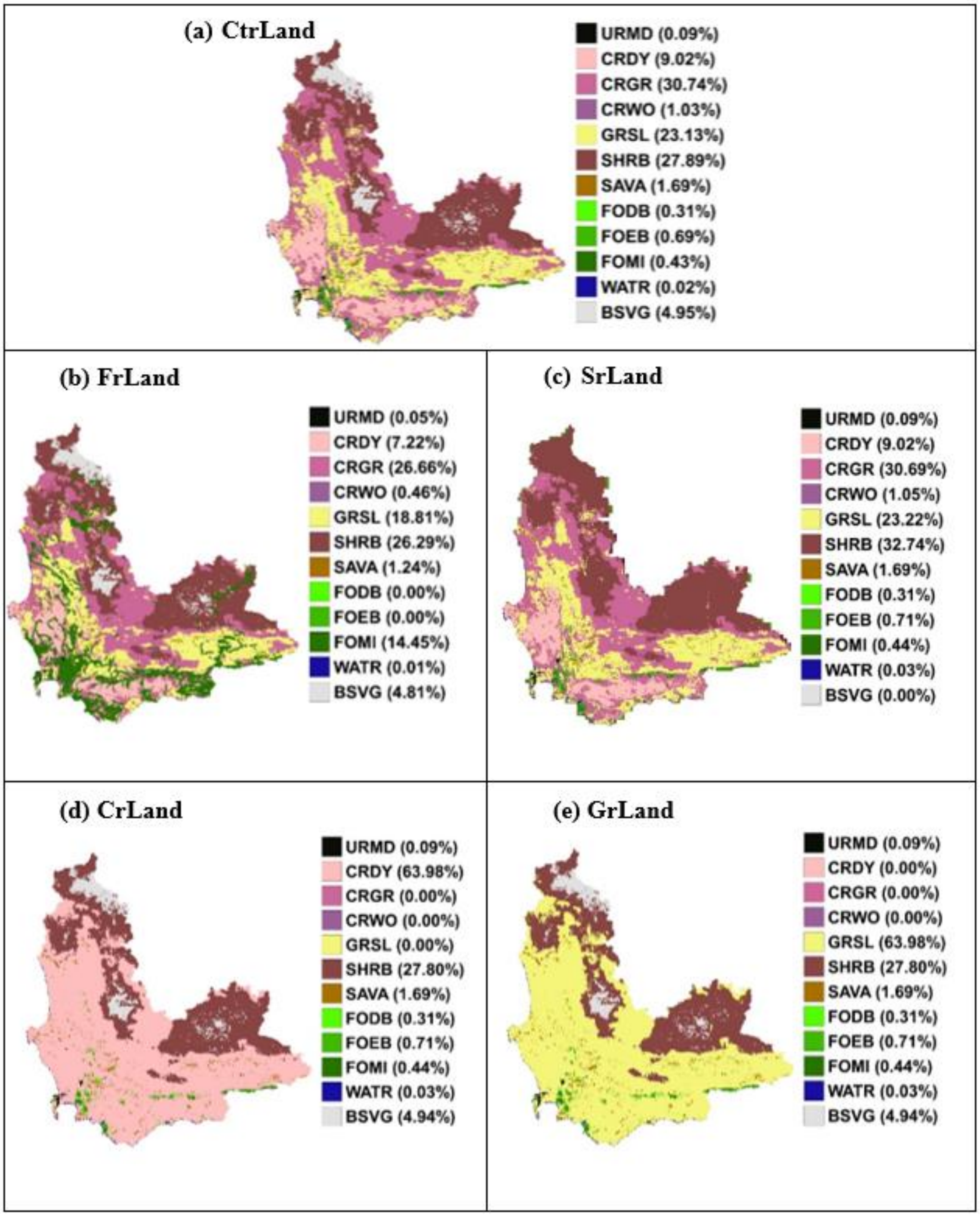

Figure 3.4: The LULC patterns used in the LULC change experiments for Western Cape River Basins: (a) CtrLand, (b) FrLand, (c) SrLand, (d) CrLand, (e) GrLand. The land-use types are urban residential medium density (URMD), cropland/dryland and pasture (CRDY), cropland/grassland mosaic (CRGR), cropland/woodland mosaic (CRWO), grassland (GRAS), shrubland (SHRB), savanna (SAVA), forest - deciduous broadleaf (FODB), forest - evergreen broadleaf (FOEB), forest - mixed (FOMI), water (WATR), and bare ground, sparsely vegetated (BSVG). The percentage of each LULC type is indicated in brackets.

Chapter 4:
Projected future changes in the characteristics of meteorological drought

In this chapter, meteorological drought both for the present-day and projected future climate are evaluated over the Western Cape River Basins (WRB). The present-day climate simulation data are first compared to observation data to determine how well the models can reproduce the temperature and moisture fields and drought. Thereafter, the future drought is projected, both for SPI and SPEI drought indices at various GWLs (1.5 °C, 2.0 °C, 2.5 °C, 3.0 °C), and a SOM was also used to classify the different drought patterns.

4.1 Climate model evaluation

The models capture the spatial distribution of major climate variables across the Western Cape region. The model ensemble (hereafter, RMEAN) reproduces all the essential climatic features in the observed temperature and moisture fields. For example, it captures the location of the temperature maxima over the West Coast (about 24 ^{o}C) and of the temperature minima along the central interior (about 6 ^{o}C over the Cape Winelands), showing good agreement with the CRU observation data (r = 0.85, 0.85 and 0.89 for maximum, minimum and mean temperatures, respectively; Figure 4.1). The models also reproduce the spatial gradient in the precipitation field and show high correlation with observations (r = 0.86) (Figure 4.2). In agreement with CRU data, the models simulate drier conditions (about 15 mm month^{-1}) over the West Coast (around 32 ° S, 18 ° E) with increasingly wet conditions (about 50 mm month^{-1}) towards the southern Cape Peninsula (between 34 ° S, 18 ° E; Figure 4.2). Nevertheless, the simulations do feature some biases. For instance, the models underestimate the magnitude of the temperature maxima, producing a cold bias (of about 4 ^{o}C) over the most parts of the Western Cape. A dry bias (about 15 mm month^{-1}) also occurs over parts of the Overberg, while a wet bias (about 5 mm month^{-1}) occurs further inland over parts of the Cape Winelands and the Central Karoo. It may be that the biases in the simulated rainfall and temperature also produce inherited biases in derived variables, such as PET (of about −20 mm month^{-1}; Figure 4.2) over the Kalahari Basin.

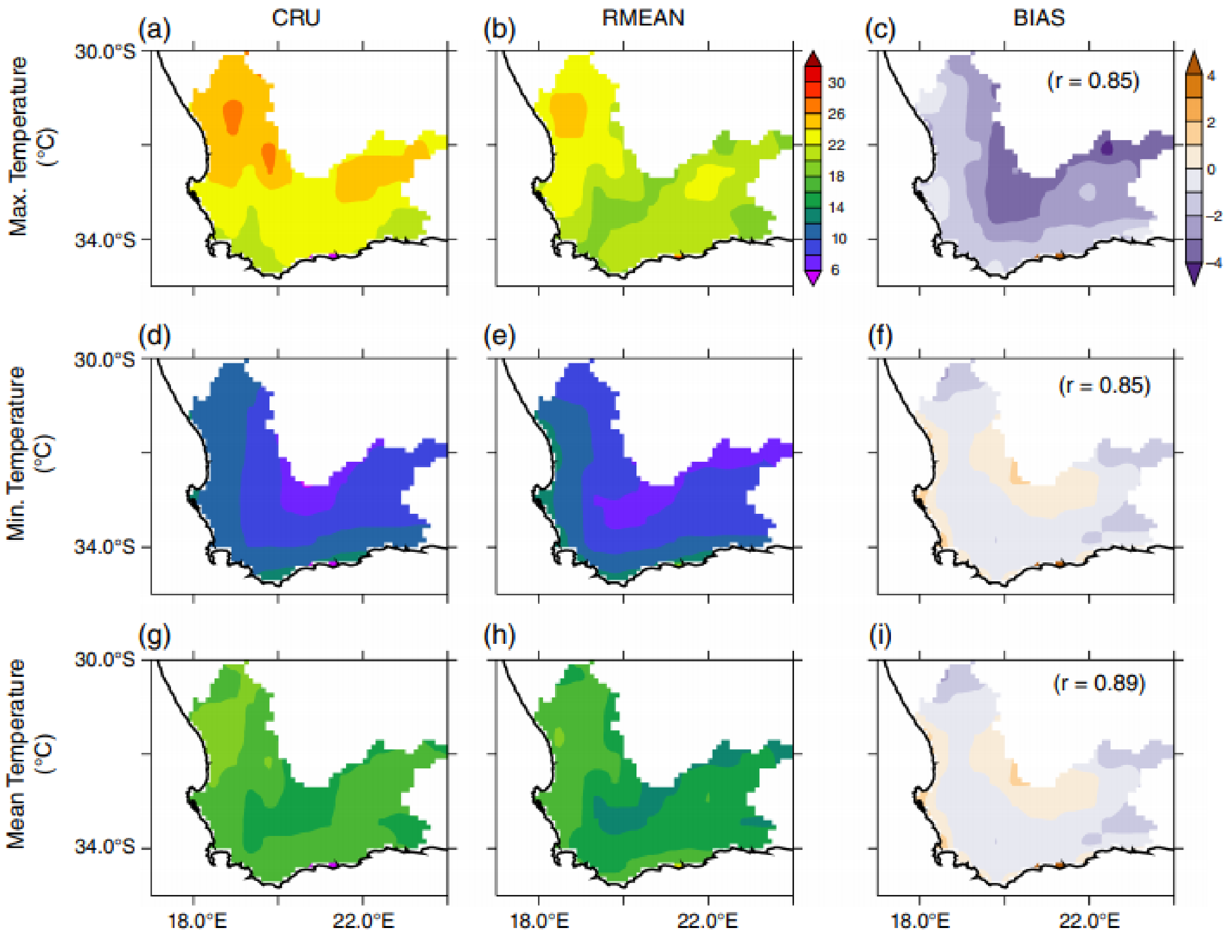

Figure 4.1: The climatology for near surface maximum, minimum and mean temperatures (°C) over Western Cape, South Africa (for 1970—2000), as observed by CRU and simulated by CORDEX models (RMEAN). The correlation (r) and difference (bias; RCM – CRU) between the observed and simulated variables are indicated.

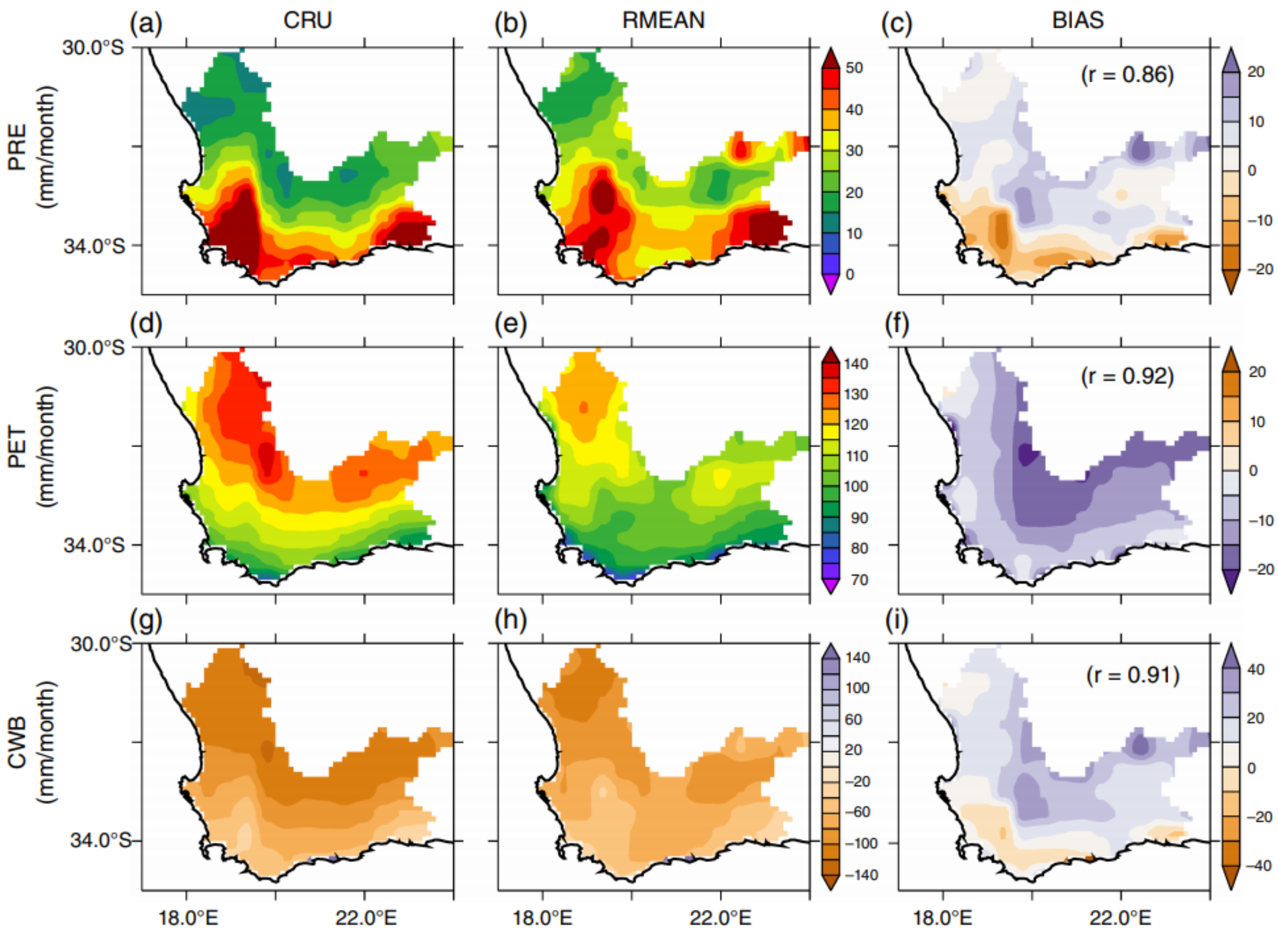

Figure 4.2: Same as Figure 4.1, but for moisture variables: precipitation (PRE), potential evapotranspiration (PET) and changes of the climatic water balance (CWB = PRE – PET).

The models also give a credible simulation of the annual cycles of the climate variables over each of the four basins (Figure 4.3). Over each basin, the simulation spread encloses the observation value, and for all the variables, RMEAN closely follows the observed annual cycle. The models also capture differences in the annual cycles over the basins. For instance, in agreement with the observation data, RMEAN shows that, while the Breede, Berg and Olifants Rivers receive their maximum precipitation (about 50, 75, 45 mm month^{-1}, respectively) during the winter months (June to August) and experience dry conditions in the summer, the Gouritz River receives rainfall throughout the year but with a peak (50 mm month^{-1}) during the summer months (January to February). This is because the Gouritz River straddles the winter-rainfall and summer-rainfall regions of the Western Cape region. However, both the models and the simulations agree that, despite differences in the annual precipitation cycle, the climate water balance (CWB) over all the basins reaches its maximum values

(–5 to +50 mm month⁻¹) during the winter months and its minimum values during the summer months, thus mirroring the PET cycles.

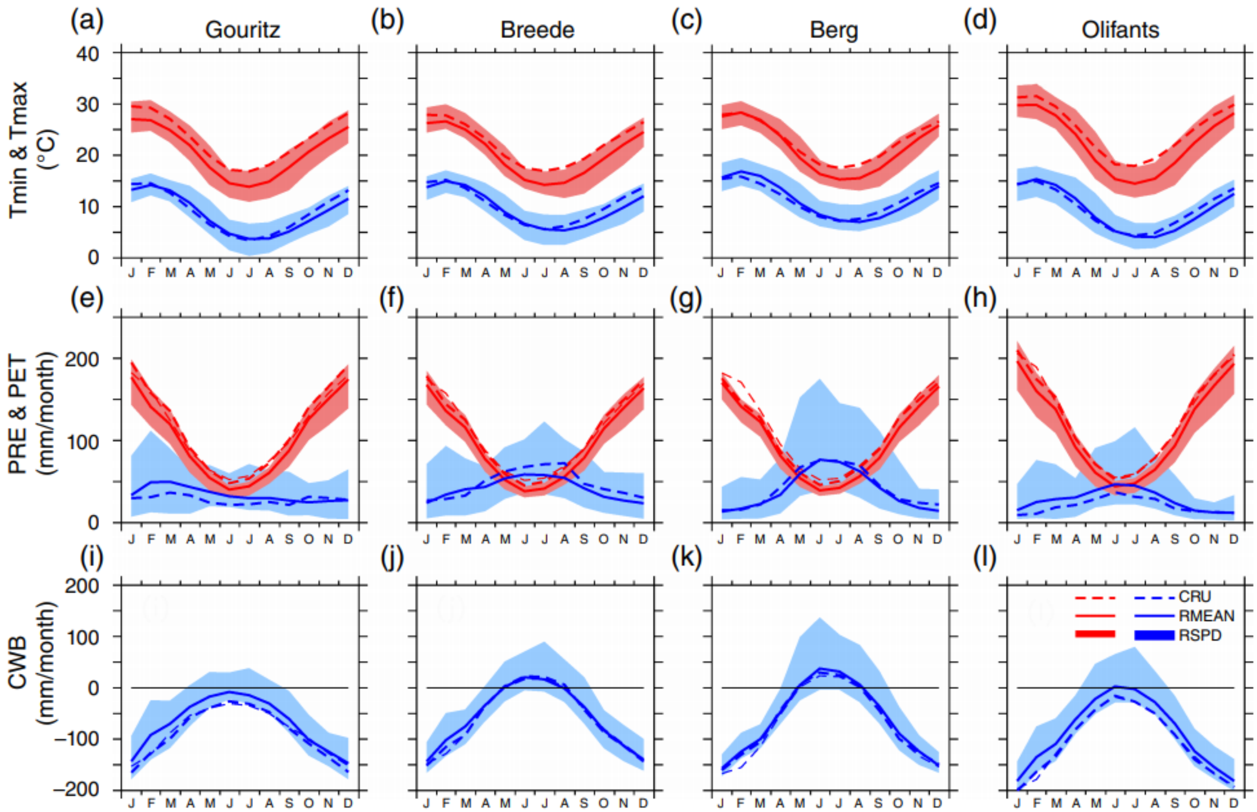

Figure 4.3: The annual cycle of climates variables over the major river basins in the Western Cape (1970—2000) as observed by CRU and simulated by CORDEX model ensemble (ENS).

The performance of the model in simulating drought intensity and frequency over the river basins depends on the index used to characterise the drought (Figure 4.4). Although the simulated spread in drought frequency resembles the observed spread (Figure 4g), there is better agreement between the observed and simulated drought patterns for SPEI (r=0.38) than for SPI (r=0.24). The SPEI also provides a better representation of drought frequency across all four basins. For instance, over the Breede River basin, the interquartile range of the drought frequency in the simulated SPI (but not the SPEI) overestimates the observed frequency.

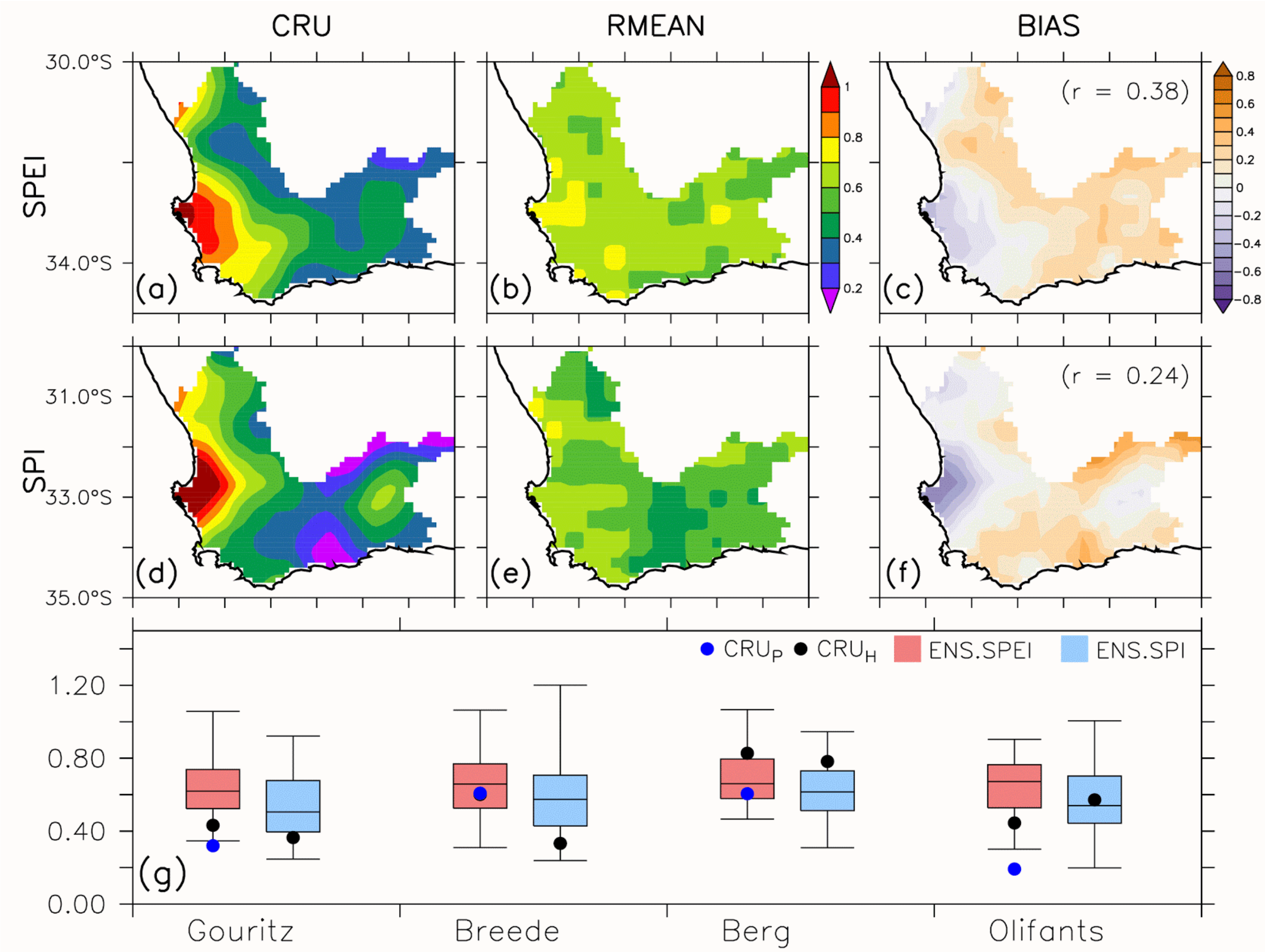

Figure 4.4: The frequency of severe drought (SPEI ≤ –1.5; SPI ≤ –1.5) over Western Cape, South Africa (panel a—f) and over each river basin (panel g), for the period 1970—2000, based on CRU and CORDEX model ensemble simulations.

4.2 Projected changes in drought characteristics over the river basins

The model projections show that the SPEI drought increases across the Western Cape for all GWLs, but the drying patterns are not homogenous across the region (Figures 4.5a–d). Projections of the SPEI drought intensity under GWL 1.5 suggest that more intense drying may occur towards the northwestern parts, particularly over the interior of the Olifants River basin (–1.0). This pattern is similar for higher GWLs (i.e., 2.0, 2.5 and 3.0), except that the intensity of the droughts increases with the GWLs (Figure 4.5b, c, and d). Projections of severe drought frequency in terms of the SPEI reflect a similar pattern, showing an enhanced occurrence over the northwestern catchments compared to the southeastern catchments for successive GWLs (Figures 4.5i–l). The peak in SPEI drought frequency across the Olifants River system increases progressively from 2 and 4 events decade^{-1} for GWL 1.5 and GWL 2.0 (respectively) to 3 and 5 events decade^{-1} for GWL 2.5 and GWL

3.0 (respectively). These results are in line with previous studies on projected circulation changes over the region. For instance, simulations by Engelbrecht et al. (2009) also suggest a displacement of frontal rain-bands south of the Southern African subcontinent due to an increase in the intensity and frequency of upper-level high pressure systems. Such changes would decrease projected rainfall over the region, which may contribute to drier conditions over the Western Cape catchments in the future, as found in the present study.

The model projections using the SPI (Figures 4.5e–h) also show that drought may increase across the region, although the intensity and the spatial distribution differ from that of SPEI. Projections of SPI drought intensity shows homogeneous drying (−0.4) for GWL 1.5 (Figures 4.5e) and a pattern of increased drying over the northwestern areas (about −1.0) compared to parts of the southeastern basins (−0.4) for the remaining GWLs. Yet the maximum drying for the SPI under GWL 3.0 does not exceed that of the SPEI under GWL 1.5 (Figures 4.5h and a, respectively). Similarly, projections of severe drought frequency using the SPI are lower than those obtained using the SPEI, and they extend across a smaller spatial area. For instance, under GWL 3.0, the severe drought frequency maxima in terms of the SPI are limited to the Berg River catchment (2 droughts decade^{-1}; Figures 4.5h). In contrast, when using the SPEI, these maxima extend across the Olifants River and are greatly enhanced (>5 droughts decade^{-1}; Figures 4.5d). These findings compare well to those of a previous study by Botai et al. (2017), which found a similar spatial contrast between parts of the Western Cape, where the southern and western parts experienced more frequent, more intense and more severe droughts than the eastern parts of the province. Similarly, Oguntunde et al. (2006) found an increase in drought intensity and spatial extent for the SPEI and SPI over the Volta River Basin (West Africa), where the magnitude of the increase was higher with the SPEI than with the SPI.

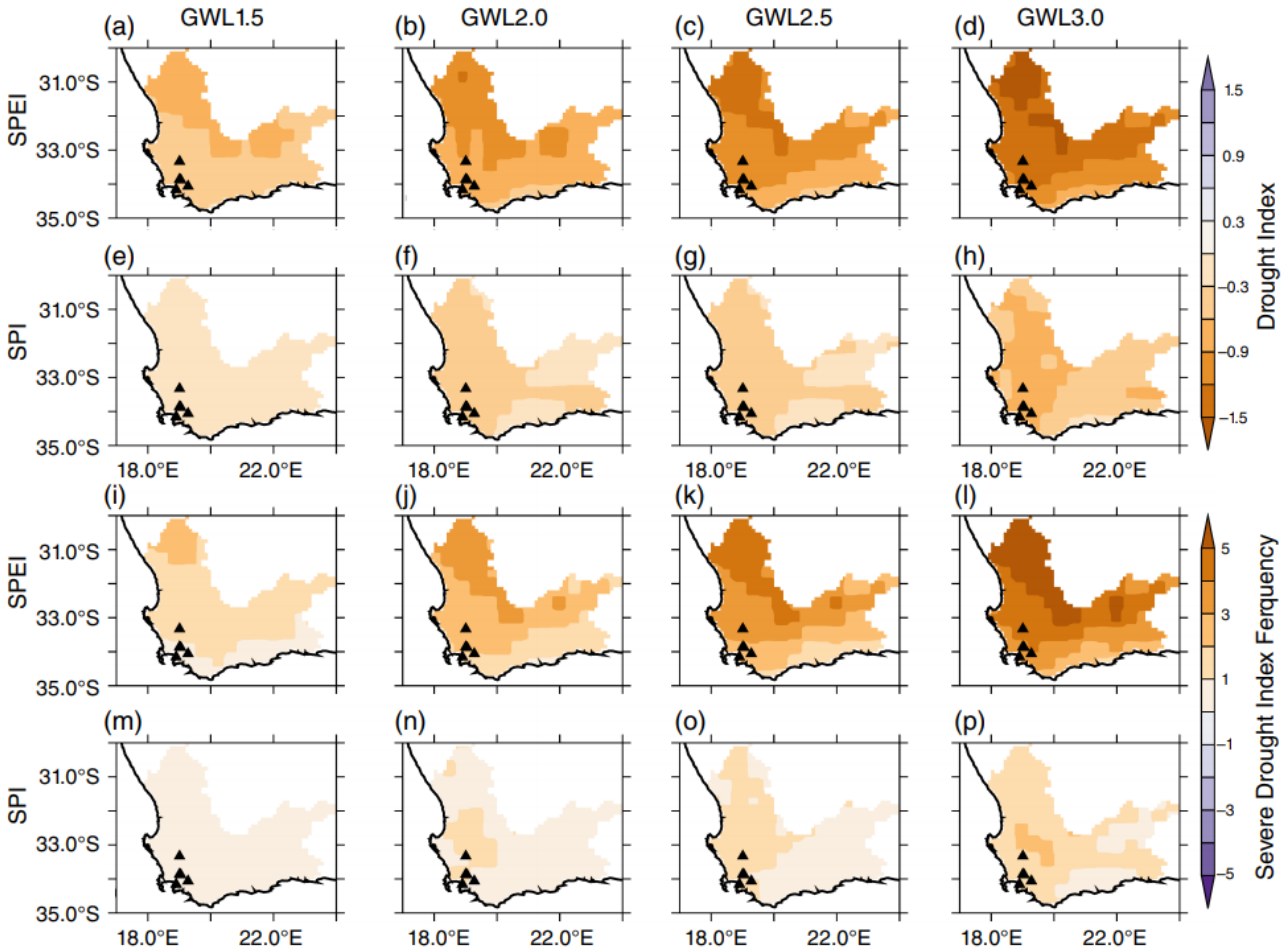

Figure 4.5: Projected changes in drought index (for SPEI and SPI; panel a – h) and severe drought frequency (for SPEI and SPI; i – p) for different global warming levels (GWL1.5, GWL2.0, GWL2.5, and GWL3.0) over Western Cape (South Africa).

The SOM classification of simulated severe drought intensity over the Western Cape region shows four extreme patterns. Each pattern is located near the edges of the SOM (Figure 4.6a) and is linked to differences between the drought indices (Figure 4.6b). In the first pattern (*i.e.*, Nodes 1, 2, 5 and 6), drying peaks over the northern parts of the Olifants and the central Gouritz River basins. The four nodes associated with the first pattern contribute a high percentage of the variability in drought intensity (25%). Model simulations contributing to this node are better explained by drought intensity using the SPEI (rather than the SPI). These drought patterns (especially nodes 1 and 5) are dominated by SPEI projections (Figure 4.6).

The second pattern (i.e. nodes 9 and 10) is characterized by severe drought (about −1.5 ^{o}C) especially over the northern parts of the Olifants River basin (Figure 4.6). The two nodes associated with this pattern also contribute to variability in drought intensity (about 22%). The second pattern, best represented by node 9, is comparable spatially to the SPEI model ensemble mean (Figure 4.5d). Model simulations contributing to this node are also better explained by drought intensity in terms of the SPEI (rather than the SPI). There is a distinct increase in the SPEI drought pattern of Node 9 in the different models at higher GWLs; in other words, one, three and 11 models feature at GWLs 2.0, 2.5 and 3.0, respectively.

In the third pattern (i.e. nodes 3, 4, 7 and 8), drought is not severe over much of the region. Nodes associated with the third pattern account for the largest percentage of the SOM variability in drought intensity (about 40%). The third pattern is well represented by node 4, which shows a weak drying signal across all four basins. Model simulations for this node are better represented by SPI drought (Figure 4.5e-h). Note that the number of simulations showing this pattern for drought severity decreases for higher GWLs (Figure 4.6b). For instance, with SPI, while ten simulations feature it at GWL1.5, only one simulation suggest it at GWL3.0.

The fourth pattern (i.e. nodes 7, 8, 11 and 12) shows a west–east spatial gradient in drought intensity. The pattern, which accounts for 30% of the projected drought, compares more to the SPI ensemble mean than the SPEI (compare Figures 4.5 and 4.6). It is well represented by node 12, which shows a peak drought intensity over the central Berg River catchment about −1) and a relative decrease towards the Breede River (about −0.5). The results of the SOM classification for simulated drought frequency are similar to that of drought intensity, although there are some differences in the number of simulations showing the respective pattern for drought frequency at higher GWLs (Figures 4.7a,b).

There is a robust drying signal across the Western Cape because the models show good agreement regarding the various river basins; this agreement varies, depending on the GWL and the drought index used (Figure 4.8). In most cases, at least 75% of the models agree on the drying signal. For example, across successive GWLs, the models show an increase in drought intensity and frequency over all the basins. Over the Olifants River, for example, the model ensemble shows that drought intensity increases across successive GWLs, both for SPI (from –0.1 to –1.0) and for SPEI (about –0.5 to –2.0) (Figure 4.8d). The model ensemble further shows that drought frequency increases across successive GWLs, both for SPI (from 0.1 to 4 events decade ^{1}) and for SPEI (from 0.1 to 4 events decade^{-1}; Figure 4.8h). This pattern in the drying signal varies over the other three basins, with some differences in the model spread. The model ensemble for drought in the Breede River basin using the SPEI is less severe than in the Olifants River, for both drought intensity (–0.1 to –1.1; Figure 4.8b) and frequency (from 0.1 to 3.5 events decade^{-1}; Figure 4.8f). Additionally, the degree of drying also varies depending on the drought index used. The SPI projects a lower value than the SPEI for drought. For instance, over the Olifants River, for GWL 3.0 (RCP8.5), the ensemble mean for SPI drought intensity (–0.5) is less than that of SPEI (–2.0), and the SPI drought frequency (0.5) is also less than that of the SPEI (7.0). The reason for this may be that, since the SPI does not incorporate PET, it may underestimate the drought.

(a)

(b)

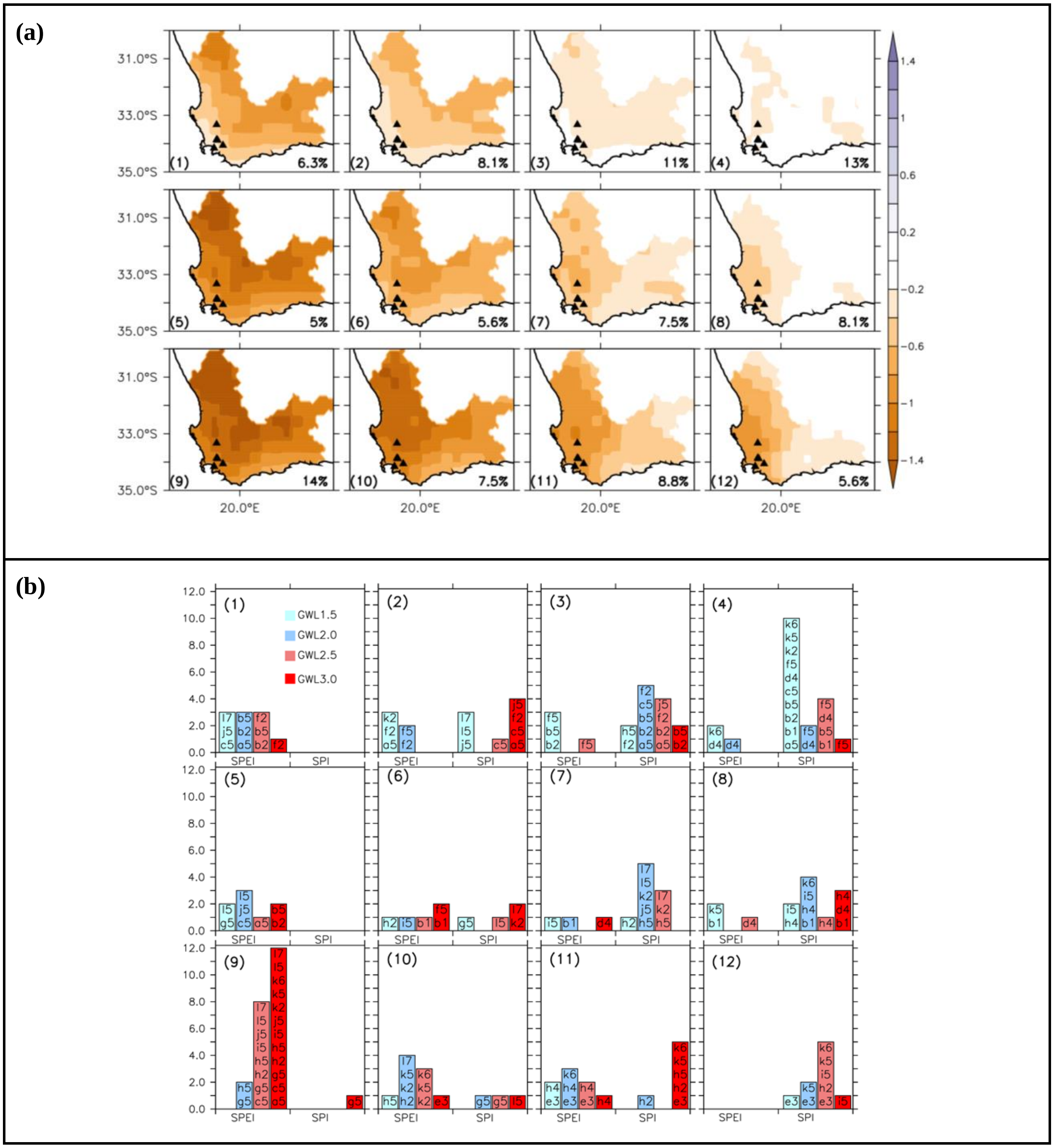

Figure 4.6: (a) Self-organizing map distribution (3 × 4 nodes) of projections for drought (Standardized Precipitation Index and Standardized Precipitation Evapotranspiration Index) patterns over the Western Cape (South Africa) for different global warming levels (GWLs) (GWL 1.5, GWL 2.0, GWL 2.5 and GWL 3.0). The numbers at the lower-left and lower-right corners of each node represent the tag and percentage contribution of each pattern, respectively; (b) the frequency of the patterns under each GWL, drought index, and simulation. The codes in each bar are the tags of the simulations make up the bar. In a simulation tag, alphabet indicates the GCM while the number denotes the RCM (e.g., a5 represents CanESM2_RCA4 simulation), see Table 3.7.

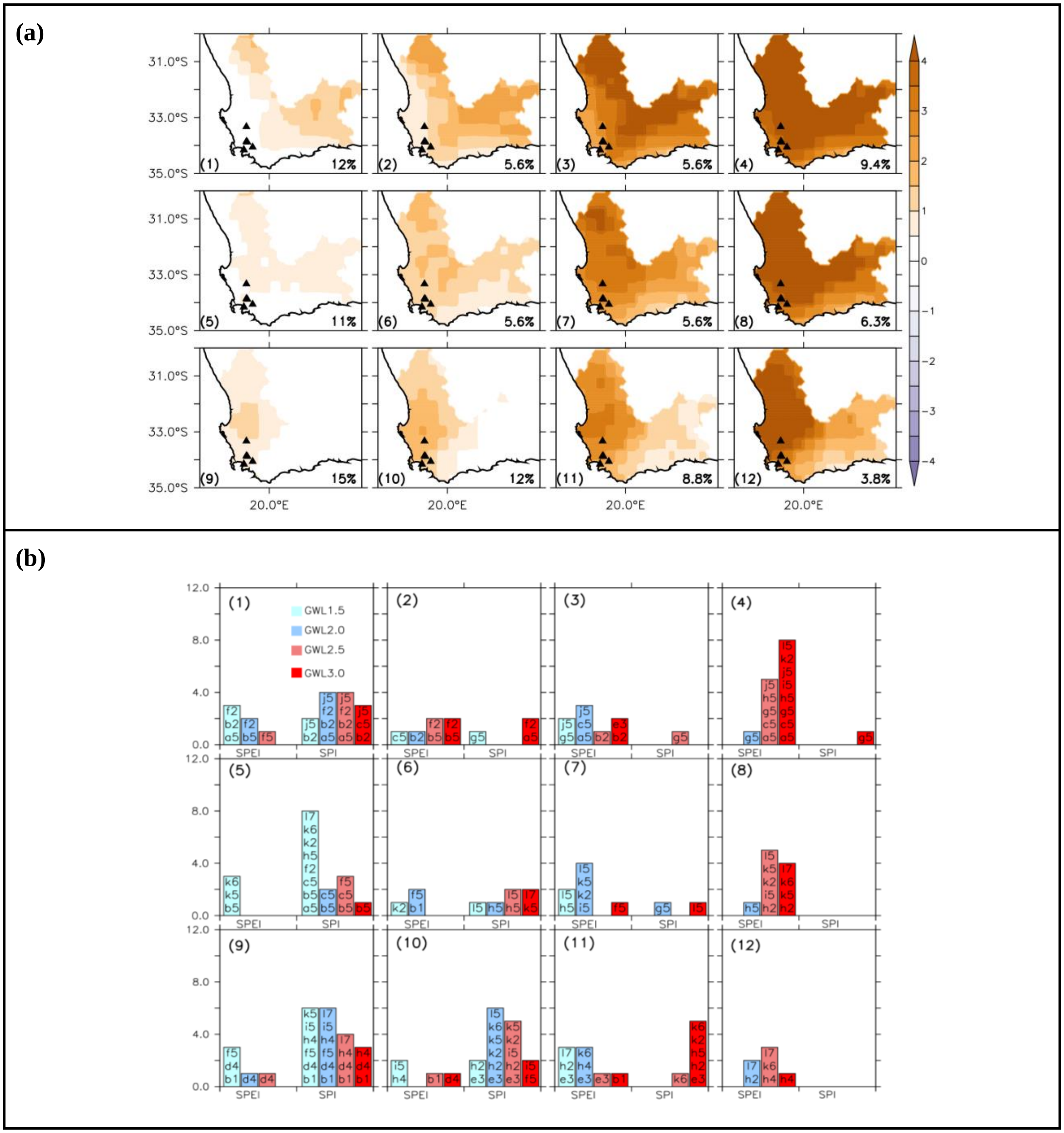

Figure 4.7: Same as Figure 4.6 but for drought frequency

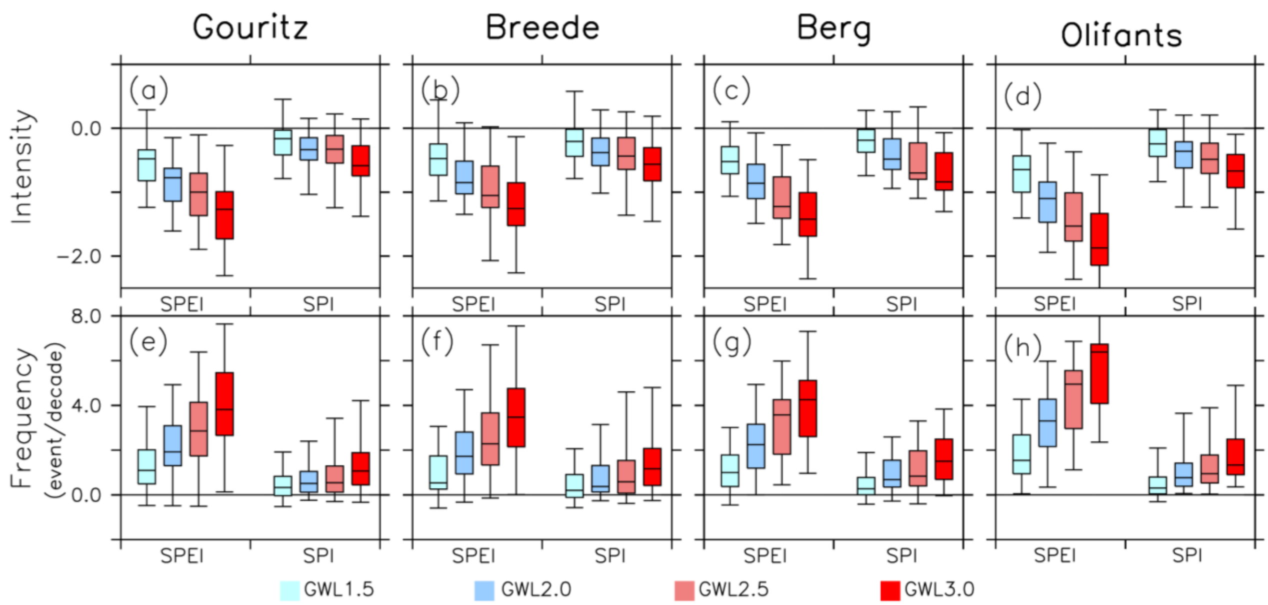

Figure 4.8: Projections of SPEI and SPI severe drought intensity (a—d), and frequency (e—h), over the four river basins in Western Cape (South Africa)

These findings have some implications for water resource managers operating in the WRB. There is good model agreement on the sign of change across the region. The robust drying signal projected for the future across the entire Province underscores the need for developing a mitigation strategy to reduce drought impacts. Additionally, it may also be necessary carefully to consider the drought index used when developing such a strategy. Depending on the drought index used, projections may indicate higher or lower values of drought impacts, thereby either overestimating or underestimating the influence of global warming on drought. As illustrated above, the SPI and SPEI drought indices produce considerable differences in the model ensemble spread. The study furthermore highlights the role of PET as a key variable, both in drought monitoring and prediction over the region, and potentially in mitigating the harmful impacts of droughts and water scarcity across the Western Cape in the future.

4.3. Summary

In this chapter, CORDEX data was used to examine the potential impacts of various GWLs (1.5 °C, 2.0 °C, 2.5 °C, 3.0 °C) on future drought in four river basins across the Western Cape. SPI and SPEI drought indices were used to quantify drought (in terms of frequency and intensity), and a SOM was also used to classify the different drought patterns. The present-day climate (1971–2000) simulations were compared with observations in order to evaluate the capability of the CORDEX simulations to reproduce the characteristics of drought variables over the region accurately; thereafter, the projected changes in future droughts were examined. The results of this chapter suggest the following:

- The CORDEX models correctly capture the spatial distribution of major climate variables over the Western Cape region and reproduce the essential climatic features in the observed temperature and moisture fields.
- The models also give a credible simulation of the annual cycles of the climate variables over each of the four basins. However, the accuracy of the model's performance in simulating the drought intensity and frequency over the river basins depends on the index used in characterising the drought.
- Projected changes in drought characteristics over the river basin show a robust drying signal, but this varies depending on the GWL, the river basin, and the drought index used.
- When using the SPEI, drought increases across the Western Cape for all GWLs, although the drying pattern is not homogenous across the region. When using the SPI, drought may also increase over the region, but the intensity and the spatial distribution is different.

This chapter highlighted the role of PET as a key variable in characterising drought in the Western Cape. It showed that droughts will be more severe and more frequent in the future under different GWLs. The research underscores the need for developing an effective mitigation strategy to reduce drought impacts, with careful consideration of the drought index being used. All these findings have significant implications for water resource managers operating in Western Cape.

Chapter 5:
Sensitivity and Performance of SWAT+ in simulating the hydrology of the Western Cape

This chapter discusses performance and sensitivity of SWAT+ simulation to model parameters in simulation of the hydrology over the Western Cape River Basins. It provides a sensitivity analysis of the SWAT+ simulation to model parameters before concluding with evaluation of model performance across four observation stations.

5.1 Sensitivity of the SWAT+ simulation to model parameters

Figure 5.1 shows the convergence of 300 model iterations during SWAT+ calibration using the NSE objective function. In general, the SWAT model converged quickly, before 125 iterations. After which, there is no further discernible improvement in the 1–NSE objective function value. The convergence progression (total of 300 model iterations) of the SWAT+ model over Western Cape is rapid with the 1–NSE objective function used for the calibration. This convergence found in this study is in line with Yen et al. (2019) that found early convergence behaviour with the IPEAT model, since hydrologic processes are generally well simulated with SWAT. For the sensitivity analysis, the selected parameters were allowed to vary by a +30 to –30 percentage change range while the other parameters remain fixed at the SWAT+ default (initial value). The corresponding parameter values for ten important parameters selected for calibration with 1–NSE are shown in Figure 5.2a—j. In general, some model parameters selected for the calibration are more sensitive than others. For some parameters, there is a limit to which the values of the parameters can be decreased. For these parameters the best value is negative. For example, parameters such as CN2 (about –6.2), EPCO (about –7.4) and FLO_MIN (about –12.9). In contrast, for other parameters, the best value is positive, such as for ESCO (about 1.9), AWC (about 8.2), and SURLAG (about 7.6). Nevertheless, the NSE objective function value appears to be most sensitive to variations in two parameters, which are crucial to calibrating the SWAT+. The curve number (CN2) parameter's variation showed a high sensitivity. Generally, increased values of CN2 imply an increase in the surface runoff (or surface flow response). Also, the soil evaporation compensation factor (ESCO) parameter showed a high sensitivity. This is because changes in the value of the ESCO may affect all major water balance components (Kannan et al., 2007). We found decreasing the percentage change for CN2 and ESCO produced better results, and that comparatively, the remaining parameters (i.e., EPCO, SOL_AWC, SOL_K, GW_DELAY, FLO_MIN, REVAP_CO and REVAP_MIN and SURLAG; see Table 5.2) did not affect the surface, subsurface or basin response as much.

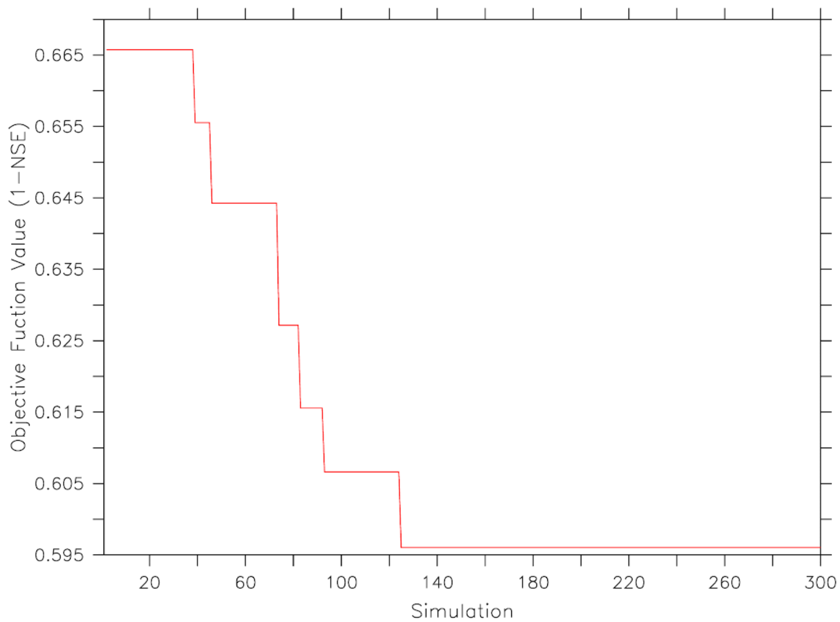

Figure 5.1: The convergence of 300 model iterations during calibration using the NSE objective function over the river basins.

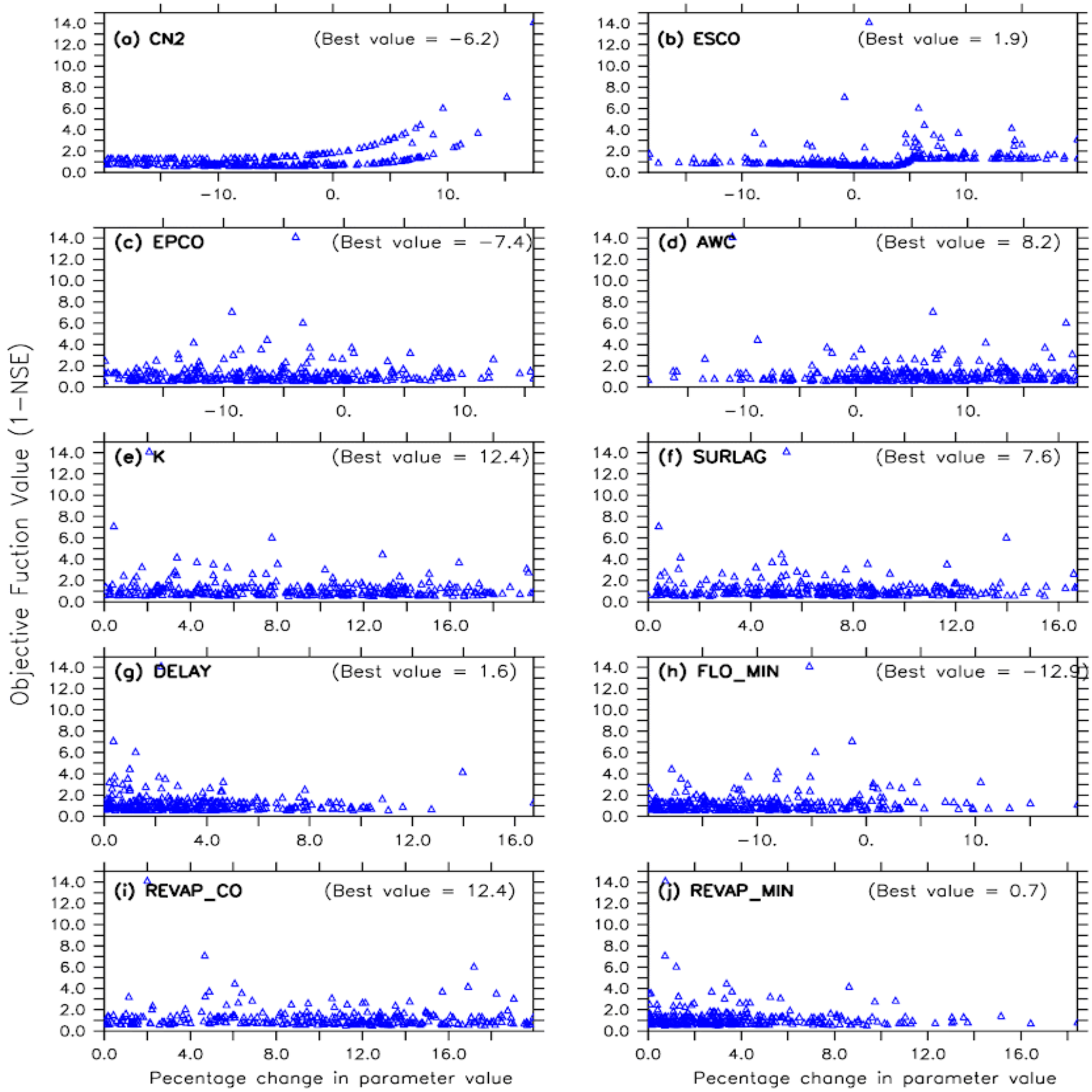

Figure 5.2: Scatter plots of the sensitivity of four objective functions (1–NSE) to different calibration parameters. Parameters were within –30% to +30% change of the default value.

5.2 Evaluation of the SWAT+ hydrological model

Comparison of the observations and the SWAT+ simulated streamflow at four hydrological stations (i.e., J1H019, E2H003, G1H013, and H7H006) in the WRB is shown in Figure 5.3. This shows that the SWAT+ model simulations capture the peaks in the observation streamflow during the calibration period. At stations E2H003 and H7H006, for instance, although the simulations underestimate (e.g., 1983, 1984, for H7H006) or overestimate (e.g., 1995, 2004, for H7H006) the observed peaks, the simulation spread is generally close to the observed value. Similarly, for station G1H013, while there are some years when all the simulations underestimate (e.g., 1992, 1996, 2001) or overestimate (e.g., 1986, 1991) the observed peaks, the simulation spread generally tracks the observed values well. For station J3H004, the paucity of the observation data is evident, and this limits our analysis. Generally, the SWAT+ simulated streamflow values closely track the observed values in reproducing seasonal and annual variations of the streamflow. The model also captures the observed peaks and their inter-annual variability, and this provides a reasonable simulation of hydrological processes over the region.

During the calibration period (1980–1990), the simulation spread often envelops the observation, particularly at stations H7H006 and E2H003. At other stations, like G1H013, the correlation (r) between the simulated and observed flow is more than 0.5 and the Nash-Sutcliffe Efficiency (NSE) value is also more than 0.5. SWAT+ also captures the magnitude of the streamflow at the stations. Streamflow is largest at H7H006 (i.e., Breede river) and G1H013 (i.e., Berg River), and lowest at J1H019 (i.e., Gouritz river). Even so, there are some notable model biases in the simulation. SWAT+ either overestimates or underestimates the magnitude of the peak streamflow in some years. The model overestimates the observed streamflow by more than 40 $m^3 s^{-1}$ at H7H006 in 1986 and underestimates by up to 120 $m^3 s^{-1}$ at H7H006 in 1983. Percentage bias (PBIAS) ranges from –43% (at G1H013) to 73% (at J1H09). The biases here may be the result of uncertainties in the model input and/or set-up, or biases may also exist within the climate and hydrological datasets themselves. For instance, the resolution of the GFMD reanalysis may not sufficiently resolve all the Western Cape climate processes and the complex topography of the region, or the resolution of the soil and land use dataset (input) may also be too coarse in representing all the hydrological processes in these river basins. A previous study by Dabrowski (2014) has also reported this problem when they applied SWAT over South African river basins. Model biases may also occur from using naturalised flow data (as observed streamflow), since this removes the effects of human impacts (e.g., reservoirs, dams). Generally, the model performance improves (or remains the same) in the validation period (1991–2005) than in the calibration period (1980–1990) (Figure 5.3). At station G1H013, for example, the model performance improves for NSE (from 0.4 to 0.5), PBIAS (–43.2% to –40.2%), and root mean square error (RMSE) (from 17.5 $m^3 s^{-1}$ to 17.2 $m^3 s^{-1}$). Similarly, at station E2H006, it improves for PBIAS (from –30.8% to –31.2%), RMSE (14.6 $m^3 s^{-1}$ to 15.4 $m^3 s^{-1}$), and for R^2 (from 0.5 to 0.7). The model improvement depends on the statistical metrics used in the performance evaluation. For example, at station H7H003, while the model performance improves for R^2 (0.5 to 0.6), RMSE (from 34.2 $m^3 s^{-1}$ to 30.7 $m^3 s^{-1}$) and PBIAS (from –25.7% to –14.3%), it remains the same for NSE (from 0.5 to 0.5). Differences in model performance during the calibration and validation periods may be due to the length of the observation data gaps in the periods, as evident in the case of station J1H019. At this station, the paucity of observation data makes the results unreliable. Generally, however, the performance of the SWAT+ model at the stations suggests that the model does indeed provide a reliable representation of hydrological processes in WRB.

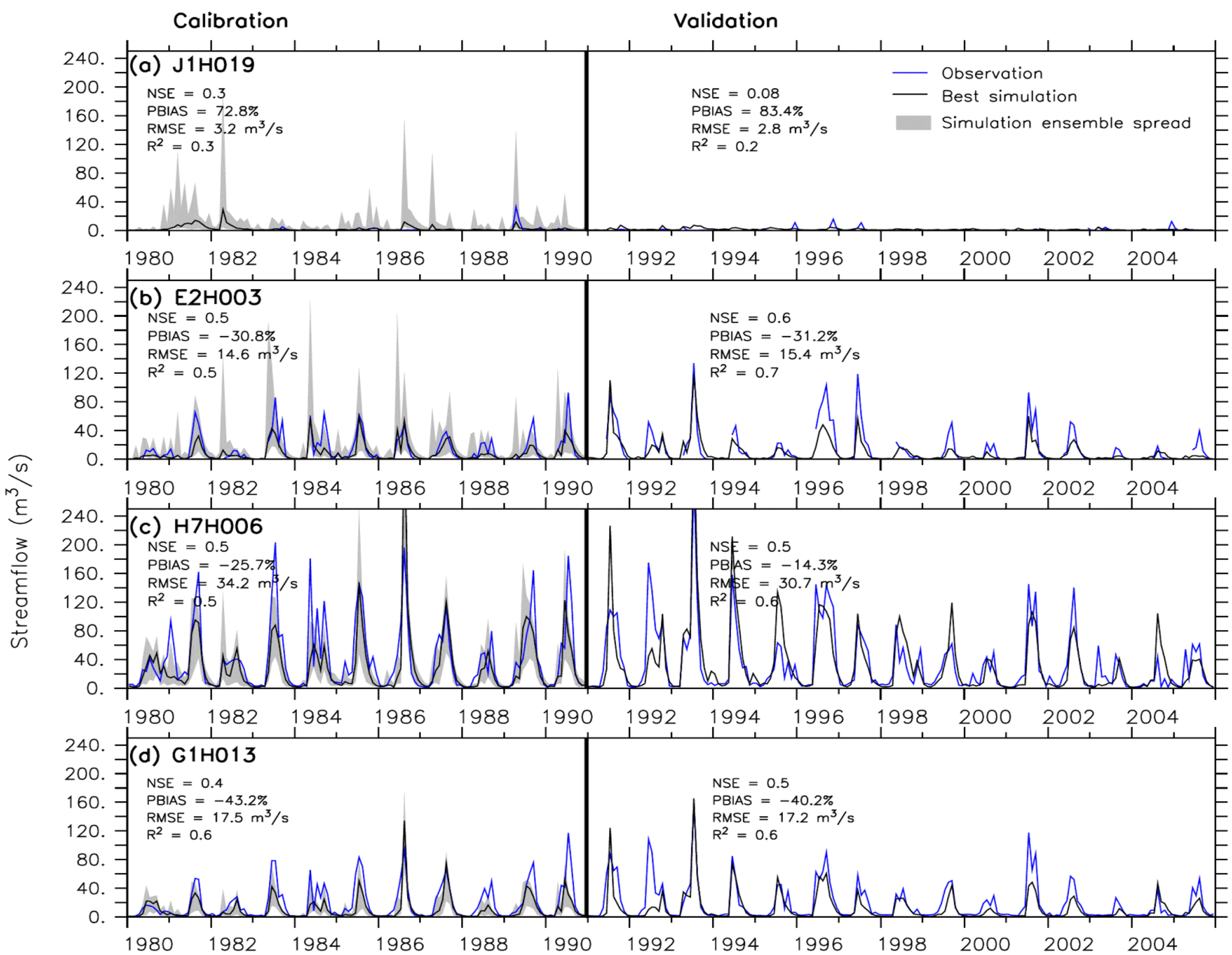

Figure 5.3: Comparison of the observations and SWAT+ simulated streamflow during the calibration period at four hydrological stations (i.e., (a), J1H019 (b) E2H003, (c) H7H006, and (d) G1H013) in the Western Cape River Basins. The values of the statistical metrics (i.e., NSE, PBIAS, RMSE, and R^2) used in quantifying the comparison are indicated.

5.3 Summary

In this chapter, the SWAT+ model was calibrated and validated over four river basins in Western Cape. The GMFD dataset (described in Chapter 3) was used as the input for the hydrological model and the simulations were compared to streamflow observation data from four stations over the basins. The results of this chapter suggest:

- In general, SWAT+ gives credible simulations over all the basins. It reproduces the annual cycle of the observed streamflow at the hydrological stations in the WRB, (i.e., G1H013, H7H006, E2H003, and J1H019) during both calibration and validation periods.
- The model also captures the timing and magnitude of most peak flows at the stations, in addition to replicating the interannual variability of the observed peaks. The coefficient of correlation (r) between the simulated and observed streamflow is more than 0.5 over most of the stations.

However, there are notable biases in the SWAT+ simulations. The biases may be attributed to several factors. They could be due to the shortcomings in the SWAT+ model or the model set-up over each river basin. SWAT+ is still undergoing a series of testing and improvements. Lack of data to represent all the physical features (e.g., dams and reservoirs) and operation rules (e.g., water abstractions and transfers) in the model set-up may influence the simulation of hydrological processes. The biases could also be due to the deficiencies in the climate input dataset (i.e., GMFD reanalysis) in capturing the influence of complex topography on the rainfall pattern. Nevertheless, the generally good performance of the SWAT+ in reproducing the peaks and annual cycle of the streamflow is encouraging and shows that the model provides a reliable representation of hydrological processes over the WRB.

Chapter 6:
Influence of bias correction of climate datasets on simulation of hydrological drought in the Western Cape

This chapter discusses the performance of the CORDEX datasets over the Western Cape. To provide confidence on the quality of the CORDEX datasets climate simulations for input data in the SWAT+ hydrological modelling, the evaluation focuses on how well the dataset reproduces different hydroclimate variables. The evaluation examines the annual cycle and the spatial distribution of hydroclimatic variables, comparing the non-bias-corrected CORDEX datasets (CORDEX_ORG) with the three bias-corrected datasets (CORDEX_QDM, CORDEX_MBCr and CORDEX_MBCn). These results are compared for different climates and hydrological variables (T_{max}, T_{min}, PRE, PET, ET, SW, Runoff, SFlow and Stream ET etc.), and drought indices. Details of the CORDEX and GMFD datasets, as well as the bias correction techniques, can be found in Chapter 3.

6.1 Annual cycle of hydroclimatic variables

Generally, the CORDEX_ORG simulations capture the annual cycle of the hydroclimatic variables across the Western Cape (Figures 6.1 and 6.2). The CORDEX_ORG ensemble simulates well the temporal distribution for temperature, for instance, both for T_{max} (about 15 to 28 °C) and T_{min} (between 5 to 15 °C) values, as observed in the GMFD (Figure 6.1). The annual cycle for PET follows that of temperature, with a summer peak (about 220 mm mon^{-1}) and a winter trough (about 50 mm mon^{-1}). Changes in these variables mimic the seasonal temperature differences during the year that correspond to the north-south movement of Earth's thermal equator. This seasonal shift is also associated with the northward shift of the mid-latitude cyclones, which bring seasonal rainfall to the Western Cape region (Tyson, 1986). The CORDEX_ORG ensemble captures this increase in PRE, with a peak (about 40 mm) in the annual cycle during winter (June–July–August). Other hydrological variables also follow this increase in PRE during winter. The CORDEX_ORG ensemble mean also reproduces a similar peak increase in winter, for variables, like ET (i.e., 25 mm mon^{-1}), SW (i.e., about 60 mm mon^{-1}), SFlow (about 80 mm mon^{-1}) over the region (Figure 6.2). The ability of the climate simulations to reproduce the annual cycle of these hydroclimate variables suggests that the

CORDEX_ORG dataset captures the general large-scale atmospheric mechanisms and the broader essential components of CWB over the region.

Nevertheless, the CORDEX_ORG simulations feature notable biases in simulating the annual cycle of hydroclimatic variables over the region (Figures 6.1 and 6.2). For temperature, for instance, the CORDEX_ORG ensemble mean simulates a cold bias for both T_{max} and T_{min}. The cold bias, which is between 2 to 4 °C, occurs throughout the annual cycle but is particularly notable during the mild, moist, winter months (May–August). The cold bias produces a negative PET (about 10 mm mon^{-1} in May–August). The simulation biases in PRE are more evident and less consistent than the temperature biases. The CORDEX_ORG PRE ensemble mean produces a wet bias (about +10 mm mon^{-1}) compared to that of GMFD, but there is a large uncertainty (i.e., spread) in the simulation ensemble. For instance, RCA-CNRM produces a wet bias (up to +35 mm mon^{-1}), while RCA-CCCma, RCA-IPSL and RCA-IPSL2 produce a dry bias (about –10 mm mon^{-1}). Consistent with this PRE bias, the CORDEX_ORG simulation mean also produces a wet bias with large uncertainty for hydrological variables: SW (i.e., about +30 mm mon^{-1}), ET (about +70 mm mon^{-1}), runoff (i.e., about +1 mm mon^{-1}), and SFlow (about +70 mm mon^{-1}). The large uncertainty in climate model variables is what guards against the use of raw simulation data in hydrological models and underscores the value of bias correction (Johnson and Sharma, 2015).

The bias corrections reduce the systematic biases in the annual cycle of the hydroclimatic variables over the Western Cape. The three bias-corrected datasets (CORDEX_QDM, CORDEX_MBCr and CORDEX_MBCn) perform better than CORDEX_ORG in tracking the annual cycle of GMFD hydroclimate variables (Figures 6.1 and 6.2). For example, the corrected datasets reduce the cold biases T_{min} and T_{max} to less than 1°C and the negative bias in PET to less than 5 mm mon^{-1}. They also improve the PRE simulations by reducing the systematic biases and large uncertainty in the simulation ensemble. The improvement of the climate datasets enhances the quality of the hydrological simulations because the systematic bias in these variables also reduce SW (i.e., about +30 mm mon^{-1}), ET (i.e., about +70 mm mon^{-1}), runoff (i.e., about +1 m^3 s^{-1}), and SFlow (about +70 m^3 s^{-1}). However, there are some notable shortcomings in the bias-corrected datasets. All the bias-corrected datasets overcorrect the dry bias in RCA_CCCma and RCA_IPSL precipitation, and produce a wet bias, leading to a positive bias in all the hydrological variables. In addition, none of the bias-correction methods correct the one-month delay bias in PRE peak simulation in RCA_IPSL.

All these indicate that the improvements of bias correction in the datasets are simulation dependent as suggested by Ayar and Mailhot (2021). Nevertheless, the bias in the ensemble of each bias-corrected dataset is smaller than that of CORDEX_ORG. Among the three bias-corrected datasets, the CORDEX_MBCn gives the best results followed by CORDEX_MBCr. These results are in line with those of Cannon et al. (2018), which found that MBCn outperformed QDM and MBCr algorithms in correcting the simulated climate variables from CanRCM4 (the Canadian Centre for Climate Modelling and Analysis Regional Climate Model) over a North American domain. Cannon et al. (2018) showed that MBCn performs better than other methods (QDM and MBCr) because it transfers all aspects of the continuous multivariate distribution of the observed variables to the corresponding multivariate distribution of the simulated variables. While QDM neglects the dependence between different variables, MBCr only corrects limited measures of joint dependence.

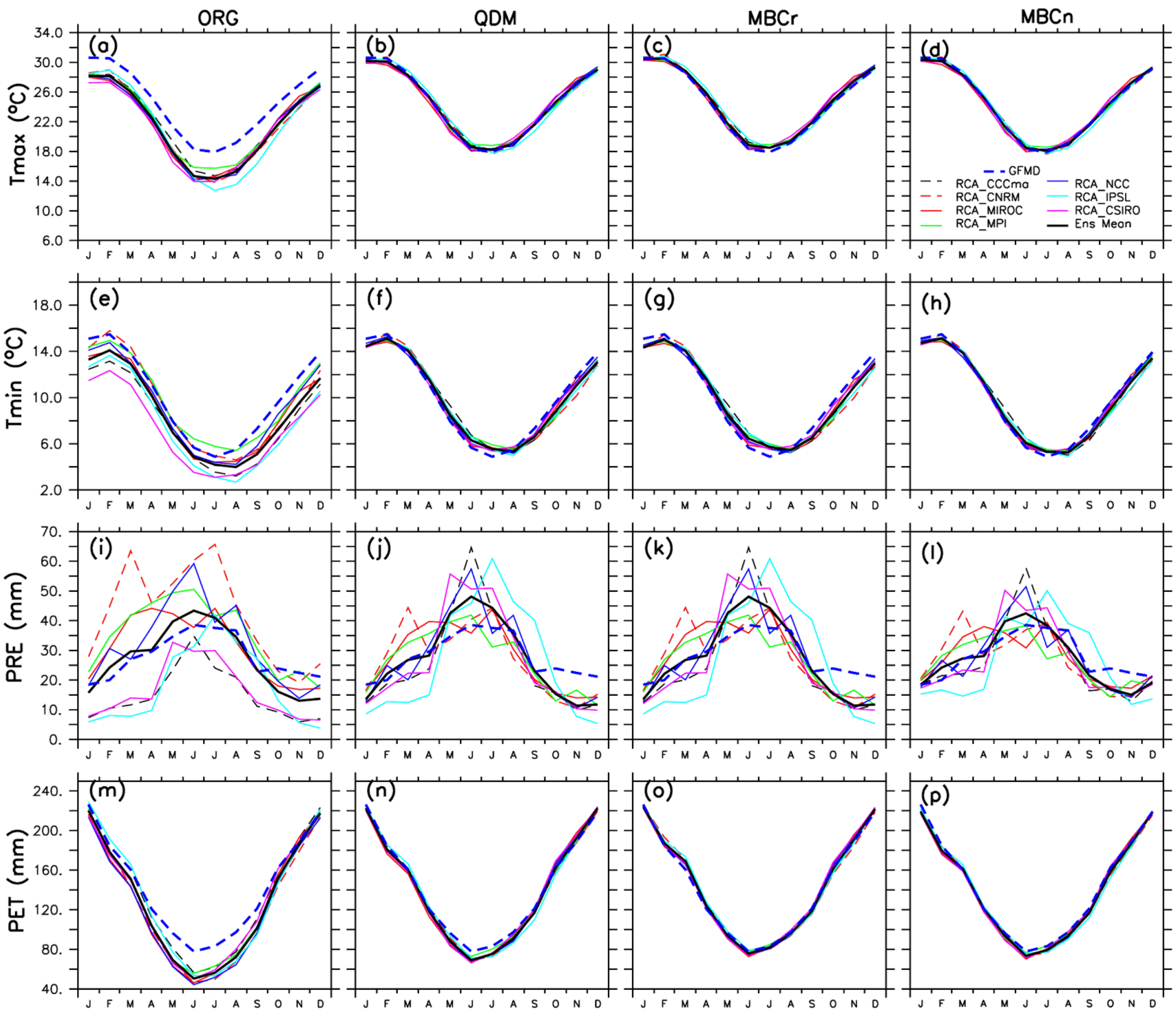

Figure 6.1: Annual cycle of climate variables [maximum and minimum temperature (T_{max} and T_{min}), precipitation (PRE), and potential evaporation (PET)] over the river basins as depicted by GMFD, original CORDEX (ORG) and bias-corrected CORDEX (QDM, MBCr, and MBCn) datasets.

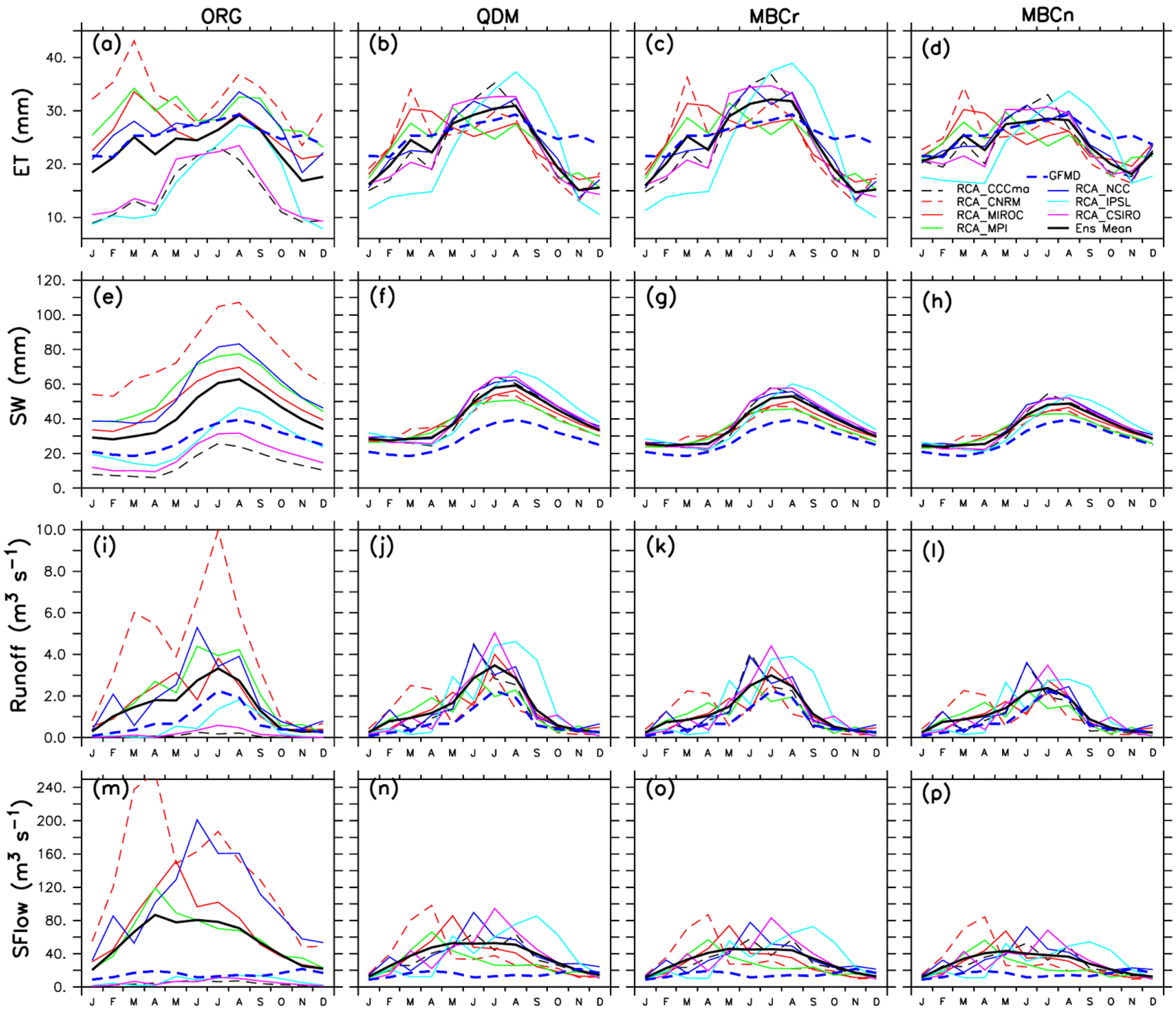

Figure 6.2: Same as Figure 6.1, except for hydroclimatic variables [evapotranspiration (ET), soil water (SW), runoff and streamflow at TWT (SFlow)].

6.2 Spatial distribution of hydroclimatic variables

The CORDEX_ORG dataset also gives realistic spatial patterns of the hydroclimatic variables over the Western Cape (Figures 6.3 and 6.4). In the temperature pattern (Figure 6.3), it captures the temperature maxima over the north-western part of the basin (about 18 °E to 31 °S) and the temperature minima over the mountain range (about 20 °E to 33 °S) as depicted by the GMFD. In the PRE pattern, it features the lowest PRE over the north-western part of the basin and the peak PRE over the mountain range. This precipitation maxima are the result of orographic rainfall due to moist air cooling rapidly when passing over areas of higher relief (Figure 3.3a). In agreement with the

GMFD, CORDEX_ORG shows that PET increases from south to north (following the temperature distribution), while ET increases from north to south (PRE distribution). In both the GMFD and CORDEX_ORG, the capability of the WRB to meet the atmospheric demand (i.e., ET/PET) decreases from south-west to north-east. For the hydrological variables, the spatial distribution is consistent with that of PRE. For instance, both the CORDEX_ORG and GMFD results feature maximum soil water and runoff over the mountain range due to the peak PRE and the steep slopes over the mountains. So, the CORDEX_ORG simulations capture the processes that control the spatial distribution of hydroclimate variables over the Western Cape.

Nevertheless, there are substantial biases in the spatial distribution of the hydroclimatic variables produced by the CORDEX_ORG dataset (Figures 6.5 and 6.6). The dataset underestimates temperature (by up to 2 °C) and PET (up to 30 mm $month^{-1}$). The CORDEX_ORG dataset locates the PRE maxima too far north of its location in the GMFD, thereby producing a dry bias over the southern part of the region (i.e., over the Berg and Breede rivers; by more than 10 mm $month^{-1}$) and a wet bias over the northern part (i.e., Olifants and Gouritz; by more than 10 mm $month^{-1}$). The biases in climate variables translate to the simulated hydrological variables. For instance, the dry bias leads to an overestimation of soil water (up to 40 mm $month^{-1}$), percolation (up to 3 mm $month^{-1}$), runoff (up to 6 m^3 s^{-1}) and streamflow (up to 1,300 m^3 s^{-1}) in the northern part of the basin and an underestimation of these variables (up to 40 mm $month^{-1}$, 2 mm $month^{-1}$, 4m^3 s^{-1}, and 1,300 m^3 s^{-1}, respectively) in the southern part of the basin.

The three bias-correction methods drastically reduce these errors and provide better spatial distribution of the climate and hydrological variables over the region. For example, in the temperature pattern, they increase the correlation between the CORDEX and GMFD datasets (from 0.87 to 1.0) and reduce the RMSE (from 2.25 to about 0.1%). In the precipitation pattern, they also enhance the correlation (from 0.7 to 1.0) and decrease the RMSE (from 9.7 to 1.1). Nevertheless, the improvement in the hydrological variables is lower than that of the climate variables. For instance, while the coefficient of correlation between the GFMD and the bias-corrected datasets is ≥ 0.99 for the climate variables, it is between 0.92 and 0.98 for the hydrological variables. Also, the PBIAS of the bias-corrected datasets, which is less than ±2% for climate variables, is up by 77% in the hydrological variables. However, among the three bias-correction techniques, the MBCn gives the best results, while the QDM performs the worst. For all the hydroclimatic variables, the coefficient of the correlation of CORDEX_ORG with GMFD is ≥ 0.94 and the PBIAS CORDEX ≤ 39%.

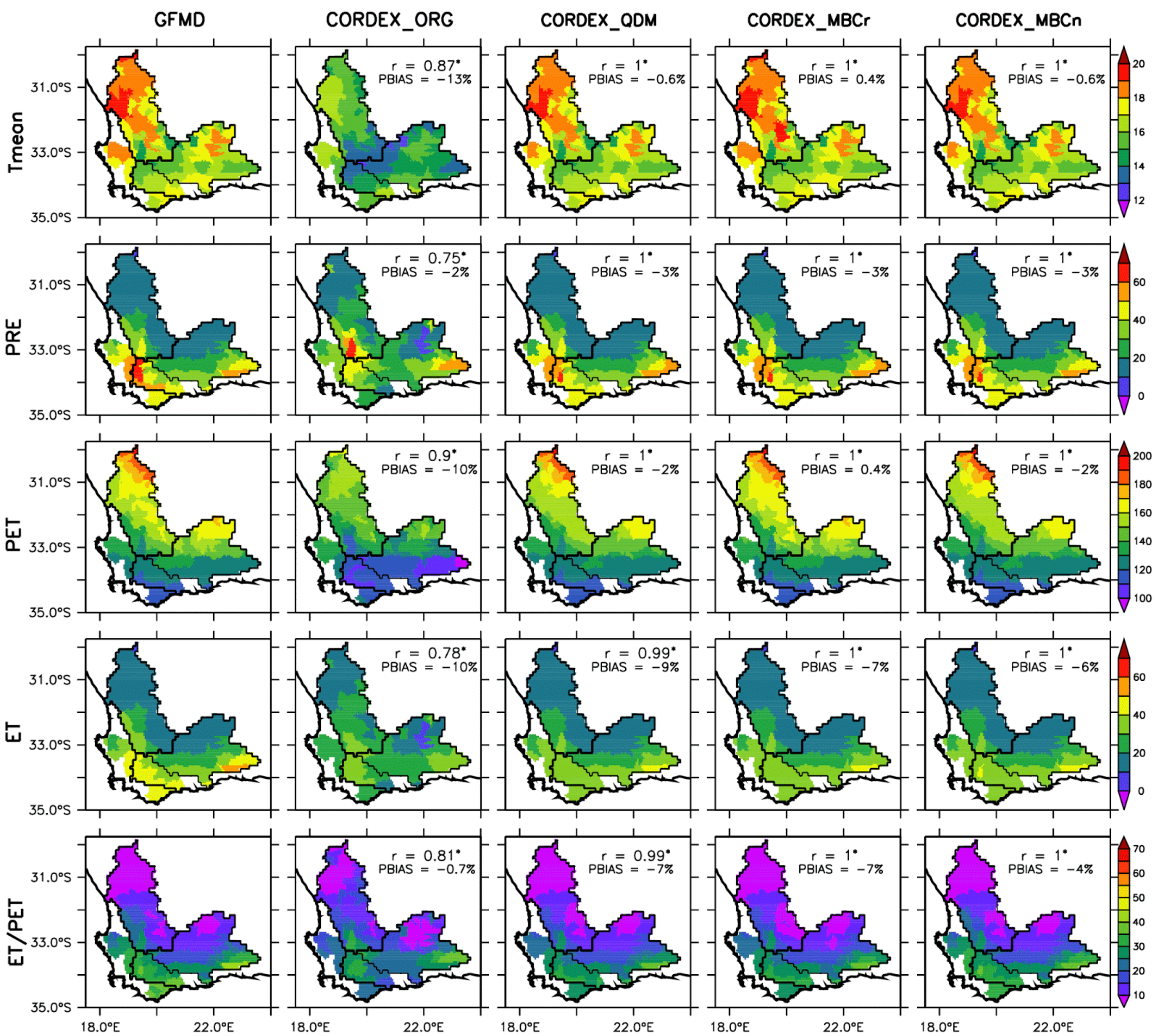

Figure 6.3: The spatial distribution for hydroclimatic variables over the Western Cape River basins as depicted by GMFD, original CORDEX (ORG) and bias-corrected CORDEX (QDM, MBCr, and MBCn) datasets.

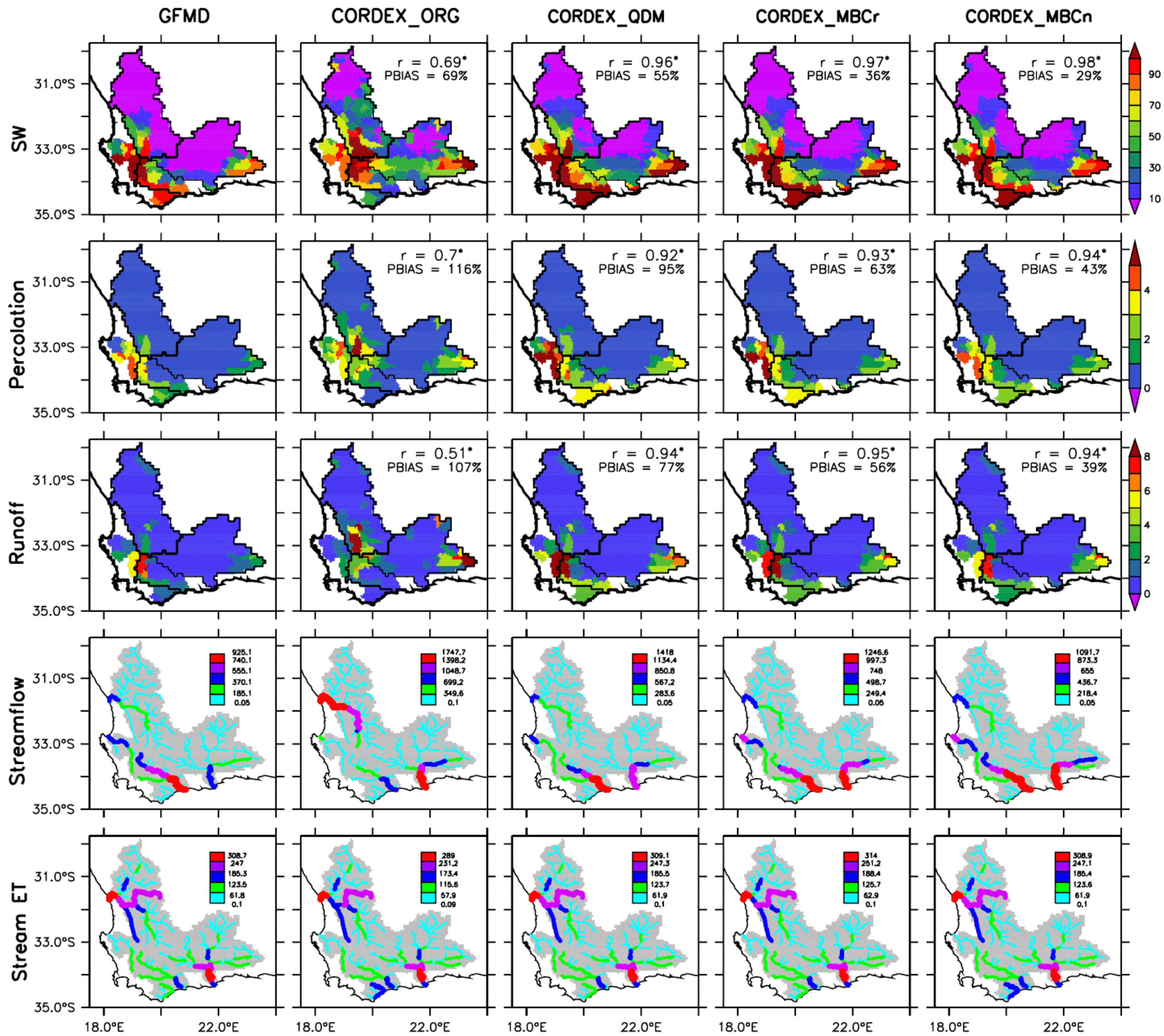

Figure 6.4: The spatial distribution for hydrological variables over the Western Cape River Basins as depicted by GMFD, original CORDEX (ORG) and bias-corrected CORDEX (QDM, MBCr, and MBCn) datasets.

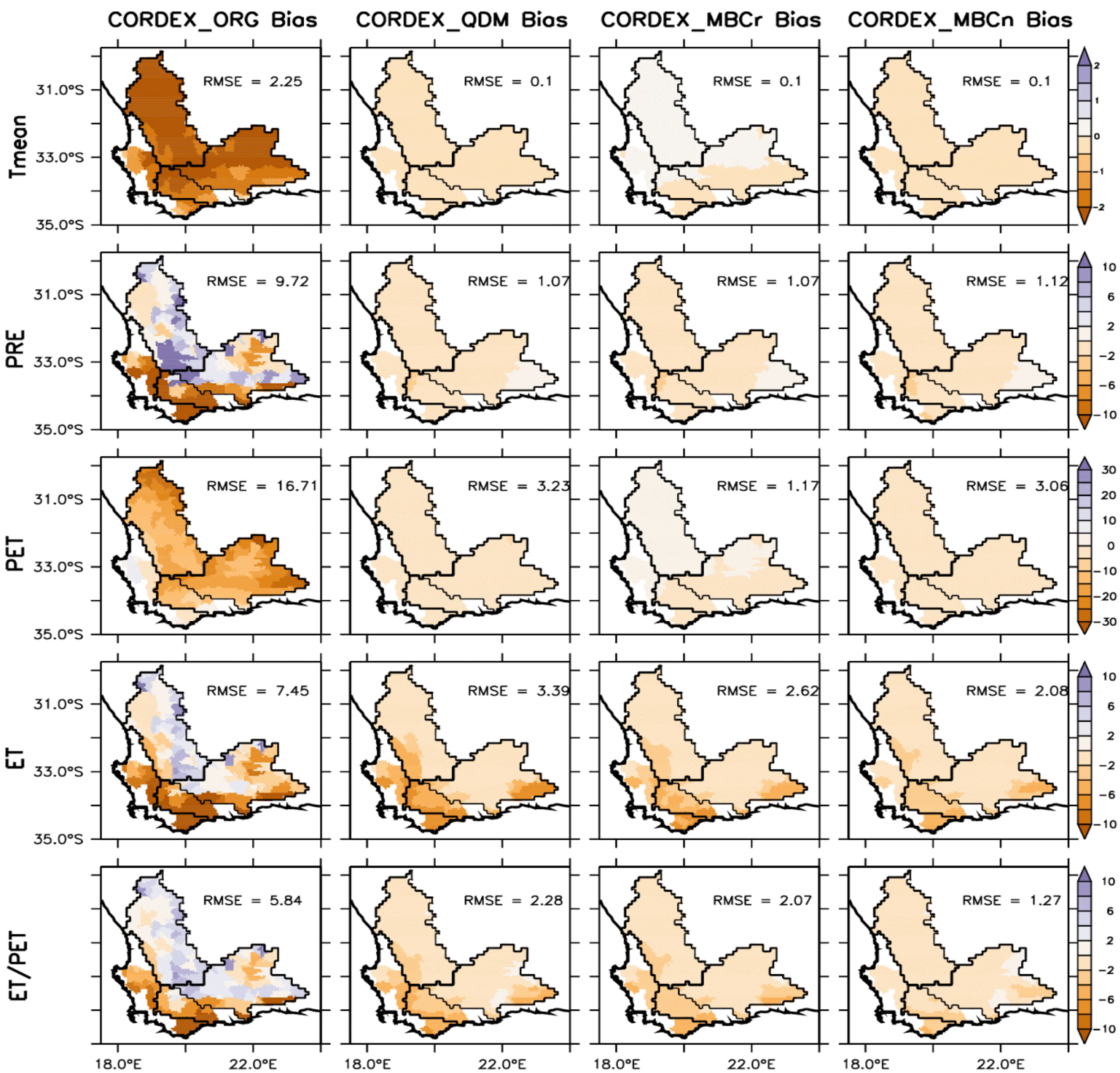

Figure 6.5: Biases in hydroclimatic variables in the original CORDEX (ORG) and bias-corrected CORDEX (QDM, MBCr, and MBCn) datasets.

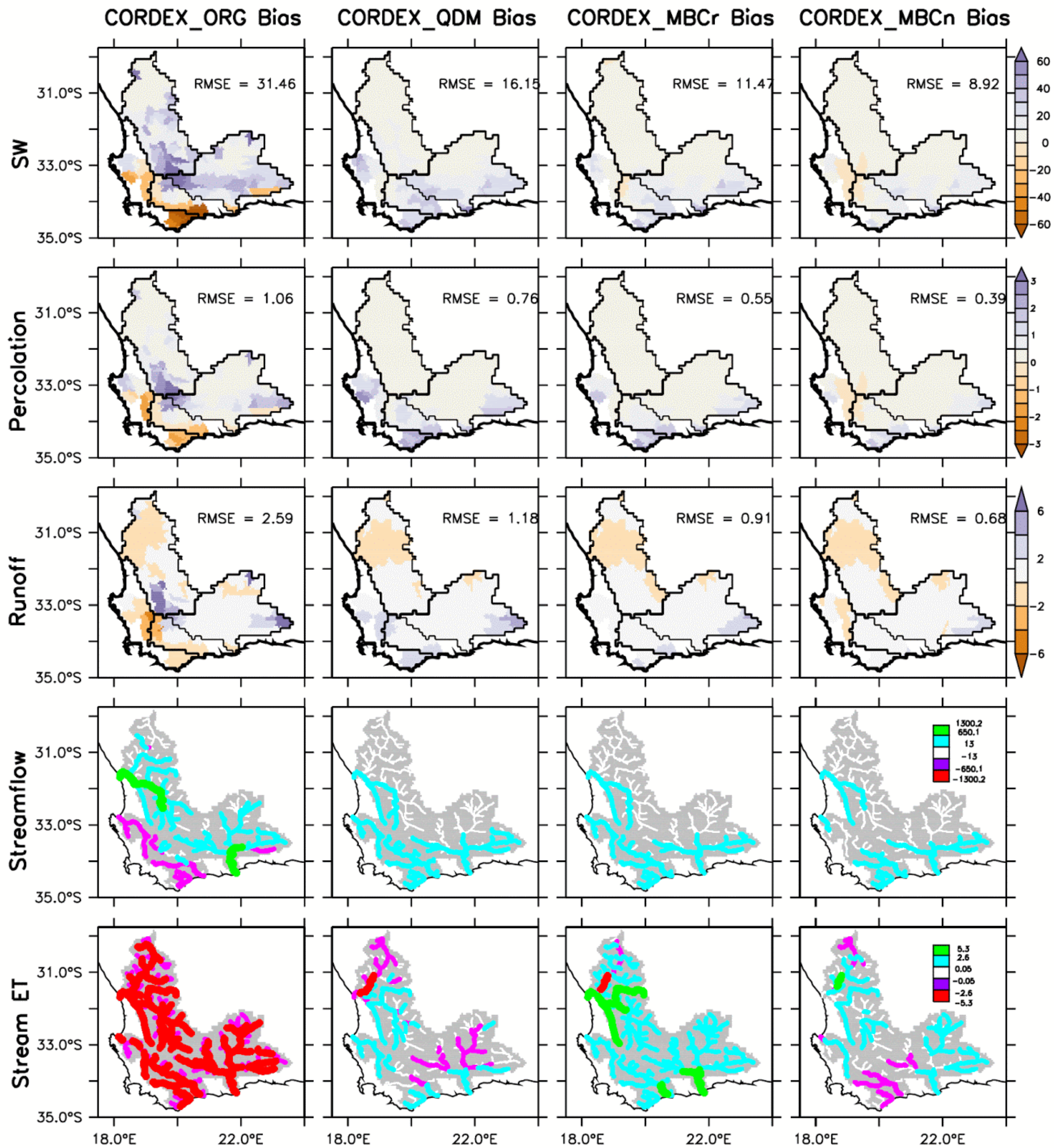

Figure 6.6: Biases in hydrological variables in the original CORDEX (ORG) and bias-corrected CORDEX (QDM, MBCr, and MBCn) datasets.

6.3 Hydroclimatic droughts

The CORDEX_ORG simulations capture the characteristics of the hydroclimatic droughts well (Figure 6.7). For most cases, the GMFD results are between the 1st and 3rd quartile of the simulations and in some cases, the simulation median or simulation ensemble mean values are very close to or the same as the GMFD values. There is only one instance where CORDEX_ORG grossly overestimates the drought characteristics (i.e., SPEI drought intensity; the 1st quartile value is higher than the GMFD result) and four instances where it grossly underestimates certain characteristics (i.e., PERCI drought intensity; RFI, WYLDI, SFI drought frequencies; the 3rd quartile value is lower than the GMFD result). The capability of the bias correction to improve these biases varies. While all the bias-corrected datasets improve on the underestimation of the PERCI drought intensity as well as the RFI and SFI drought frequencies, only CORDEX_QDM and CORDEX_MBCr improve on the underestimation of the WYLDI drought frequency, but no dataset improves on the underestimation of the SPEI drought intensity. However, there are cases when the bias correction worsens the CORDEX results. For example, in comparison with CORDEX_ORG, all the datasets perform worse in RFI drought intensity; CORDEX_QDM and CORDEX_MBCr give less credible SFI drought intensity, while CORDEX_MBCr has a higher bias in WYLDI drought. Hence, the bias-correction improvements to the hydroclimatic drought characteristics are not as distinct as they are in relation to the hydroclimatic variables.

These findings suggest that, while bias correction is critical for the correction of hydrological variables, it is less critical when considering drought characteristics. This is because multivariate bias-correction approaches (MBCr and MBCn) are a generalisation of the QDM method. QDM bias correction preserves the quantiles of observed historical series and applies them on top of the relative changes in quantiles from model simulations (Cannon, 2015). The preservation of quantiles reduces the systematic errors in the climate data and is akin to the standardisation process used for the calculation of drought indices. Note that the drought indices also require normalisation of variables, and transformation of the climate data to a normal distribution (with mean zero and standard deviation of one) (Vicente-Serrano et al., 2010). Thus, the lack of substantial bias-correction improvement in the drought characteristics occurs because the systematic biases that QDM tries to correct are already removed in the process of standardisation when calculating the drought indices.

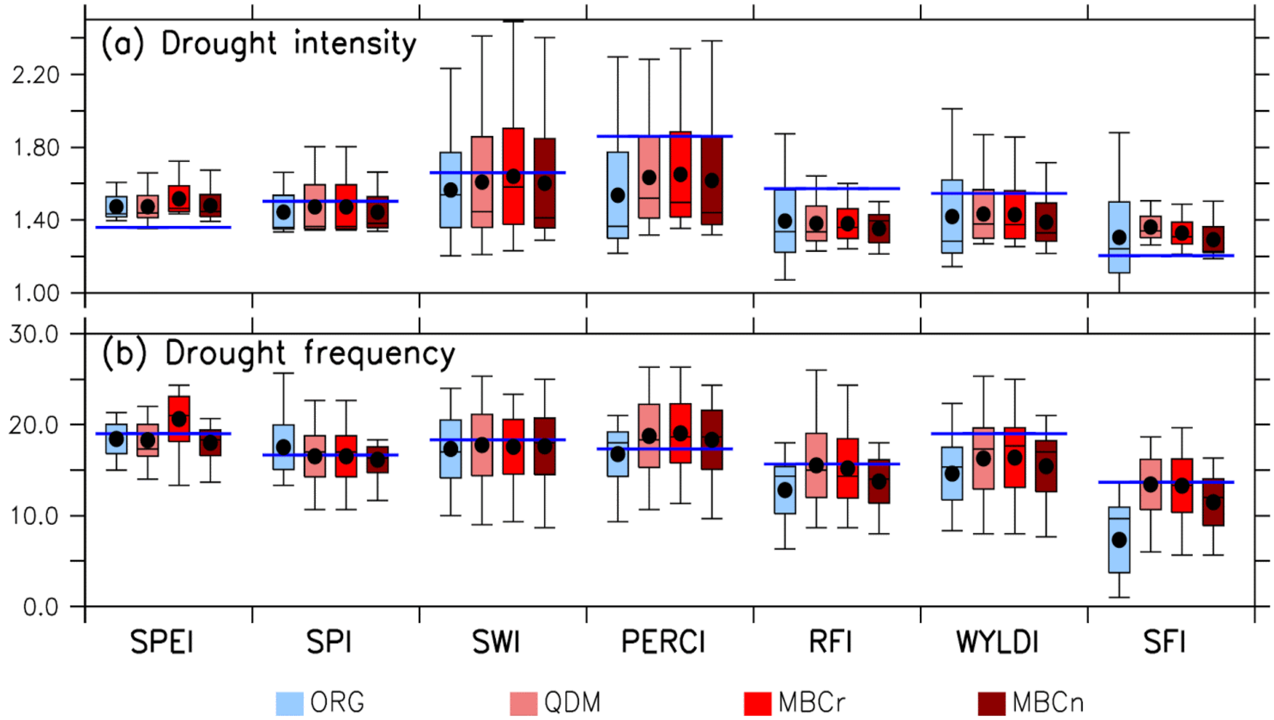

Figure 6.7: The characteristics of 12 months droughts (drought index < –1.0) as depicted by CORDEX (ORG) and bias-corrected CORDEX (QDM, MBCr, and MBCn) datasets. Panel (a) shows the absolute value of the drought intensity while Panel (b) shows the drought frequency as the number of drought months per decade. The blue lines show the GMFD observed value while boxplots show the CORDEX simulation spread (minimum, first quarter, median, third quarter, and maximum).

6.4. Summary

In order to emphasise the quality of hydrological simulations in the Western Cape, this chapter examined the influence of three bias-correction methods (QDM, MBCr and MBCn) on CORDEX climate variables and the associated simulated hydrodynamic variables. The GMFD dataset was used as the reference for the bias correction, and the SWAT+ was used to perform the hydrological simulations. Using the GFMD data as the input, the SWAT+ model was calibrated and validated using four hydrological stations in the region. The calibrated SWAT+ results were used to evaluate the SWAT+ simulations that were forced with the original dataset (CORDEX_ORG) and the bias-corrected datasets (CORDEX_QDM, CORDEX_MBCr, CORDEX_MBCn). The results of the study can be summarised as follows:

- The GFMD-forced SWAT+ model gives a realistic simulation of hydrology in the WRB, where the simulated monthly streamflow in the SWAT+ model closely tracked the observed values.
- While the CORDEX_ORG-forced SWAT+ simulations capture the annual cycle and spatial variation of the hydroclimatic variables over the basins, there are substantial biases and large uncertainties in the simulated variables.
- All the bias-correction methods reduce the magnitude of the biases (by more than 50%), improved the correlation between the GFMD and CORDEX simulations, and lowered the level of the uncertainty in the simulated hydroclimatic variables. However, the MBCn method performs better than the other methods in this regard.
- There is a good agreement between the CORDEX_ORG and GMFD results in relation to the characteristics of hydrodynamic droughts over the basins.
- There is no substantial bias-correction improvement in the characteristics of the hydroclimatic droughts, possibly because the standardisation inherent in the calculations of the drought indices has already reduced the systematic biases in the hydroclimatic variables.

The results emphasise the importance of performing the bias correction of climate datasets before using them as input into SWAT+ hydrological modelling. Nevertheless, before doing a bias correction of any climate dataset over a basin, it is essential to ensure that the dataset gives realistic simulations of climate variables over the basin. This is to ensure that the dataset captures all the important climate processes over the basin. It is important to emphasise that bias correction cannot compensate for the inability of a climate dataset to capture all the essential large-scale atmospheric processes over a basin.

Chapter 7:

Projected future impacts of climate change on hydrological drought

This chapter presents and discusses the results of the potential impacts of climate change on hydrological drought in the Western Cape River Basins (WRB). The results detail the impacts on the spatial and temporal distribution of hydrological variables (e.g., ET, ET/PET, soil water (SW), percolation (PERC), Runoff, water yield (WYLD), and streamflow over the WRB, and are discussed for different global warming levels (GWLs; i.e., 1.5 °C, 2.0 °C, 2.5 °C and 3.0 °C, hereafter referred to as GWL 1.5, GWL 2.0, GWL 2.5 and GWL 3.0, respectively)).

7.1 Impacts of climate change

Figure 7.1 shows the time series of projected climate changes across the Western Cape for the period 1980 – 2100. These projections show a gradual increase in mean temperature (T_{mean}), from about 1°C in 2030, and reaching about +4 °C by the end of the century. The spatial distribution of the warming is generally uniform across the region and robust (i.e., the simulations agree on the sign of the changes and the change is of statistical significance), but the magnitude of the warming increases with the GWLs (Figure 7.2). For example, the temperature increase may be between 1.5 – 2.5 °C, under GWL1.5 and GWL2.0, or as high as 3.0 – 4.5 °C, under GWL2.5 and GWL3.0 across the basins. These climate projections for temperature are in line with those of the previous study, which suggests increased temperatures (up to 4°C) could occur in this region before the end of the century (Haensler et al., 2011; Field, 2014; Naik and Abiodun, 2016). Note that for higher GWLs, increased warming tends to occur further inland, over the north-eastern regions. For example, under GWL3.0, the increase is about 4.5°C, over the north-eastern parts of the Olifants basin, but about 2.5 °C along southern parts of the Berg and Breede. This is in line with previous projections and may be due to the moderating effects of the ocean on temperature along the coastline (e.g., Mbokodo et al., 2020; Naik and Abiodun, 2016). This projected increase in temperature leads to an increase in potential evaporation (PET), which also shows a gradual increase by the end of the century (from about +10 mm month^{-1} in 2030, and to about +20 mm month^{-1} by 2100; Figure 7.1). The areas where the largest changes in PET occur compare well spatially to areas where the largest changes in T_{mean} occur (Figure 7.2), and the magnitude of the PET change increases with higher GWLs (2.0, 2.5 and 3.0). The changes in PET are also robust across the region. The largest increase occurs over the north-eastern parts of the Olifants and northern Gouritz basins, where PET may increase by between +10 mm month^{-1} (GWL1.5) to more than +20 mm month^{-1} (GWL3.0), respectively. Several studies confirm that PET rates may increase with higher temperatures in the future (Dai et al., 2018; Yuan and Bai, 2018). This is because global warming (and associated higher temperatures) lead to an increase in the vapour pressure deficit of air and increased atmospheric evaporative demand.

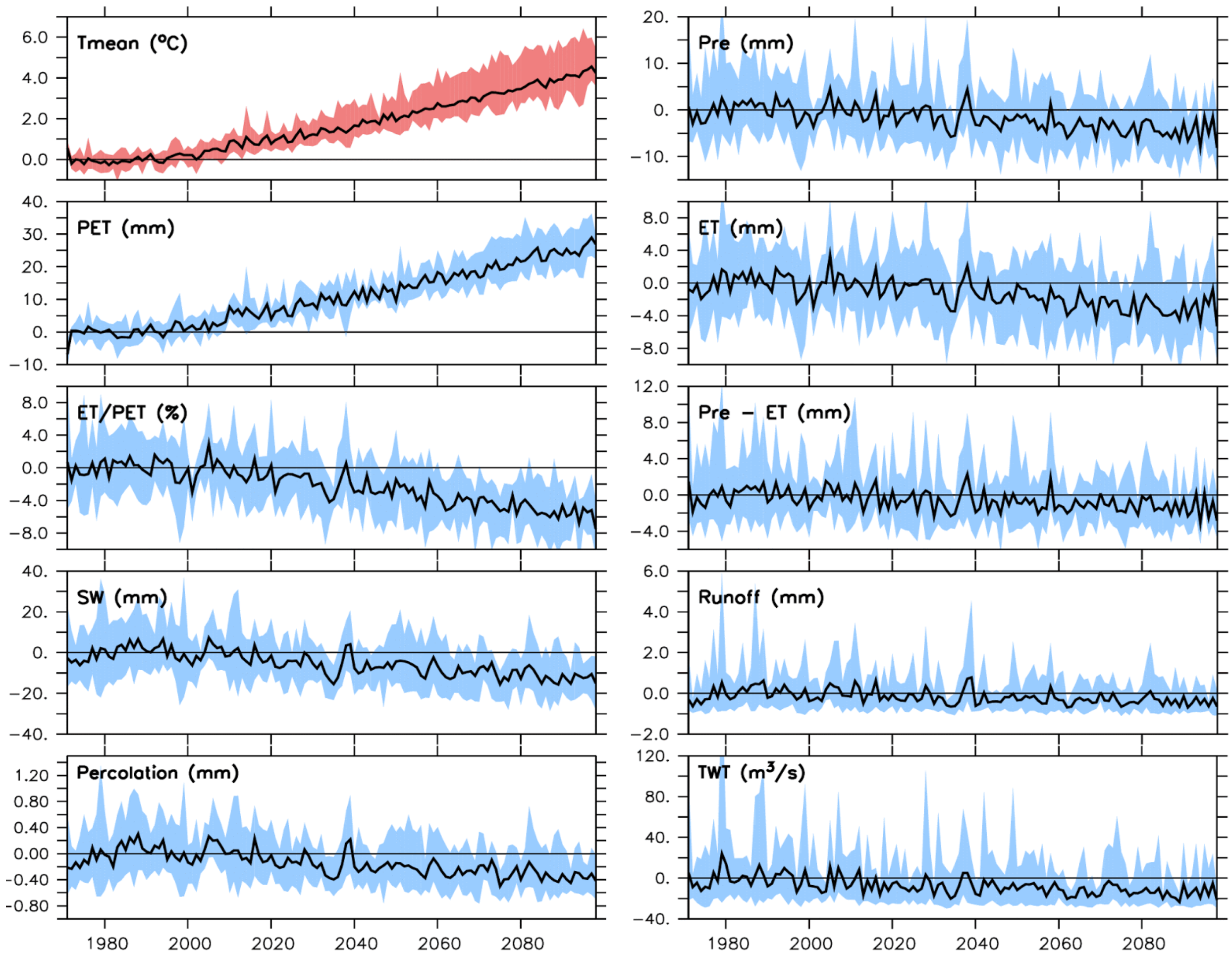

Figure 7.1: Temporal variation of the changes in hydroclimatological variables over the Western Cape River Basins in the period (1971–2099) under the RCP8.5 climate scenarios. The changes are calculated with reference to the present-day climate (1971–2000). The solid lines represent the multi-model ensemble mean of selected climate models and the spreads represent the range of selected climate models.

The projected changes in precipitation (PRE) are more complex than those of T_{mean}. PRE projections show no discernible change in the trend before 2040, but a decreasing trend afterwards until the end of the century. However, changes in the spatial distribution do occur (Figure 7.2). Nonetheless, the pattern of the PRE change differs spatially across the Western Cape basins. While there is a general decrease in PRE across the region, the projections under GWL 1.5 suggest more drying (about –2 mm month^{-1}) may occur over some areas, like parts of the southern Gouritz and the south-eastern Breede, while only modest change occurs over other areas like the central Olifants. Generally, this pattern is similar across the GWLs, only that the magnitude of the change increases under higher GWLs and that the spatial extent of the drying increases. For instance, the area of maximum drying includes the southern margin of the Gouritz and Berg (–1.5 mm month^{-1}) for GLW2.0, and it extends cross the entire Gouritz, Breede, and parts of the Berg and Olifants, where it exceeds –2.5 mm month^{-1} for GWL 3.0. Only few areas show wetter conditions over the Western Cape in the future. The exception to the general drying over the region occurs over a limited area of the central Berg (near a large dam), where increased PRE (+2 mm month^{-1}) occurs, and over central-southern parts of the Olifants (+1 mm month^{-1}). However, this occurs for GWL1.5, but not under higher GWLs, when a robust drying signal dominates. The large-scale forcing mechanisms potentially responsible for the decreased rainfall across the Western Cape region may include an increase in the intensity and frequency of upper-level highs, and migration of subtropical anticyclones towards the mid-latitudes across the southern African subcontinent (Sousa et al., 2018). The poleward shift of the Southern Hemisphere moisture corridor and the displacement of the South Atlantic storm-track may create significantly drier conditions under conditions of future climate change. The projected evaporation (ET) can be linked to the changes in PRE. While there is no discernible trend in future ET time series projections over the Western Cape (Figure 7.1), there are changes spatially. The spatial pattern of the ET change is not uniform across the Western Cape for GWL1.5. ET may decrease over some basins, such as the Gouritz (–2 mm month^{-1}), but increase over others, such as the south-central Olifants (+1 mm month^{-1}) or the Berg (+1 mm mon^{-1}). Generally, however, the areas where the largest changes in ET occur are comparable to the areas where PRE changes occur. The robustness of the signal and the magnitude of the ET change also increases with higher GWLs (2.0, 2.5 and 3.0). For example, the projections show that, for higher GWLs, ET may decrease over much of the region (–1.5 mm month^{-1}), and particularly over the south-western Gouritz and central Olifants. This decrease may be up to –1.5 mm month^{-1} under GWL1.5, –2 mm month^{-1} under GWL2.0 and exceed –2.5 mm month^{-1} under GWL3.0.

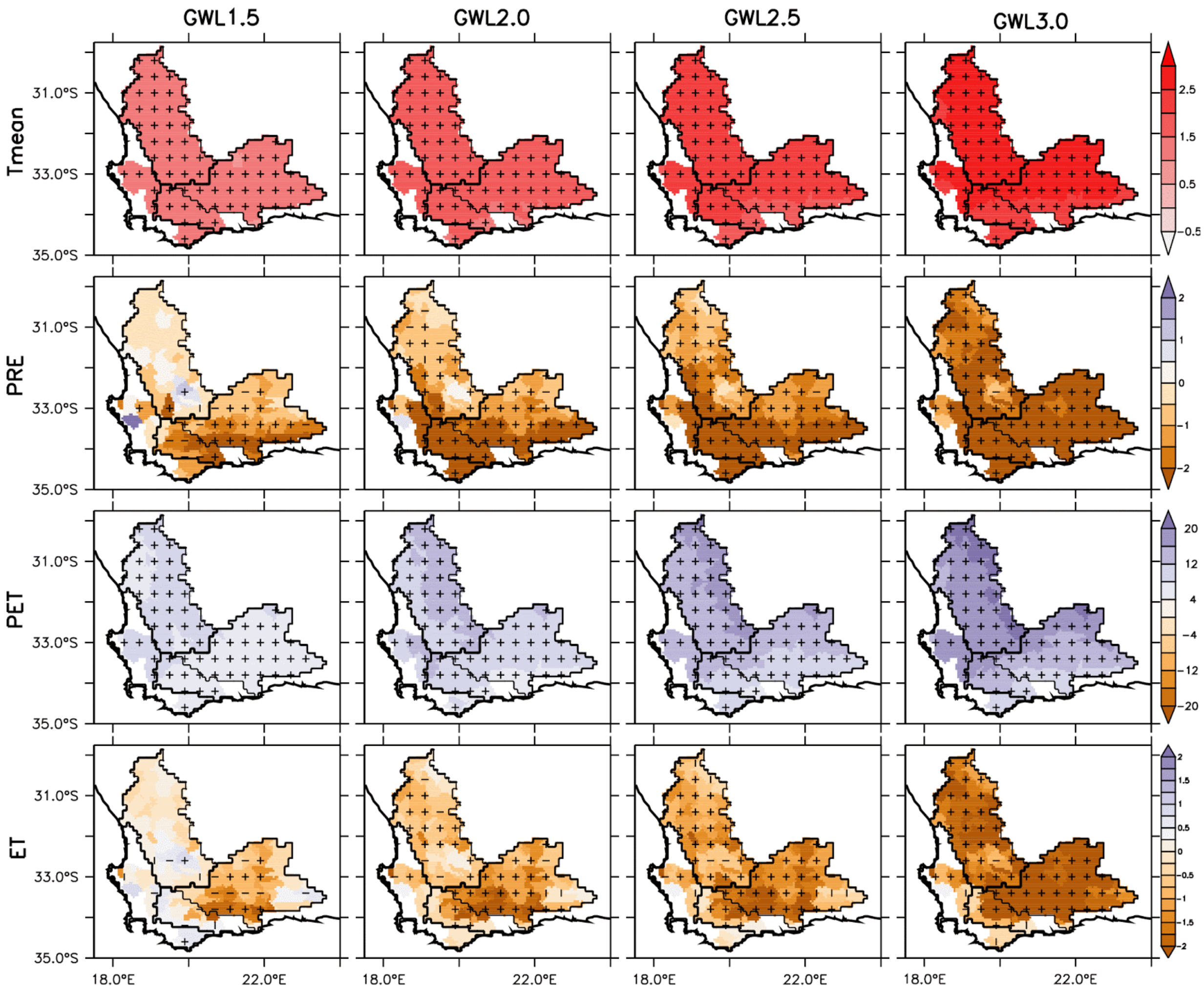

Figure 7.2: Spatial distribution of the projected changes in temperature (°C), precipitation (mm month^{-1}), potential evapotranspiration (PET, mm month^{-1}) and evapotranspiration (ET, mm month^{-1}) over the Western Cape River Basins at different global warming levels (GWL1.5, GWL2.0, GWL2.5, and GWL3.0). Note that the vertical line (|) indicates where at least 80% of the simulations agree on the sign of the changes, and a horizontal line (−) indicates where at least 80% of the simulations agree that the change is of statistical significance (at 99% confidence level). The cross (+) shows where the change is robust, that is, if both conditions are satisfied.

The projected decrease in hydrological variables can be linked to the decrease in PRE (Figures. 7.3 and 7.2, respectively). The spatial distribution of these hydrological changes is consistent with that of PRE. For example, the projections show a general decrease in soil water across the region (–10 mm month^{-1}), that is enhanced over the eastern Olifants (–20 mm month^{-1}) and the central Berg (–20 mm month^{-1}), under GWL3.0. The spatial distribution of the drying is comparable for higher

GWLs, except that the magnitude of the drying increases with the GWLs and the signal is more robust. This is because the projected decrease in PRE negatively affects the overall soil water budget of the affected areas. With time, this causes a gradual decrease in volumetric water content of soil over the region (soil water; about –10 mm) from 2050–2100 (Figure 7.1). This negative change in storage (i.e., soil water content) occurs when outputs, such as percolation (PERC) and surface runoff (runoff) exceed PRE. As seen in Figure 7.3, the distribution of the future drying is spatially comparable for these variables. Since the soil does not reach saturation, reduced PERC occurs and there is also a consistent decrease in overland runoff. (Note the differences in PERC and runoff are comparable to the spatial variation in soil types (Figure 3.3c) because loam and sandy loam textures differ in their water-holding capacity). This is consistent with our projected changes in hydrological variables over channels (Figure 7.4). There is a decrease in channel precipitation over many areas of the Western Cape (Stream PRE; –10 mm month^{-1}), and this drying increases under higher GWLs. For instance, drying of –8.4 mm month^{-1} occurs along channels of the southern Gouritz and Breede, under GLW2.0, and it extends across the entire Western Cape, where it exceeds up to 16.9 mm month^{-1} for GWL 3.0. The projected increase in PET leads to an increase in stream ET, which occurs for all GWLS, and over all the Western Cape basins, but is enhanced over the Olifants and Gouritz basins (+19 mm month^{-1}). Since more water is lost through evaporation, there is an associated decrease in streamflow over many of the region's channels (+10 mm month^{-1}), but particularly over the Olifants and Gouritz basins (+19 mm month^{-1}). This is consistent with the decreasing trend in future projection of channel discharge entering the largest dam in the Western Cape at Theewaterskloof (TWT; Figure 7.1) and reaching about –2 m^3 s^{-1} by the end of the century. While there are few studies on the hydrological projections for the Western Cape, several studies recognize that this region has historically experienced increased surface aridity due to decreased precipitation. The hydrological projections here are in line with historical analysis, which found increased surface temperature, decreases in precipitation, and occurrence of dry spells, which have depleted water resources in the Southwest Cape (Jury, 2018).

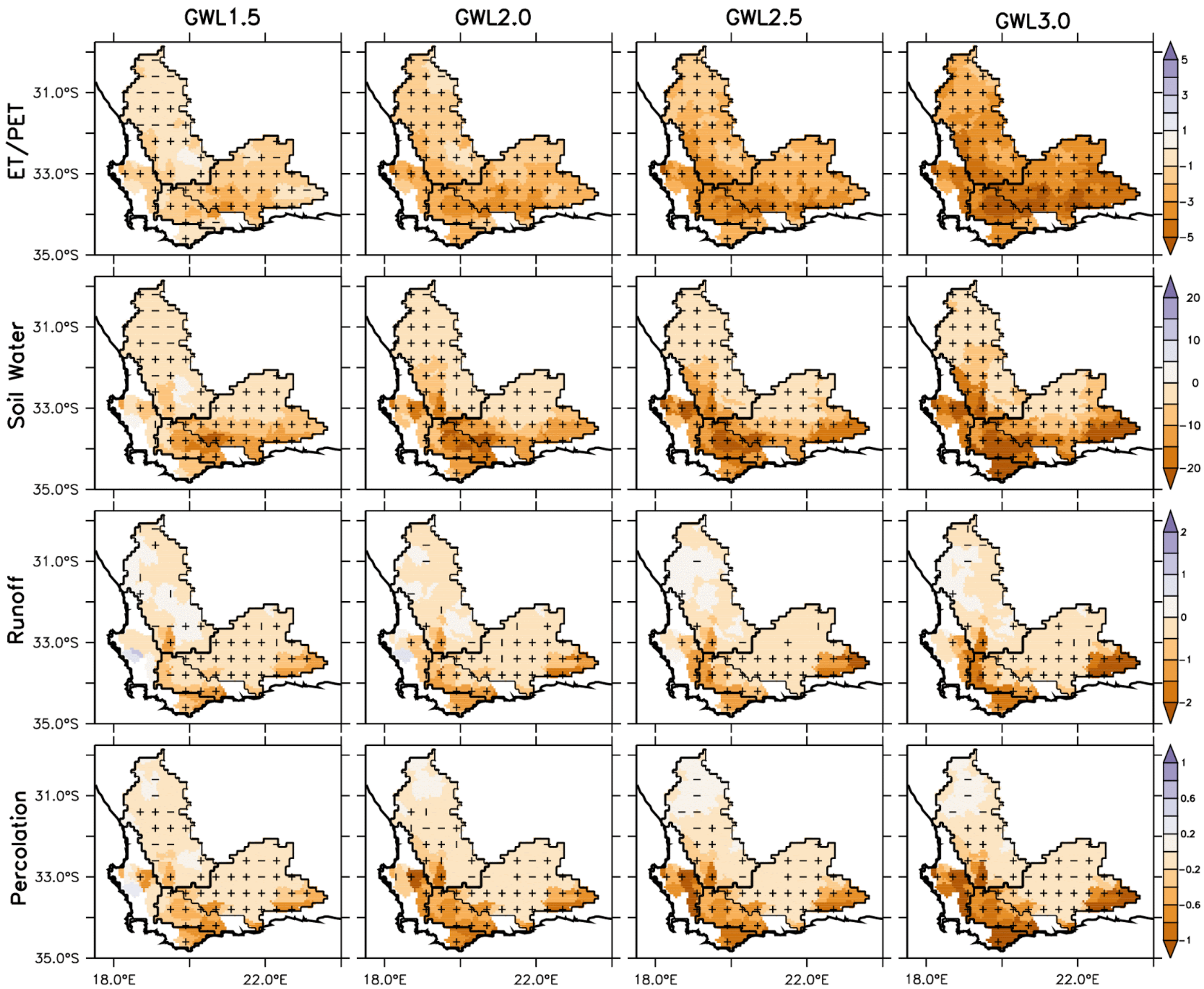

Figure 7.3: Same as Figure 7.2, except for ET/PET (%), soil water (mm month^{-1}), surface runoff (Runoff, m^3 s^{-1}) and percolation (mm month^{-1}).

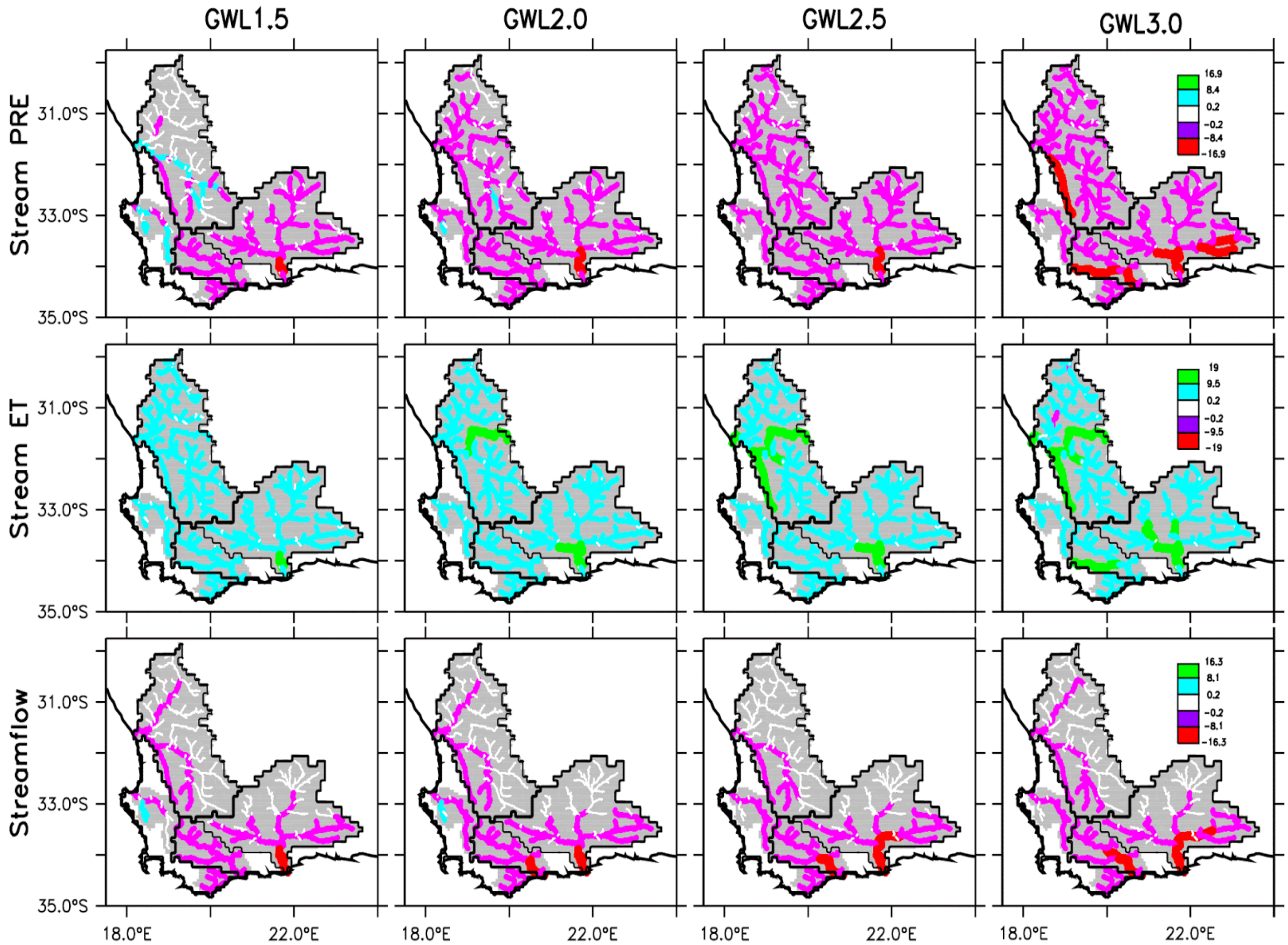

Figure 7.4: Same as Figure 7.2, but for channel variables: precipitation (mm month^{-1}), stream ET (mm month^{-1}), and streamflow (m^{3} s^{-1}).

7.4. Summary

This chapter has examined the projected impacts of climate change on hydrological drought in the WRB. We applied the calibrated SWAT+ model with biased corrected CORDEX datasets to simulate future spatial and temporal hydrological conditions over the basins for different GWLs. The results of this chapter suggest:

- The time series of projected climate changes across the Western Cape feature an increase in temperature and potential evaporation, but a decrease in precipitation and all the hydrological variables.
- The projected changes in precipitation (PRE) are more complex than those of T_{mean}.

- The projected decrease in hydrological variables can be linked to the decrease in PRE, and the spatial distribution of these hydrological changes is consistent with that of PRE.

These results of this chapter highlight the potential impacts of climate change on hydrological drought and detail the impacts on the spatial and temporal distribution of hydrological variables in the WRB. These streamflow and hydrological drought projections are essential sources of information for future water resources strategic planning and management, particularly in water-scarce regions such as Western Cape. As such, the results of the study have application in improving water security in the WRB.

Chapter 8:
Using land-use change to mitigate future impacts of climate change on hydrological drought in the Western Cape.

This chapter presents and discusses the results of the potential impacts of climate change and land use change on hydrological drought in the Western Cape River Basins (WRB). The results are presented and discussed in two parts. The first section details the impacts of each LULC changes (i.e., FrLand, SrLand, CrLand, and GrLand) on the hydrological variables (e.g., curve number (CN), ET, ET/PET, soil water (SW), percolation (PERC), Runoff, water yield (WYLD), and streamflow over the Western Cape River Basin, and are discussed for different global warming levels (GWLs; i.e., 1.5 °C, 2.0 °C, 2.5 °C and 3.0 °C, hereafter referred to as GWL 1.5, GWL 2.0, GWL 2.5 and GWL 3.0, respectively). The second section details a comparison of the impacts of land-use change with climate change projections as linked to changes in drought frequency.

8.1 Impacts of land-use change

The impacts of the LULC changes (*i.e.,* FrLand, SrLand, CrLand, and GrLand) on the hydrological projections can be explained through the influence of the LULC changes on the curve number (CN2; Figure 8.1). With FrLand, there is a decrease in CN2, which is consistent with the area of mixed forest land-use change (CN of about –3; Figure 8.1 and Figure 3.4b). The lower runoff potential is linked to more permeable soil surface and hence, there is less runoff from rainfall. As such, FrLand increases the amount of soil water available over the basin. For instance, soil water increases occur over parts of the southern Berg (+2 mm month^{-1}) basin, and the southwest Breede (+2 mm month^{-1}) basin. The increase in soil water may be due to the deeper rooting network of trees, which alters the physical properties of the upper soil layers, improving infiltration and percolation. As the amount of available soil water at the surface increases, more water is available for conversion through evapotranspiration (ET). Thus, for FOMI, ET also increases over these parts of the Berg and Breede (+0.5 mm month^{-1}) that are spatially comparable to that of soil water. However, although FrLand generally decreases runoff over the region (–0.2 mm month^{-1}), particularly over parts of the central Berg and western Breede (–0.5 mm month^{-1}), FrLand also increases the streamflow over most basins. The largest increases in streamflow occur over parts of the western Olifants, the northern Berg and the south-eastern Gouritz (about +61.9 $m^3 s^{-1}$; Figure 8.1). Decreases in streamflow occur only in some sub-basins of the western Breede and southern Berg (about –61.9 $m^3 s^{-1}$). These hydrological changes suggest the increase in streamflow is unlikely due to surface runoff (from precipitation runoff over the landscape i.e., overland flow) but rather due to percolation of water past the soil profile (subsurface) to become groundwater recharge, or via lateral movement in the profile (interflow), which eventually reaches streamflow (not shown). Several studies confirm that forests may have a positive impact on soil hydraulic properties, by functioning as water harvesters and contributing to infiltration, deeper drainage, and groundwater recharge (e.g., Bargués Tobella et al., 2014; Luo et al., 2020).

The hydrological impact of SrLand is similar to that of FrLand. With SrLand, there is a decrease in CN (of about 8) over the areas where shrubland restoration replaces bare ground (Figure 8.1 and Figure 3.4c). This occurs particularly over sub-basins of the northern and central Olifants and northern Gouritz. Over the central and northern Olifants sub-basins, SrLand increases soil water (+2.0 mm $month^{-1}$) and increases ET (+0.4 mm $month^{-1}$). But SrLand decreases runoff over the region (–0.2 mm $month^{-1}$), particularly over the central Olifants and northern Gouritz (–0.5 mm $month^{-1}$). However, unlike FrLand, SrLand decreases water yield over most Western Cape basins. The streamflow decreases (about –61.9 $m^3 s^{-1}$) occur over the Olifants, Gouritz and Breede. However, SrLand does not influence water yield over the Berg since no land-use change occurred in this basin. Overall, these hydrological changes suggest that the restoration of shrubland may decrease streamflow and may have negative impacts on the water security of the region.

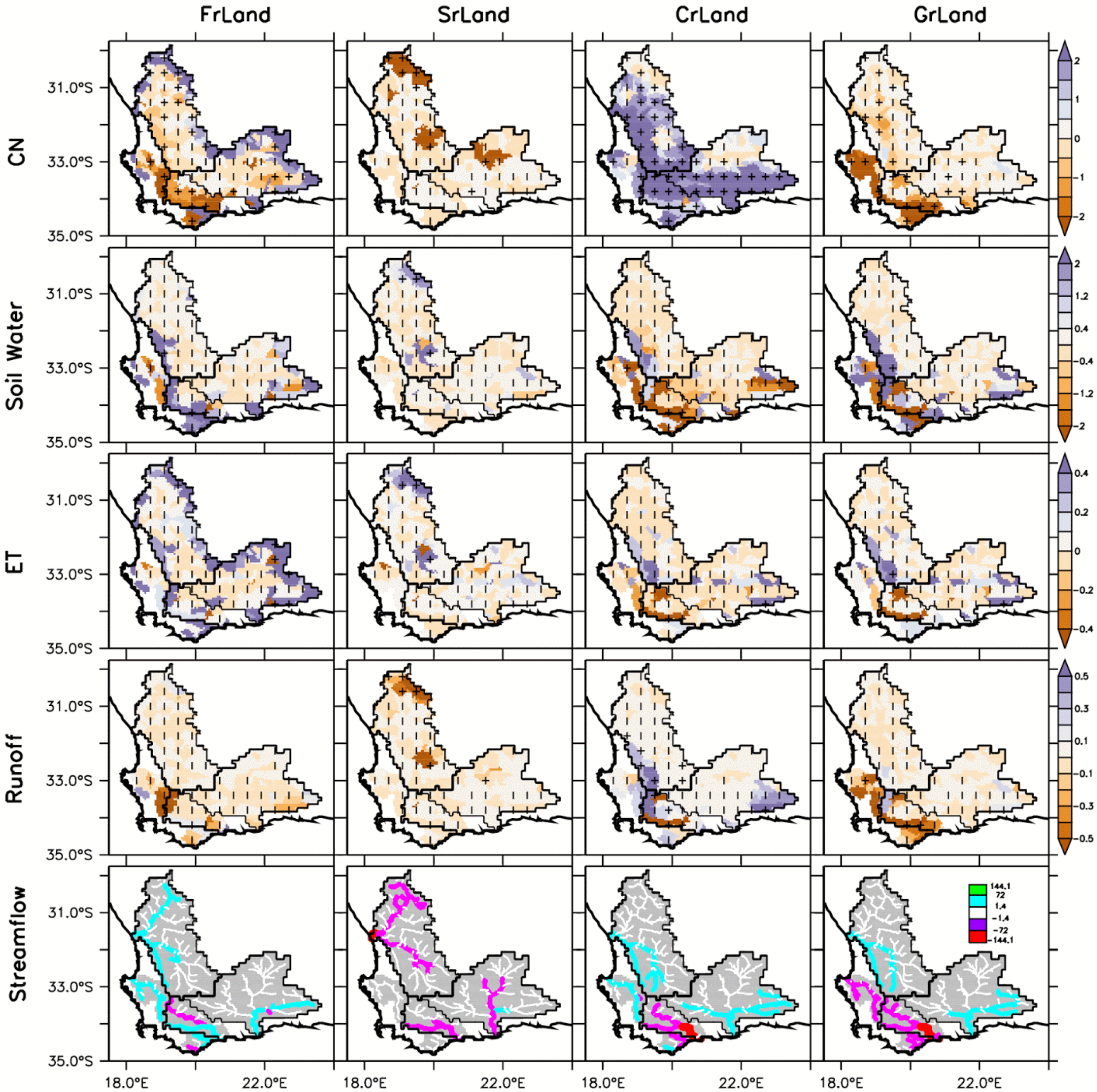

Figure 8.1**:** Impacts of LULC changes on hydrological variables over the Western Cape River Basins: CN (unitless), soil water (mm month^{-1}), surface runoff (Runoff, m^3 s^{-1}) and streamflow (m^3 s^{-1}). Note that the vertical line (|) indicates where at least 80% of the simulations agree on the sign of the changes, and a horizontal line (−) indicates where at least 80% of the simulations agree that the change is of statistical significance (at 99% confidence level). The cross (+) shows where the change is robust, that is, if both conditions are satisfied.

The response of CrLand is complex, as it includes both increases and decreases in hydrological conditions. CrLand (i.e., expansion of cropland/dryland area) increases the curve number (CN), such that the area of LUC is spatially consistent with the area of higher CN (about +5; Figure 8.1 and Figure 3.4d). While CrLand decreases soil water over some sub-basins, it increases it in other sub-basins. For instance, it decreases soil water over the eastern and southern Berg (–2 mm month^{-1}), the northern and southern Breede (–2 mm month^{-1}) and the eastern Gouritz (–1.6 mm month^{-1}), but it increases soil water over southwestern Olifants (+0.8 mm month^{-1}). However, the hydrological response of CrLand differs from FrLand, in that, while the soil water changes are spatially consistent with ET in some basins, they are not consistent in others. For instance, the decrease in ET (–2 mm month^{-1}) over the Breede is consistent with the decrease in soil water over the basin, and the increase in ET (+0.4 mm month^{-1}) over the southwestern Olifants also agrees with the increase in soil water over this sub-basin. However, the increase in ET (+0.2 mm month^{-1}) over the southern Breede is not consistent with the decrease in soil water over the sub-basins. Moreover, CrLand increases runoff and streamflow over the southern Olifants and eastern Gouritz (+0.5 mm month^{-1} and about +61.9 m^3 s^{-1}) but decreases them over much of the Breede (–0.5 mm month^{-1} and up to about –123.8 m^3 s^{-1}, respectively). Unlike with FrLand, the increase in the streamflow obtained with CrLand is likely due to an increase in surface runoff over the landscape. It may be that the percolation rate is slower with CrLand than with FrLand. Nevertheless, the CrLand changes have complex impacts on the hydrology of the region, possibly due to the complex topography and local soil conditions.

The hydrological response to GrLand is also complex. GrLand (i.e., restoration of grassland) generally decreases the curve number (CN), with areas of lowest CN_2 spatially consistent with areas converted from CrLand to GrLand (CN about –4; Figures 8.1 and 3.4e). GrLand is associated with a lower curve number (compared to CrLand) and hence, less runoff from rainfall. Compared to CrLand, GrLand increases soil water over many basins. For example, soil water increases occur over the southwestern Olifants (+2 mm month^{-1}), the eastern Gouritz (+2 mm month^{-1}) and several sub-basins of the Berg. Although, like CrLand, for GrLand soil water decreases occur over the southern margins of the Breede (–2 mm month^{-1}). Even so, the changes in ET for the two land-uses (CrLand and GrLand) are spatially comparable. Nevertheless, unlike CrLand, GrLand reduces runoff (–0.5 mm month^{-1}) over many basin areas. And, while changes in streamflow for the two land-uses are similar over the Olifants and Gouritz basins (increases), and over the Breede (decreases), unlike CrLand, GrLand reduces streamflow over the Berg (–61.9 m^3 s^{-1}).

8.2 A comparison of the impacts of land-use change with climate change projections

The impacts of projected future climate change decrease all the hydrological variables over the basins studied herein, but the percentage of the decrease varies among the variables and with the GWL (Figure 8.2). Generally, the magnitude of the projection increases for higher GWLs, with the largest impacts of land-use change under GWL3.0. For instance, at GWL3.0 while the ET decreases by only 10%, the percolation (PERC) decreases by more than 40%. The decrease in ET may be linked to the projected decreases in PRE, which makes less water available for evaporation over the basins. The capability of the basin to meet atmospheric water demand (ET/PET) also decreases (by –20%), not only because the ET decreases, but because PET, the atmospheric water demand, is also projected to increase across the basins (Figure 8.2). These changes drive the decrease in other hydrological variables because they alter the overall soil water (SW) of the river basin areas, inducing a 30% decrease in soil water, a 40% decrease in PERC and a 30% decrease in runoff. Since less water percolates into deep soil layers, it also decreases the water yield (WYLD). Hence, there is also a decrease in water yield (–30%) and discharge (–35%) at the Theewaterskloof dam (TWT). This pattern is similar for successive GWLs (1.5, 2.0, and 2.5; Figure 8.2a, b, and c, respectively), except that the magnitude of the decrease in hydrological variables is lower than that of GWL3.0.

The impacts of some land-use changes offset the climate change impacts on the mean hydrological variables (Figure 8.2). For example, CrLand may increase the runoff by 10% under GWL3.0. This may mitigate the impacts of climate change on runoff (to about 30%). While not across the entire Western Cape, CrLand may also offer potential climate change offset due to its impact on water yield at the Theewaterskloof dam (TWT), where CrLand may increase discharge (+5%). For FrLand, SrLand, and GrLand land-use changes, the impact on the hydrological variables is almost negligible relative to the impact of future climate change.

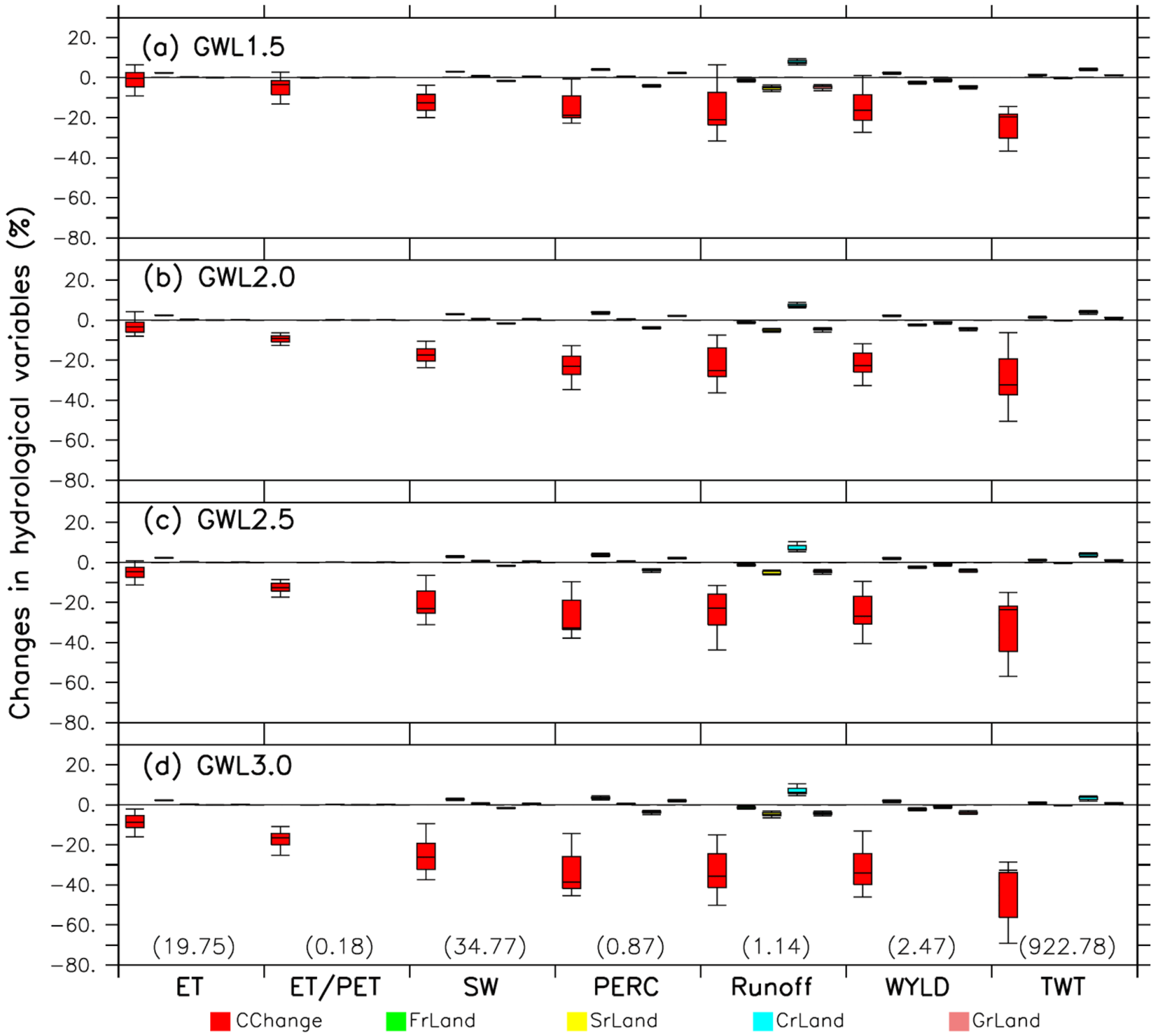

Figure 8.2: A comparison of the impacts of climate change and LULC change (FrLand, SrLand, CrLand, and GrLand) on hydrological variables: ET, ET/PET, soil water (SW), percolation (PERC), Runoff (RF), water yield (WYLD) and streamflow at Theewaterskloof (TWT), over the Western Cape River Basin at different global warming level. The present-day climatological value for each variable is indicated in the bracket.

The changes in the hydrological variables are also linked to changes in drought frequency (Figure 8.3). The projections indicate that impacts of climate change may increase drought frequency in the future. Climate change may increase both Standardized Precipitation Evapotranspiration Index (SPEI; about +75 months decade^{-1}) and Standardized Precipitation Index (SPI; +20 months decade^{-1}) drought frequency (Figure 8.3). Note that, while SPEI is more severe than SPI drought, for both indices, a moderate drought is defined as a condition in which the drought index (SPI or SPEI) is less than or equal to −1.0. These projections are in line with those of a previous study, which suggests that changes in the intensity and frequency of droughts are weaker when using the SPI than the SPEI, and that SPI projections may in fact underestimate the influence of global warming on drought because they do not account for the influence of PET (Naik and Abiodun, 2020). The changes in the SPEI/SPI drought provide the upper/lower range that is linked to changes in hydrological drought for other variables. For instance, climate change may increase the frequency of the soil water drought index (SWI) by +38 months decade^{-1}, the percolation drought index (PERCI) by +30 months decade^{-1}, the runoff drought index (RFI) by +10 months decade^{-1}, and the water yield drought index (WYLDI) by +12 months decade^{-1}.

Some land-use changes may offset the climate change impacts on the hydrological drought variables (Figure 8.3). Most notably changes occur under GWL3.0, where FrLand may decrease the SWI, PERCI and the WYDLI, and it may thus mitigate the impacts of climate change on both types of droughts by about –3 to –5 months decade^{-1}. SrLand may increase the RFI by –3 months decade^{-1}. Similarly, CrLand may also decrease the RFI and may thus mitigate the impacts of climate change by about –5 months decade^{-1}. However, while GrLand may decrease the PERCI by about –3 months decade^{-1}, it may increase the impacts of climate change on RFI by about +5 months decade^{-1}. This pattern is similar for successive GWLs (1.5, 2.0, and 2.5; Figure 8.3 a, b, and c, respectively). Generally, however, the impact of the hydrological variable's drought is almost negligible relative to the frequency of future climate change drought.

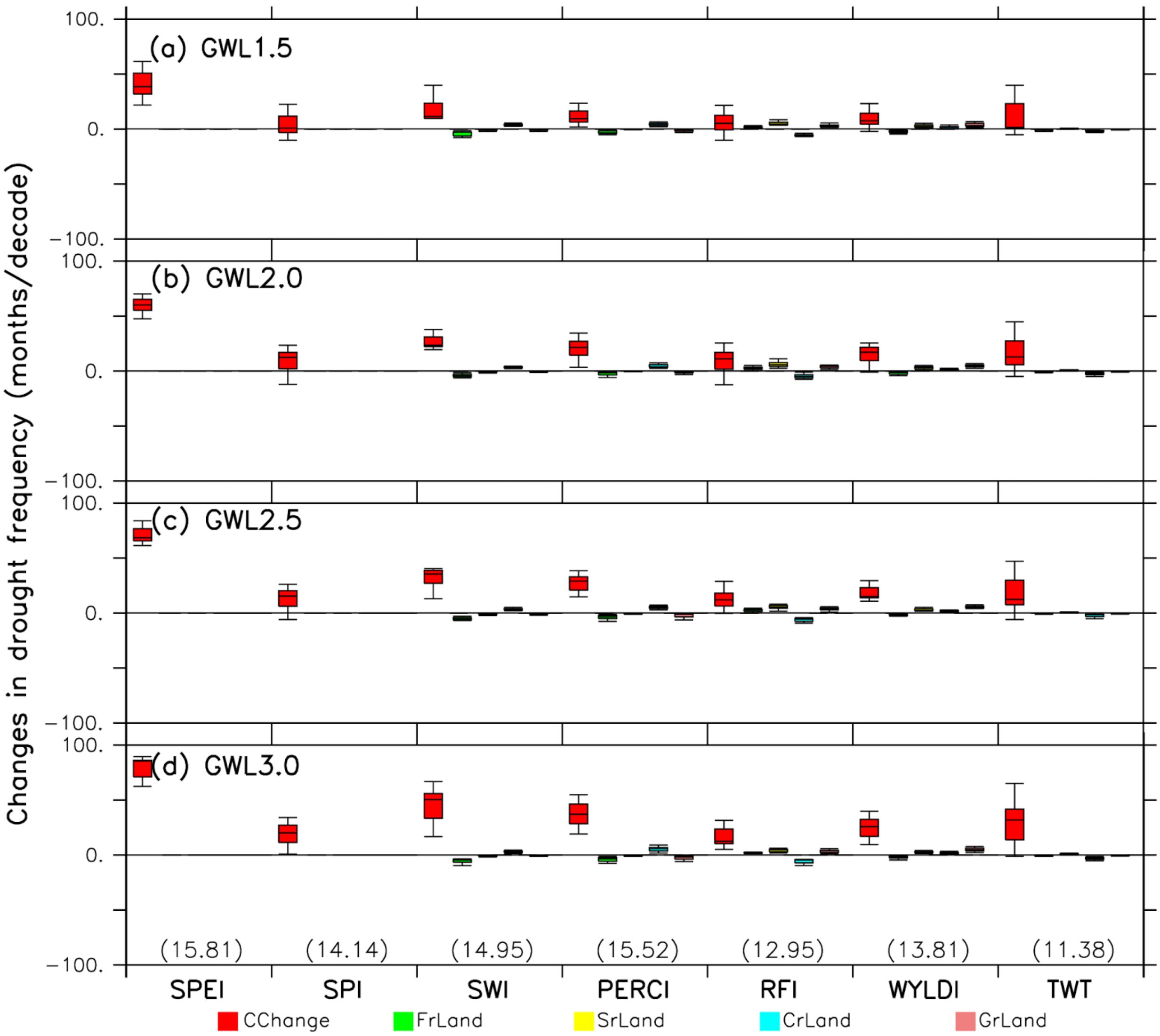

Figure 8.3: A comparison of the impacts of climate change (CChange) and LULC change (FrLand, SrLand, CrLand, and GrLand) on the frequency of droughts (SPEI, SPI, SWI, PERCI, RFI, WYLDI and TWT) over the Western Cape River Basin at different global warming level (GWL1.5, GWL2.0, GWL2.5 and GWL3.0). The present-day climatological value for each variable is indicated in the bracket.

8.3 Summary

This chapter has examined the extent to which LULC changes can reduce the projected impacts of climate change on hydrological drought in the WRB. We applied the calibrated SWAT+ model with biased corrected CORDEX datasets to simulate future hydrological conditions over the basin under different LULC changes and studied the sensitivity of the hydrological variables and drought indices to the LULC changes. The land-use scenarios considered are the spread of forest, the restoration of shrubland, the expansion of cropland, and the restoration of grassland. The results of this chapter suggest:

- The climate change projections feature an increase in temperature and potential evaporation, but a decrease in precipitation and all the hydrological variables.
- The drying occurs across the Western Cape, with the magnitude increasing with higher global warming levels (GWLs).
- The land-use changes alter these climate change impacts through changes in the hydrological water balance.
- The spread of forest (FrLand) increases streamflow and decreases runoff, while the restoration of shrubland (SrLand) decreases streamflow and runoff.
- The hydrological responses of cropland (CrLand) and grassland (GrLand) are more complex as it includes both increases and decreases in hydrological conditions.

These results suggest that the impacts of FrLand, SrLand, CrLand and GrLand on the hydrological variables and drought frequency are negligible relative to the impact of future climate change. Note that the simulations agree on the sign of the changes for some hydrological variables, for some parts of WRB, but the change is generally not statistically significant. Hence, land-use changes in the Western Cape may not be the most efficient strategies for mitigating the impacts of climate change on hydrological drought over the region. The results of the study have application in improving water security in the WRB.

Chapter 9:
Conclusion & Recommendations

9.1 Conclusion

In an effort to better characterize and mitigate future drought impacts, this dissertation examined the extent to which LULC changes can reduce the projected impacts of climate change on hydrological drought in the Western Cape River Basins (in South Africa). To that end, this dissertation has successfully calibrated, validated, and applied the SWAT+ model. We applied the calibrated SWAT+ model with biased-corrected CORDEX datasets to simulate future hydrological conditions over the basin under different LULC changes and studied the sensitivity of the hydrological variables and drought indices to the LULC changes. This research investigated the influence of bias-correction of climate datasets on the quality of the hydrological simulation before quantifying the impacts of climate change and LULC scenarios on characteristics of hydrological drought in the future (under the RCP8.5 scenario). The land-use scenarios considered are the spread of forest, the restoration of shrubland, the expansion of cropland, and the restoration of grassland. The results of this research can be summarized as follows:

- The SWAT+ gives satisfactory simulation of hydrological processes over the WRB. It captures the annual cycle and inter-annual variability of the observed streamflow at the hydrological stations (i.e., E2H003, G1H013, H7H006, and J1H019) during both calibration and validation periods. It also reproduces the timing and magnitude of most peak flows at the stations and shows good agreement between the simulated and observed monthly streamflows. The coefficient of correlation (r) between the simulated and observed streamflow is more than 0.5 over most of the stations. However, there are notable biases in the simulations. Generally, the model provided a satisfactory representation of hydrological processes in Western Cape basins.

- The CORDEX models correctly capture the spatial distribution of major climate variables over the Western Cape region and reproduce the essential climatic features. The models also give a credible simulation of the annual cycles of the climate variables over each of the four basins. However, the accuracy of the model's performance in simulating the drought intensity and frequency over the river basins depends on the index used in characterising the drought.

The SWAT+ simulation that used the bias-corrected CORDEX datasets (QDM, MBCr and MBCn methods) better capture the spatial distribution of hydroclimatic variables than the simulation that used original CORDEX datasets. Bias-correction also improves the annual cycles of hydroclimatic variables over the basin.

- The future climate change projections over the river basins features an increase in temperature and potential evaporation. A robust drying signal occurs across the Western Cape, but this varies depending on the GWL (i.e., increases with higher global warming levels), the river basin, and the drought index used. For instance, when using the SPEI, drought increases across the Western Cape for all GWLs, although the drying pattern is not homogenous across the region. When using the SPI, drought may also increase over the region, but the intensity and the spatial distribution is different. Nevertheless, there is no substantial trend in the time series of precipitation and hydrological variables. However, a decrease in precipitation and hydrological variables (soil water, runoff, and streamflow) is projected over the Western Cape region, inducing an increase in frequency and intensity hydrological drought.
- Over the WRB, the spread of forest enhances the climate changes impacts on runoff (by further decreasing runoff) and reduces the climate change impacts on the streamflow and streamflow droughts (by further decreasing the streamflow). The restoration of shrubland enhances the climate change impacts by runoff and streamflow and the associated droughts (by decreasing both variables). The expansion of cropland and the restoration of grassland produce more complex changes, featuring increases and decreases in hydrological variables in different parts of the river basins. The impacts of FrLand, SrLand, CrLand and GrLand on the hydrological variables and drought frequency are negligible relative to the impact of future climate change. The results suggest that these land-use changes may not be the most efficient strategies for mitigating the impacts of climate change on hydrological drought over the Western Cape region.

The results of the research show that while LULC change scenarios can reduce the impacts of climate change on some hydrological drought in some parts of the river basins, they can also enhance the impacts on other types of hydrological drought. Nevertheless, the impacts of the land-use change scenarios are small compared to the climate change impacts. That is, while these extreme LULC change scenarios could either mitigate or aggravate the climate change impacts on hydrological drought frequency over the river basins, the magnitude of the impacts is in most cases less than 30% of the climate change impacts. This implies that LULC changes may not be sufficient in offsetting the climate impacts over the basin; hence, there is a need to explore other climate change mitigation options over the basins. In addition, as all the LULC changes reduce the climate change impacts on one hydrological drought and aggravate the impacts on another, there is a need to weigh the pros and cons of any LULC change before implementing it. That is, the local impacts of the land-use changes on hydrological variables are subjective and likely dependent on the end user upstream/downstream in each basin area.

The approach used in this study only offers insight into the potential hydrological impacts of using LULC changes to mitigate droughts in the WRB. It is by no means intended to be prescriptive with regard to land-use activities for a river basin, but it may assist stakeholders and decision makers in making better decisions for land management and water resource planning in a future impacted by drought due to climate change. Hence, it is broadly anticipated that the results of the study may have application in improving water security in the WRB. Future research avenues may support a further understanding of the potential for land-use to mitigate drought due to climate change.

9.2 Recommendations

For simplicity and ease of interpretation, all the LULC change experiments in this project have assumed that the future climate projection would sustain the prescribed LULC patterns, so the vegetation did respond to the climate variability and change. This may not be the case in reality. Hence, there is a need to extend this study to perform more sophisticated experiments that would enable vegetation to respond to future atmospheric conditions (modelling using vegetation-climate feedbacks under climate change). The results of such experiments may alter the magnitude of the LULC changes obtained in this study. Nevertheless, the present project has provided the framework for model set-up and foundation for interpretation for such experiments.

Solar radiation management (SRM) has been proposed as a global and more effective option to mitigate climate change impacts. SRM aims to eliminate global warming by artificially reflecting a small amount of inbound sunlight out into space. However, although SRM is still in its early stage of research, controversy exists because its full effect on different components of the earth system is unknown. Several studies have shown that some types of SRM may, at high latitudes, alter snow depth, and sea ice, or reduce the current rate of permafrost degradation, partially offset the poleward shift or alter the storm-tracks, or impact tropical and subtropical atmospheric circulation changes (e.g., Lee 2019; Karami, 2020; Gertler, 2020). Substantial precipitation changes may result from stratospheric heating which generally leads to drying in many wet tropical regions (Simpson, 2019). Over Sub-Saharan Africa, Pinto et al (2020) found the benefit of SRM as mitigation strategy is larger for temperature than precipitation and that there is a regional diversity in the climate response: while SRM is effective over Central and East Africa, changes over West and Southern Africa are mixed. Hence, there is now a need to investigate the potential impacts of SRM on the hydrological drought over the basins and compare the results with that of LULC obtained in the present project. This will provide an opportunity for comparing global and local climate change mitigation strategies over the basins.

It may also be that, as ensemble climate change projections (like CORDEX datasets here) improve, SWAT+ may better simulate the local hydrology. Future research avenues may also consider different future emissions trajectories (e.g., a newly built range of the "Shared Socio-economic Pathways"; SSPs). Further studies may also make use of alternative drought indices (for comparison) that have not been considered here or translate these future climate change drought projections to hydrological drought impacts in selected river basins. As was illustrated in this research, different indices have different strengths and weaknesses.

The robustness of the bias correction results can also be improved in several ways. The results are based on only one approach of bias correction (QDM) and its variants (MBCr and MBCn). Future studies might test alternative bias-correction approaches, like linear scaling (LS), power transformation of precipitation, empirical quantile mapping, gamma quantile mapping, and gamma-pareto quantile mapping (Mendez et al., 2020). In addition, only one climate dataset is investigated in this study. Future research may also explore other datasets (e.g., Coupled Model Intercomparison Project Phase 6, CMIP6) to determine whether the influence of bias correction is specific to this climate ensemble dataset. Moreover, the results presented here may be region specific. For example, our contemporary analysis (not included here) indicates that the performance of QDM differs in the tropical regions (where QDM seems to outperform MBC). Hence, there is a need to expand the analysis provided here over the entire African domain. Furthermore, the study has only considered the simulation for present-day climate (1970–2031), but the influence of bias correction on future climate change projections for different GWLs need to be considered too. Such studies would better inform policymakers in their efforts to manage water resources sustainably and to adapt to drought more effectively. Nevertheless, the results of the present study have shown that applying bias correction on climate model data before using this as input data for SWAT+ is valuable because it improves simulations of the hydrological processes and makes the simulated variables closer to the observed. However, the bias-correction improvements are minimal in the case of the drought indices themselves.

While the focus of the research here was on meteorological and hydrological drought, future work may consider the agricultural and socio-economic aspects of LULC mitigation strategies for the region. Research may also consider how other alternative land-use change combinations (e.g., by the expansion of viticulture or urbanization expansion of Cape Town city), which is also relevant in the Western Cape, may affect future drought. Such analysis may also be useful to assess the potential for the mitigation of PET through LULC changes, and would better inform water policymakers in efforts to create sustainable and effective drought adaptation efforts.

Appendix

Table A1: CN values of different soil types and land use types.

SWAT+ land cover classification	Description	CN for different Hydrological Soil Group				Hydrological condition
		A	B	C	D	
URMD	Urban	98	98	98	98	Poor
CRDY	Straight row crops	72	81	88	91	Poor
CRGR	Straight row crops	67	78	85	89	Good
CRWO	Woods-grass combination	43	65	76	82	Fair
GRAS	Pasture-grassland	39	61	74	80	Good
SHRB	Brush-weed-grass mixture	30	48	65	73	Good
SAVA	Woods-grass combination	32	58	72	79	Good
FODB	Deciduous evergreen forest	33	58	72	77	–
FOEB	Evergreen broadleaf forest	30	55	70	77	–
FOMI	Mixed forest	32	57	71	77	–
WATR	Water	100	100	100	100	–
BSVG	Fallow	77	86	91	94	–

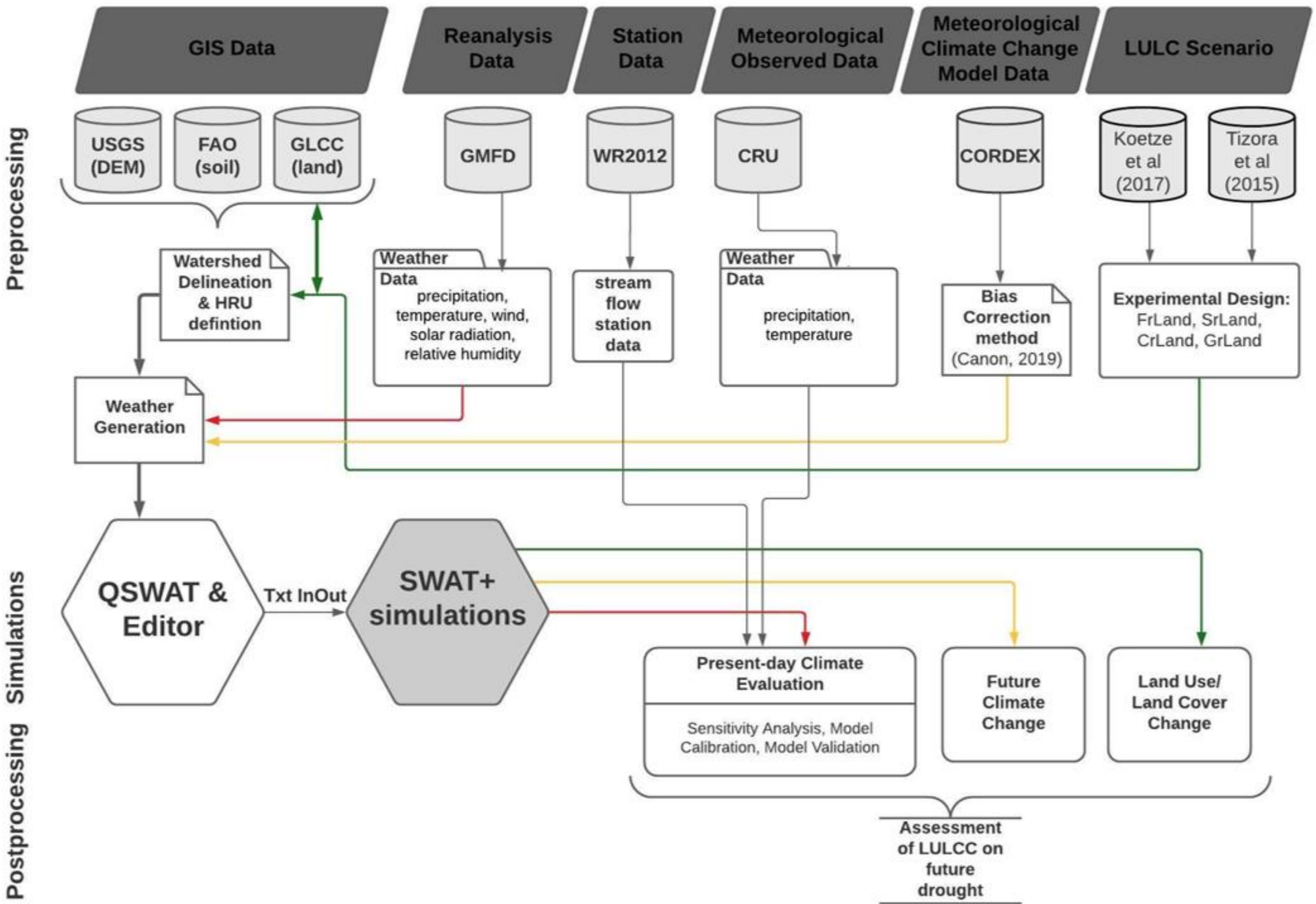

Figure A1: Schematic flow diagram of the Soil and Water Assessment Tool+ user-defined methodology for simulations produced.

Declaration III

- Conflicts of interest/Competing interests:

  The author declares that there is no conflict of interest and no competing interest in this research dissertation.

- Availability of data and material & Code availability:

  The datasets generated and/or analysed during this study are available from the author on reasonable request. All the scripts, datasets and FORTRAN coding materials used in this study can be freely made available but are subject to approval from the University of Cape Town's (via their data sharing policy). Please email myranaik@gmail.com with your request.

- Ethics approval & Consent to participate: Not applicable.

References

Aadhar, S. and Mishra, V., 2017. High-resolution near real-time drought monitoring in South Asia. Scientific Data, 4(1), pp.1–14.

Abbott, M.B., Bathurst, J.C., Cunge, J.A., O'Connell, P.E. and Rasmussen, J., 1986. An introduction to the European Hydrological System – Systeme Hydrologique European, "SHE" 1: History and philosophy of a physically-based, distributed modelling system. Journal of Hydrology, 87(1-2), pp.45–59.

Abiodun, B., Ujeneza, E.L., Meque, A., Naik, M., Omar, S.A., Lawal, S., Nguvava, M., Gore, M., Molepo, K., Maoyi, M. and Mukwenha, P., 2018. Regionally extensive droughts and climate change in southern Africa: Mechanisms, model reliability and projections. Water Research Commission Report, Project No. 2317/1, pp.1–18. ISBN 978-1-4312-0973-6.

Abiodun, B.J., Makhanya, N., Petja, B., Abatan, A.A. and Oguntunde, P. G. 2019. Future projection of droughts over major river basins in Southern Africa at specific global warming levels. Theoretical and Applied Climatology, 137(3), pp.1785–1799.

Abiodun, B.J., Mogebisa, T.O., Petja, B., Abatan, A.A. and Roland, T.R., 2020. Potential impacts of specific global warming levels on extreme rainfall events over southern Africa in CORDEX and NEX-GDDP ensembles. International Journal of Climatology, 40(6), pp.3118–3141.

Abiodun, B.J., Abatan, A.A., Petja, B., Nguvava, Naik, M., Mogebisa T., Makhanya N., and Yocgo R. 2021. Using land cover changes to reduce climate change impacts on hydrological droughts in the Vaal River Basin (under review).

AghaKouchak, A., Farahmand, A., Melton, F.S., Teixeira, J., Anderson, M.C., Wardlow, B.D. and Hain, C.R. 2015. Remote sensing of drought: Progress, challenges, and opportunities. Reviews of Geophysics, 53(2), pp. 452–480.

Ahmed, K.F., 2011. Bias Correction and Downscaling of Climate Model Outputs Required for Impact Assessments of Climate Change in the US Northeast. Master's Thesis. 212. https://opencommons.uconn.edu/gs_theses/212.

Akinsanola, A.A. and Ogunjobi, K.O. 2017. Evaluation of present-day rainfall simulations over West Africa in CORDEX regional climate models. Environmental Earth Sciences, 76(10), pp.1–20.

Albhaisi, M., Brendonck, L. and Batelaan, O., 2013. Predicted impacts of land use change on groundwater recharge of the upper Berg catchment, South Africa. Water SA, 39(2), pp.211–220.

Al-Quraishi, A.M., Gaznayee, H.A. and Crespi, M., 2021. Drought trend analysis in a semi-arid area of Iraq based on Normalized Difference Vegetation Index, Normalized Difference Water Index and Standardized Precipitation Index. Journal of Arid Land, 13(4), pp.413–430.

Andreadis, K.M., Clark, E.A., Wood, A.W., Hamlet, A.F. and Lettenmaier, D.P. 2005. Twentieth-century drought in the conterminous United States. Journal of Hydrometeorology, 6(6), pp. 985–1001.

Angelidis, P., Maris, F., Kotsovinos, N. and Hrissanthou, V., 2012. Computation of drought index SPI with alternative distribution functions. Water Resources Management, 26(9), pp.2453–2473.

Araujo, J.A., Abiodun, B.J. and Crespo, O. 2016. Impacts of drought on grape yields in Western Cape, South Africa. Theoretical and applied climatology, 123(1), pp.117–130.

Arnold, J.G., Moriasi, D.N., Gassman, P.W., Abbaspour, K.C., White, M.J., Srinivasan, R., Santhi, C., Harmel, R.D., Van Griensven, A. and Van Liew, M.W. 2012. SWAT: Model use, calibration, and validation. Transactions of the ASABE, 55(4), pp.1491–1508.

Ashrafi, S.M., Gholami, H. and Najafi, M.R., 2020. Uncertainties in runoff projection and hydrological drought assessment over Gharesu basin under CMIP5 RCP scenarios. Journal of Water and Climate Change, 11(S1), pp.145–163.

Asoka, A., Gleeson, T., Wada, Y. and Mishra, V. 2017. Relative contribution of monsoon precipitation and pumping to changes in groundwater storage in India. Nature Geoscience, 10(2), pp.109–117.

Astuti, I.S., Sahoo, K., Milewski, A. and Mishra, D.R., 2019. Impact of land use land cover (LULC) change on surface runoff in an increasingly urbanized tropical watershed. Water Resources Management, 33(12), pp.4087–4103.

Ayar, P.V., Vrac, M. and Mailhot, A., 2021. Ensemble bias correction of climate simulations: preserving internal variability. Scientific Reports, 11(1), pp.1–9.

Ayugi, B., Tan, G., Ruoyun, N., Babaousmail, H., Ojara, M., Wido, H., Mumo, L., Ngoma, N.H., Nooni, I.K. and Ongoma, V., 2020. Quantile mapping bias correction on Rossby centre regional climate models for precipitation analysis over Kenya, East Africa. Water, 12(3), pp.1–16.

Azmi, M., Rüdiger, C. and Walker, J.P., 2016. A data fusion-based drought index. Water Resources Research, 52(3), pp.2222–2239.

Baker, T.J. and Miller, S.N., 2013. Using the Soil and Water Assessment Tool (SWAT) to assess land use impact on water resources in an East African watershed. Journal of Hydrology, 486, pp.100–111.

Bargués Tobella, A., Reese, H., Almaw, A., Bayala, J., Malmer, A., Laudon, H., and Ilstedt, U., 2014. The effect of trees on preferential flow and soil infiltrability in an agroforestry parkland in semiarid Burkina Faso. Water Resources Research, 50(4), pp.3342–3354.

Beguería, S. and Vicente-Serrano, S.M., 2013. SPEI: calculation of the standardised precipitation-evapotranspiration index. R package version, 1(6).

Beguería, S., Vicente-Serrano, S.M., Reig, F. and Latorre, B. 2014. Standardized precipitation evapotranspiration index (SPEI) revisited: Parameter fitting, evapotranspiration models, tools, datasets and drought monitoring. International Journal of Climatology, 34(10), pp. 3001–3023.

Behera, S.K. and Yamagata, T. 2001. Subtropical SST dipole events in the southern Indian Ocean. Geophysical Research Letters, 28(2), pp.327–330.

Bergström, S., 1995. The HBV model. Computer models of watershed hydrology., pp.443-476.

Betts, A.K., Ball, J.H. and Viterbo, P., 1999. Basin-scale surface water and energy budgets for the Mississippi from the ECMWF reanalysis. Journal of Geophysical Research: Atmospheres, 104(D16), pp.19293–19306.

Betts, A.K., Viterbo, P. and Wood, E., 1998. Surface energy and water balance for the Arkansas–Red River basin from the ECMWF reanalysis. Journal of Climate, 11(11), pp.2881-2897.

Bieger, K., Arnold, J.G., Rathjens, H., White, M.J., Bosch, D.D., Allen, P.M., Volk, M., and Srinivasan, R., 2017. Introduction to SWAT+, a completely restructured version of the soil and water assessment tool. JAWRA Journal of the American Water Resources Association, 53(1), pp.115-130.

Bischoff-Mattson, Z., Maree, G., Vogel, C., Lynch, A., Olivier, D. and Terblanche, D. 2020. Shape of a water crisis: Practitioner perspectives on urban water scarcity and 'Day Zero' in South Africa. Water Policy, 22(2), pp.193–210.

Blamey, R. and Reason, C.J.C. 2007. Relationships between Antarctic sea-ice and South African winter rainfall. Climate Research, 33(2), pp.183–193.

Bloomfield, J.P., Gong, M., Marchant, B.P., Coxon, G. and Addor, N., 2021. How is Baseflow Index (BFI) impacted by water resource management practices? Hydrology and Earth System Sciences, 25(10), pp.5355-5379.

Bonaccorso, B., Peres, D.J., Cancelliere, A. and Rossi, G., 2013. Large scale probabilistic drought characterization over Europe. Water Resources Management, 27(6), pp.1675–1692.

Botai, C.M., Botai, J.O., De Wit, J.P., Ncongwane, K.P. and Adeola, A.M., 2017. Drought characteristics over the Western Cape province, South Africa. Water, 9(11), pp.1–16.

Burke, E.J. and Brown, S.J., 2008. Evaluating uncertainties in the projection of future drought. Journal of Hydrometeorology, 9(2), pp.292–299.

Bohatch, T. 2017. What's causing Cape Town's water crisis? Population growth, drought and climate change threaten the city's water supply. GroundUp News, Cape Town.

Boken, V.K., Cracknell, A.P. and Heathcote, R.L. 2005. Monitoring and predicting agricultural drought: a global study. Oxford University Press.

Bridgman, H.A. and Oliver, J.E. 2014. The global climate system: Patterns, processes, and teleconnections. Cambridge University Press.

Cai, W., Cowan, T., Briggs, P. and Raupach, M. 2009. Rising temperature depletes soil moisture and exacerbates severe drought conditions across southeast Australia. Geophysical Research Letters, 36(21), pp.1–5.

Calzi, D.L., 2013. Dams, Drought and Energy-Water Interdependencies, pp.178. Nova Publishers. New York.

Campbell, I. and Barlow, C., 2020. Hydropower development and the loss of fisheries in the Mekong River Basin. Frontiers in Environmental Science, (8), pp.1–10.

Cannistra, T., 2016. Challenges, Solutions, and Future Directions for Statistical and Dynamical Downscaling of Global Climate Models, pp.1–11.

Cannon, A.J., Sobie, S.R. and Murdock, T.Q., 2015. Bias correction of simulated precipitation by quantile mapping: How well do methods preserve relative changes in quantiles and extremes? Journal of Climate, 28(17), pp.6938–6959. doi:10.1175/JCLI-D-14-00754.1

Cannon, A.J., 2018. Multivariate quantile mapping bias correction: An N-dimensional probability density function transform for climate model simulations of multiple variables. Climate Dynamics, 50(1), pp.31–49.

Chang, H. 2007. Comparative streamflow characteristics in urbanizing basins in the Portland Metropolitan Area, Oregon, USA, Hydrological Process., 21, pp.211-222.

Chattopadhyay, S., Edwards, D.R., Yu, Y. and Hamidisepehr, A., 2017. An assessment of climate change impacts on future water availability and droughts in the Kentucky River Basin. Environmental Processes, 4(3), pp.477–507.

Chen, J., Brissette, F.P., Chaumont, D. and Braun, M., 2013. Finding appropriate bias correction methods in downscaling precipitation for hydrologic impact studies over North America. Water Resources Research, 49(7), pp.4187–4205.

Chokkavarapu, N. and Mandla, V.R., 2019. Comparative study of GCMs, RCMs, downscaling and hydrological models: a review toward future climate change impact estimation. SN Applied Sciences, 1(12), pp.1–15.

City of Cape Town Day Zero Dashboard – Accessed 17 August 2021. http://coct.co/water-dashboard/.

Cole, M.J., Bailey, R.M., Cullis, J.D. and New, M.G. 2018. Water for sustainable development in the berg water management area, South Africa. South African Journal of Science, 114(3–4), pp. 1–10.

Crawford, N.H. and Linsley, R.K., 1963. A conceptual model of the hydrologic cycle. International Association of Scientific Hydrology Publication, 63, pp.573–587.

Dai, A. 2011. Drought under global warming: A review. Wiley Interdisciplinary Reviews: Climate Change, 2(1), pp.45–65.

Dai, A., 2013. Increasing drought under global warming in observations and models. Nature Climate Change, 3(1), pp.52–58.

Dai, A., Zhao, T., and Chen, J., 2018. Climate change and drought: A precipitation and evaporation perspective. Current Climate Change Reports, 4(3), pp.301–312.

Dee, D.P., Uppala, S.M., Simmons, A.J., Berrisford, P., Poli, P., Kobayashi, S., Andrae, U., Balmaseda, M.A., Balsamo, G., Bauer, D.P. and Bechtold, P., 2011. The ERA-Interim reanalysis: Configuration and performance of the data assimilation system. Journal of the Royal Meteorological Society, 137(656), pp.553–597.

DEADP, 2011. Department of Environmental Affairs and Development Planning. Western Cape (Integrated Water Resource Management) Action Plan: Status Quo Report Final Draft. Provincial Government, Department of Environmental Affairs and Development Planning, South Africa. Chapters 1–13, pp.1–288.

DeFries, R. and Eshleman, K.N., 2004. Land-use change and hydrologic processes: a major focus for the future. Hydrological Processes, 18(11), pp.2183-2186.

Dennis, I. and Dennis, R. 2012. Climate change vulnerability index for South African aquifers. Water SA, 38(3), pp.417–426.

Déqué, M., Calmanti, S., Christensen, O.B., Aquila, A.D., Maule, C.F., Haensler, A., Nikulin, G., and Teichmann, C., 2017. A multi-model climate response over tropical Africa at +2 °C. Climate Services 7, pp.87–95. doi.org/10.1016/J.CLISER.2016.06.002.

Devia, G.K., Ganasri, B.P. and Dwarakish, G.S., 2015. A review on hydrological models. Aquatic procedia, 4, pp.1001–1007.

Dile, Y.T., Daggupati, P., George, C., Srinivasan, R. and Arnold, J., 2016. Introducing a new open-source GIS user interface for the SWAT model. Environmental Modelling & Software, 85, pp.129–138.

Dow, C. L. 2007. Assessing regional land-use/cover influences on New Jersey Pinelands streamflow through hydrograph analysis, Hydrological Process., 21, pp.185-197.

Donaldson, S. 2004. The effects of urbanization on the water cycle. Nevada Cooperative Extension. Nonpoint Education for Municipal Officials. Fact Sheet, pp.04–43.

Dutra, E., Viterbo, P. and Miranda, P.M., 2008. ERA-40 reanalysis hydrological applications in the characterization of regional drought. Geophysical Research Letters, 35(19), pp.1–5.

Dutra, E., Giuseppe, F.D., Wetterhall, F. and Pappenberger, F., 2013. Seasonal forecasts of droughts in African basins using the Standardized Precipitation Index. Hydrology and Earth System Sciences, 17(6), pp.2359–2373.

Dieppois, B., Rouault, M. and New, M. 2015. The impact of ENSO on Southern African rainfall in CMIP5 ocean atmosphere coupled climate models. Climate Dynamics, 45(9), pp.2425–2442.

Du Plessis, J.A. and Schloms, B. 2017. An investigation into the evidence of seasonal rainfall pattern shifts in the Western Cape, South Africa. Journal of the South African Institution of Civil Engineering, 59(4), pp.47–55.

DWA. 2021. Department of Water Affairs Hydrological Services: Data, Dams and Flow Information. Available online: www.dws.gov.za/Hydrology. Accessed on: 17 August 2021.

Edwards, D.C. and T. B. McKee. 1997. Characteristics of 20th century drought in the United States at multiple timescales. Atmospheric Science, 634, pp.1–30.

Ehret, U., Zehe, E., Wulfmeyer, V., Warrach-Sagi, K. and Liebert, J., 2012. HESS Opinions: “Should we apply bias correction to global and regional climate model data?” Hydrology and Earth System Sciences, 16(9), pp.3391–3404.

Ek, M.A. and Holtslag, A.A.M. 2004. Influence of soil moisture on boundary layer cloud development. Journal of Hydrometeorology, 5(1), pp.86–99.

Emam, A.R., Kappas, M., Fassnacht, S. and Linh, N.H.K., 2018. Uncertainty analysis of hydrological modeling in a tropical area using different algorithms. Frontiers of Earth Science, 12(4), pp.661–671.

Engelbrecht, F.A., McGregor, J.L. and Engelbrecht, C.J., 2009. Dynamics of the Conformal‐Cubic Atmospheric Model projected climate‐change signal over southern Africa. International Journal of Climatology: Royal Meteorological Society, 29(7), pp.1013–1033.

Eslamian S. 2014. Handbook of engineering hydrology: modelling, climate change, and variability, 1st edition. CRC Press, London.

FAO. Food and Agricultural Organization. 2004. Drought Impact Mitigation and Prevention in the Limpopo River Basin: A Situation Analysis. Land and Water Discussion Paper. Rome, Italy.

Falkenmark, M., Andersson, L., Castensson, R., Sundblad, K., Batchelor, C., Gardiner, J., Lyle, C., Peters, N., Pettersen, B., Quinn, P., Rockstrom, J. and Yapijakis, C. 1999. Water: A reflection of land use. Swedish Natural Science Research Council, Sweden.

Farley, K.A., Jobbágy, E.G., and Jackson, R.B., 2005. Effects of afforestation on water yield: A global synthesis with implications for policy. Global Change Biology, 11(10), pp.1565–1576.

Field, C.B., Barros, V.R., Mastrandrea, M.D., Mach, K.J., Abdrabo, M.K., Adger, N., Anokhin, Y.A., Anisimov, O.A., Arent, D.J., Barnett, J., and Burkett, V.R., 2014. Summary for policymakers. In Climate change 2014: impacts, adaptation, and vulnerability. Part A: global and sectoral aspects. Contribution of Working Group II to the Fifth Assessment Report of the Intergovernmental Panel on Climate Change, pp.1–32. Cambridge University Press.

Flato, G., Marotzke, J., Abiodun, B., Braconnot, P., Chou, S.C., Collins, W., Cox, P., Driouech, F., Emori, S., Eyring, V. and Forest, C., 2014. Evaluation of climate models. In: Climate change 2013: The physical science basis. Contribution of Working Group I to the Fifth Assessment Report of the Intergovernmental Panel on Climate Change. pp.741–866. Cambridge University Press.

Flemming, B. and Martin, K. 2021. The Breede River estuary (Cape Province, South Africa): A historical perspective on hydrology, geomorphology, and sedimentology. Geo-Marine Letters, 41(1), pp.1–27.

Florenchie, P., Lutjeharms, J.R., Reason, C.J.C., Masson, S. and Rouault, M. 2003. The source of Benguela Niños in the south Atlantic Ocean. Geophysical Research Letters, 30(10), pp.1–4. doi:10.1029/2003GL017172, 2003.

Gassman, P.W., Reyes, M.R., Green, C.H. and Arnold, J.G., 2007. The soil and water assessment tool: Historical development, applications, and future research directions. Transactions of the American Society of Agricultural and Biological Engineers (ASABE), 50(4), pp. 1211-1250.

Gawith, D., Kingston, D.G. and McMillan, H., 2012. The effects of climate change on runoff in the Lindis and Matukituki catchments, Otago, New Zealand. Journal of Hydrology (New Zealand), pp.121-135.

Gertler, C.G., O'Gorman, P.A., Kravitz, B., Moore, J.C., Phipps, S.J. and Watanabe, S., 2020. Weakening of the extratropical storm tracks in solar geoengineering scenarios. Geophysical Research Letters, 47(11), p.e2020GL087348.

Giannini, A., Saravanan, R. and Chang, P. 2003. Oceanic forcing of Sahel rainfall on interannual to interdecadal timescales. Science, 302(5647), pp.1027–1030.

Gibson, D., 2018. Water crisis in cape town: Lessons to be learnt. Voices of South Africa (Febrero). Konrad-Adenauer-Stiftung eV, pp.1–4.

Gibbs, W.J. and Maher, J.V., 1967. Rainfall Deciles as Drought Indicators Bulletin 48, Commonwealth Bureau of Meteorology, Australia.

Gibson, D., 2018. Water crisis in cape town: Lessons to be learnt. Voices of South Africa. Konrad-Adenauer-Stiftung eV, Ciudad del Cabo, pp. 1–5.

Gillette, H.P. 1950. A creeping drought under way. Water and sewage work, 104(5), pp. 1–4.

Giorgi, F., 1990. Simulation of regional climate using a limited area model nested in a general circulation model. Journal of Climate, 3(9), pp. 941–963.

Giorgi, F. and Mearns, L.O., 1999. Introduction to special section: Regional climate modelling revisited. Journal of Geophysical Research. Atmospheres, pp.6335–6352.

Giorgi, F., Jones, C. and Asrar, G.R. 2009. Addressing climate information needs at the regional level: The CORDEX framework. World Meteorological Organization (WMO) Bulletin, 58(3), pp.175–183.

Githui, F., Gitau, W., Mutua, F. and Bauwens, W., 2009. Climate change impact on SWAT simulated streamflow in western Kenya. International Journal of Climatology: A Journal of the Royal Meteorological Society, 29(12), pp.1823–1834.

Glantz, M.H. 2001. Currents of change: Impacts of El Niño and La Niña on Climate and Society. 2nd Edition. Cambridge University Press, Cambridge, UK.

Golmohammadi, G., Prasher, S., Madani, A. and Rudra, R. 2014. Evaluating three hydrological distributed watershed models: MIKE-SHE, APEX, SWAT. Hydrology, 1(1), pp.20–39.

Graham, L.P., Andersson, L., Horan, M., Kunz, R., Lumsden, T., Schulze, R., Warburton, M., Wilk, J. and Yang, W., 2011. Using multiple climate projections for assessing hydrological response to climate change in the Thukela River Basin, South Africa. Physics and Chemistry of the Earth, Parts A/B/C, 36(14-15), pp.727–735.

Green Cape, 2019. Sustainable Agriculture 2019 Market Intelligence Report. Cape Town, South Africa. Available online: www.greencape.co.za. Accessed on: 17 August 2021.

Gropp, W., Lusk, E., Doss, N., Skjellum, A., 1996. A high-performance, portable implementation of the MPI message passing interface standard. Parallel Computer 22, pp.828.

Ground Up, 2018. Aliens are the greatest threat to Cape Town’s water security. Ground Up. Available online: www.groundup.org.za.

Guenang, G.M., Komkoua, M.A.J., Pokam, M.W., Tanessong, R.S., Tchakoutio, S.A., Vondou, A., Tamoffo, A.T., Djiotang, L., Yepdo, Z. and Mkankam, K.F., 2019. Sensitivity of SPI to distribution functions and correlation between its values at different timescales in Central Africa. Earth Systems and Environment, 3(2), pp.203–214.

Guo, J.T., Zhang, Z.Q., Wang, S.P., Strauss, P. and Yao, A.K. 2014. Appling SWAT model to explore the impact of changes in land-use and climate on the streamflow in a Watershed of Northern China. Acta Ecologica Sinica, 34(6), pp.1559–1567.

Gupta, H.V., Sorooshian, S. and Yapo, P.O. 1999. Status of automatic calibration for hydrologic models: Comparison with multilevel expert calibration. Journal of Hydrologic Engineering, 4(2), pp.135–143.

Gutowski, W. J., Jr., Y. Chen, and Z. Otles (1997), Atmospheric water vapor transport in NCEP – NCAR reanalyses: Comparison with river dis-charge in the central United States, Bulletin of the American Meteorological Society, 78, pp.1957 –1969.

Guttman, N.B. 1998. Comparing the Palmer Drought Index and the Standardized Precipitation Index. Journal of the American Water Resources Association 34(1), pp.113–121.

Gyamfi, C., Ndambuki, J.M. and Salim, R.W., 2016a. Hydrological responses to land use/cover changes in the Olifants Basin, South Africa. Water, 8(12), pp.1–16.

Gyamfi, C., Ndambuki, J.M. and Salim, R.W., 2016b. Application of SWAT model to the Olifants Basin: calibration, validation, and uncertainty analysis. Journal of Water Resource and Protection, 8(03), pp.1–14.

Haensler, A., Hagemann, S. and Jacob, D., 2011. Dynamical downscaling of ERA40 reanalysis data over southern Africa: added value in the simulation of the seasonal rainfall characteristics. International Journal of Climatology, 31(15), pp.2338–2349. doi./10.1002/joc.2242.

Hagemann, S., Machenhauer, B., Jones, R., Christensen, O.B., Déqué, M., Jacob, D. and Vidale, P.L., 2004. Evaluation of water and energy budgets in regional climate models applied over Europe. Climate Dynamics, 23(5), pp.547-567.

Hagemann, S., Arpe, K., & Bengtsson, L. 2005. Validation of the hydrological cycle of ERA 40. Berichte zur Erdsystemforschung, 10, pp.1-53.

Hargreaves, G.H. and Samani, Z.A. 1985. Reference crop evapotranspiration from temperature. Applied Engineering in Agriculture, 1(2), pp. 96–99.

Haile, G.G., Tang, Q., Hosseini-Moghari, S.M., Liu, X., Gebremicael, T.G., Leng, G., Kebede, A., Xu, X. and Yun, X., 2020. Projected impacts of climate change on drought patterns over East Africa. Earth's Future, 8(7) , pp. 1–23.

Hakala, K., Addor, N. and Seibert, J., 2018. Hydrological modeling to evaluate climate model simulations and their bias correction. Journal of Hydrometeorology, 19(8), pp.1321–1337.

Hansingo, K. and Reason, C.J.C. 2009. Modelling the atmospheric response over southern Africa to SST forcing in the southeast tropical Atlantic and southwest subtropical Indian Oceans. International Journal of Climatology: A Journal of the Royal Meteorological Society, 29(7), pp.1001–1012.

Hao, Z. and Singh, V.P., 2015. Drought characterization from a multivariate perspective: A review. Journal of Hydrology, 527, pp.668–678.

Harris, I.P.D.J., Jones, P.D., Osborn, T.J. and Lister, D.H., 2014. Updated high-resolution grids of monthly climatic observations–the CRU TS3. 10 Dataset. International journal of climatology, 34(3), pp.623–642.

Hasan, H.H., Mohd Razali, S.F., Muhammad, N.S. and Ahmad, A., 2019. Research trends of hydrological drought: A systematic review. Water, 11(11), pp.1–19.

Havenga, C.F.B., Pitman, W.V. and Bailey, A.K., 2007. Hydrological and hydraulic modelling of the Nyl River floodplain Part 1. Background and hydrological modelling. Water South Africa, 33(1).

Hayes, 2006: Drought Indices. Van Nostrand's Scientific Encyclopedia, John Wiley & Sons, Inc., doi:10.1002/0471743984.vse8593.

Hayes, M.J., Svoboda, M.D., Wiihite, D.A. and Vanyarkho, O.V., 1999. Monitoring the 1996 drought using the standardized precipitation index. Bulletin of the American Meteorological Society, 80(3), pp.429–438.

Herold, C.E. and Bailey, A.K. 2016. Water Resources of South Africa Study (WR2012). River Streamflow Gauging and Reservoir Inflow Database. Available online: https://waterresourceswr2012.co.za/. Accessed on: 17 August 2021.

Hewitson, B.C., Daron, J., Crane, R.G., Zermoglio, M.F. and Jack, C., 2014. Interrogating empirical statistical downscaling. Climatic Change, 122, pp.539-554.

Hirschi, M., S. L. Seneviratne, and C. H. Schar (2006), Seasonal variations in terrestrial water storage for major mid-latitude river basins, Journal of Hydrometeorology, 7, pp.39–60.

Hoell, A., Funk, C., Magadzire, T., Zinke, J. and Husak, G. 2015. El Niño–Southern Oscillation diversity and southern Africa teleconnections during austral summer. Climate Dynamics, 45(5), pp.1583–1599.

Hoell, A. and Cheng, L. 2018. Austral summer Southern Africa precipitation extremes forced by the El Niño-Southern oscillation and the subtropical Indian Ocean dipole. Climate Dynamics, 50(9), pp.3219–3236.

Hoell, A., Gaughan, A.E., Magadzire, T. and Harrison, L. 2021. The Modulation of Daily Southern Africa Precipitation by El Niño–Southern Oscillation across the Summertime Wet Season. Journal of Climate, 34(3), pp.1115–1134.

Hoerling, M., Hurrell, J., Eischeid, J. and Phillips, A. 2006. Detection and attribution of twentieth-century northern and southern African rainfall change. Journal of Climate, 19(16), pp.3989–4008.

Holden, P.B., Rebelo, A.J. and New, M.G., 2021. Mapping invasive alien trees in water towers: A combined approach using satellite data fusion, drone technology and expert engagement. Remote Sensing Applications: Society and Environment, 21, pp.1–14.

Holder, A.J., Rowe, R., McNamara, N.P., Donnison, I.S., and McCalmont, J.P., 2019. Soil & Water Assessment Tool (SWAT) simulated hydrological impacts of land-use change from temperate grassland to energy crops: A case study in the western UK. Bioenergy, 11(11), pp.1298–1317.

Hughes, D.A., 2013. A review of 40 years of hydrological science and practice in southern Africa using the Pitman rainfall-runoff model. Journal of Hydrology, 501, pp.111-124.

Hurry, L., Van Heerden, J., 1982. Southern Africa's weather patterns : a guide to the interpretation of synoptic maps. Via Afrika, Goodwood.

Hurry, L. and Van Heerden, J. 1982. Southern Africa's weather patterns: A guide to the interpretation of synoptic maps. Via Afrika, Goodwood.

Ibebuchi, C.C. 2021. On the Relationship between Circulation Patterns, the Southern Annular Mode, and Rainfall Variability in Western Cape. Atmosphere, 12(6), pp.1–16.

Jacobson, M.Z., 2005. Fundamentals of Atmospheric Modeling. Cambridge University Press: Cambridge, UK.

Janža, M., 2013. Impact assessment of projected climate change on the hydrological regime in the SE Alps, Upper Soča River basin, Slovenia. Natural Hazards, 67(3), pp.1025–1043.

Jarvis, A., Reuter, H.I., Nelson, A. and Guevara, E., 2008. Hole-filled SRTM for the globe Version 4, available from the CGIAR-CSI SRTM 90m Database. http://srtm.csi.cgiar.org.

Jehanzaib, M., Sattar, M.N., Lee, J.H. and Kim, T.W., 2020. Investigating effect of climate change on drought propagation from meteorological to hydrological drought using multi-model ensemble projections. Stochastic Environmental Research and Risk Assessment, 34(1), pp.7–21.

Jia, X., Zhu, Y. and Luo, Y., 2017. Soil moisture decline due to afforestation across the Loess Plateau, China. Journal of Hydrology, 546, pp.113–122.

Jiang, R., Xie, J., He, H., Luo, J. and Zhu, J. 2015. Use of four drought indices for evaluating drought characteristics under climate change in Shaanxi, China: 1951–2012. Natural Hazards, 75(3), pp. 2885–2903.

Jiao, S., Li, J., Li, Y., Xu, Z., Kong, B., Li, Y. and Shen, Y. 2020. Variation of soil organic carbon and physical properties in relation to land uses in the Yellow River Delta, China. Scientific Reports, 10(1), pp.1–12.

Joetzjer, E., Douville, H., Delire, C., Ciais, P., Decharme, B. and Tyteca, S., 2013. Hydrologic benchmarking of meteorological drought indices at interannual to climate change timescales: a case study over the Amazon and Mississippi river basins. Hydrology and Earth System Sciences, 17(12), pp.4885–4895.

Johnson, F. and Sharma, A., 2015. What are the impacts of bias correction on future drought projections? Journal of Hydrology, 525, pp.472–485.

Jones, C., Giorgi, F. and Asrar, G., 2011. The Coordinated Regional Downscaling Experiment: CORDEX–an international downscaling link to CMIP5. CLIVAR exchanges, 16(2), pp.34–40.

Joorabian Shooshtari, S., Shayesteh, K., Gholamalifard, M., Azari, M., Serrano-Notivoli, R. and López-Moreno, J.I. 2017. Impacts of future land cover and climate change on the water balance in northern Iran. Hydrological Sciences Journal, 62(16), pp.2655–2673.

Juang, J.Y., Katul, G.G., Porporato, A., Stoy, P.C., Siqueira, M.S., Detto, M., KIM, H.S. and Oren, R., 2007. Eco-hydrological controls on summertime convective rainfall triggers. Global Change Biology, 13(4), pp.887–896.

Juckem, P. F., Hunt, R. J., Anderson, M. P., and Robertson, D. M. 2008. Effects of climate and land 590 management change on streamflow in the driftless area of Wisconsin, Journal of Hydrology, 355, pp.123-130.

Jury, M.R., 2018. The climate of desiccation in the SW Cape. Hydrology and Earth System Sciences Discussions, pp.1–19.

Kalnay, E., 2003. Atmospheric modelling, data assimilation and predictability. Cambridge University Press.

Karami, K., Tilmes, S., Muri, H. and Mousavi, S.V., 2020. Storm track changes in the Middle East and North Africa under stratospheric aerosol geoengineering. Geophysical Research Letters, 47(14), p.e2020GL086954.

Kamali, B., Houshmand Kouchi, D., Yang, H. and Abbaspour, K.C., 2017. Multilevel drought hazard assessment under climate change scenarios in semi-arid regions: A case study of the Karkheh River basin in Iran. Water, 9(4), pp.1–17.

Kane, R.P. 2009. Periodicities, ENSO effects and trends of some South African rainfall series: An update. South African Journal of Science, 105(5), pp.199–207.

Karl, T.R., 1986. The sensitivity of the Palmer Drought Severity Index and Palmer's Z-index to their calibration coefficients including potential evapotranspiration. Journal of Climate and Applied Meteorology, pp.77-86.

Kienzle, S.W., Nemeth, M.W., Byrne, J.M. and MacDonald, R.J., 2012. Simulating the hydrological impacts of climate change in the upper North Saskatchewan River basin, Alberta, Canada. Journal of Hydrology, 412, pp.76–89.

Kiros, G., Shetty, A. and Nandagiri, L. 2015. Performance Evaluation of SWAT Model for Land-use and Land Cover Changes in Semi-Arid Climatic Conditions: A Review. Hydrology: Current Research, 6(3), pp.1–7. doi.org/10.4172/2157-7587.1000216.

Kohonen, T., Hynninen, J., Kangas, J. and Laaksonen, J., 1996. Som pak: The self-organizing map program package. University of Technology–Laboratory of Computer and Information Science, Helsinki, Finland. Technical Report, pp.1–31.

Kotzé, I., Beukes, H., Van den Berg, E. and Newby, T., 2010. National invasive alien plant survey. Report number: gw/a/2010/21, pp.1–55.

Kruger, A.C., South African Weather Service, 2004a. Climate of South Africa - Climate Regions. Pretoria: South African Weather Service.

Kruger, A.C., 2004b. Climate of South Africa: Climate controls. Pretoria: South African Weather Service.

Kubiak-Wójcicka, K., Nagy, P., Zeleňáková, M., Hlavatá, H. and Abd-Elhamid, H.F., 2021. Identification of Extreme Weather Events Using Meteorological and Hydrological Indicators in the Laborec River Catchment, Slovakia. Water, 13(10) , pp.1–20.

Kumar, N., Singh, S.K., Singh, V.G. and Dzwairo, B., 2018. Investigation of impacts of land use/land cover change on water availability of Tons River Basin, Madhya Pradesh, India. Modeling Earth Systems and Environments, 4(1), pp.295-310.

Kusangaya, S., Warburton, M.L., Archer van Garderen, E., Jewitt, G.P.W., 2014. Impacts of climate change on water resources in southern Africa: A review. Physics and Chemistry of Earth, Parts A/B/C 67–69, pp.47–54.

Lake, P.S. 2011. Drought and Aquatic Ecosystems: Effects and Responses, 402pp. Wiley-Blackwell.

Lakhraj-Govender, R. and Grab, S.W. 2019. Rainfall and river flow trends for the Western Cape Province, South Africa. South African Journal of Science, 115(9-10), pp.1–6.

Lau, K. M., J. H. Him, and Y. Sud. 1996. Intercomparison of hydrologic processes in AMIP GCMs, Bull. Am. Meteorological Society, 77, pp.2209– 2227.

Lerner, D.N. 1990. Groundwater recharge in urban areas. Atmospheric Environment. Part B. Urban Atmosphere, 24(1), pp.29–33.

Li, K.Y., Coe, M.T., Ramankutty, N. and De Jong, R., 2007. Modeling the hydrological impact of land-use change in West Africa. Journal of hydrology, 337(3-4), pp.258-268.

Li, H., Sheffield, J. and Wood, E.F., 2010. Bias correction of monthly precipitation and temperature fields from Intergovernmental Panel on Climate Change AR4 models using equidistant quantile matching. Journal of Geophysical Research: Atmospheres, 115(D10), pp.1-20.

Li, L., Diallo, I., Xu, C.Y. and Stordal, F., 2015. Hydrological projections under climate change in the near future by RegCM4 in Southern Africa using a large-scale hydrological model. Journal of Hydrology, 528, pp.1-16.

Li, Y.L., Tao, H., Yao, J. and Zhang, Q., 2016. Application of a distributed catchment model to investigate hydrological impacts of climate change within Poyang Lake catchment (China). Hydrology Research, 47(S1), pp.120-135.

Li, S., Yang. H., Lacayo. M., Liu, J., Lei, G., 2018. Impacts of land-use and land-cover changes on water yield: A case study in Jing-Jin-Ji, China. Sustainability. Apr;10(4):960.

Liu, Y. and Gupta, H.V., 2007. Uncertainty in hydrologic modeling: Toward an integrated data assimilation framework. Water Resources Research, 43(7), pp.1–18.

Liu, Z., Ming, Y., Wang, L., Bollasina, M., Luo, M., Lau, N.C. and Yim, S.H.L., 2019. A model investigation of aerosol-induced changes in the East Asian winter monsoon. Geophysical research letters, 46(16), pp.10186–10195.

Liu, Z., & Wang, Y., & Xu, Z., & Duan, Q., 2017. Conceptual Hydrological Models. 10.1007/978-3-642-40457-3_22-1.

Le Goff, Y., Sedrati, M. and Ettalibi, M., 1985, November. Variabilité interannuelle des précipitations au Maroc, pp.21–24.

Le Maitre, D.C., Versfeld, D.B. and Chapman, R.A., 2000. Impact of invading alien plants on surface water resources in South Africa: A preliminary assessment, Water SA, 26(3), pp.1–12.

Le Maitre, D., Colvin, C. and Maherry, A. 2009. Water resources in the Klein Karoo: The challenge of sustainable development in a water-scarce area. South African Journal of Science, 105(1-2), pp.39–48.

Le Maitre, D.C., Forsyth, G.G., Dzikiti, S., and Gush, M.B., 2016. Estimates of the impacts of invasive alien plants on water flows in South Africa. Water SA, 42(4), pp.659–672.

Le Maitre, D., Görgens, A., Howard, G. and Walker, N., 2019. Impacts of alien plant invasions on water resources and yields from the Western Cape Water Supply System (WCWSS). Water SA, 45(4), pp.568–579.

Lloyd-Hughes, B., 2014. The impracticality of a universal drought definition. Theoretical and Applied Climatology, 117(3), pp.607–611.

Louw, E.J.M. 2007. Climate Change in the Western Cape: a Disaster Risk Assessment of the impact on human health. Doctoral dissertation. University of Stellenbosch.

Lucarini, V., Danihlik, R., Kriegerova, I., & Speranza, A. 2007. Does the Danube exist? Versions of reality given by various regional climate models and climatological data sets. Journal of Geophysical Research: Atmospheres, 112, pp.1–17.

Lumsden, T.G., Jewitt, G.P.W., Schulze, R.E., 2003. Modelling the Impacts of Land Cover and Land Management Practices on Runoff Responses. WRC Report No. 1015/1/03. Pretoria, RSA.

Luo, J., Zhou, X., Rubinato, M., Li, G., Tian, Y. and Zhou, J., 2020. Impact of multiple vegetation covers on surface runoff and sediment yield in the small basin of Nverzhai, Hunan Province, China. Forests, 11(3), pp.1–18.

Macron, C., Pohl, B., Richard, Y. and Bessafi, M. 2014. How do tropical temperate troughs form and develop over southern Africa? Journal of Climate, 27(4), pp.1633–1647.

Mahlalela, P.T., Blamey, R.C. and Reason, C.J.C. 2019. Mechanisms behind early winter rainfall variability in the southwestern Cape, South Africa. Climate Dynamics, 53(1), pp. 21–39.

Maity, R. and Suman, M., 2019. Predictability of hydrological systems using the wavelet transformation: Application to drought prediction. Hydrology in a Changing World. pp. 109–137.

McGrane, S. J.2016. Impacts of urbanisation on hydrological and water quality dynamics, and urban water management: a review. Hydrological Sciences Journal, 615(61), pp.2295-2311.

Mahmud, T., Sifa, S.F., Islam, N.N., Rafsan, M.A., Kamal, A.M., Hossain, M.S., Rahman, M.Z. and Chakraborty, T.R., 2021. Drought dynamics of Northwestern Teesta Floodplain of Bangladesh: A remote sensing approach to ascertain the cause and effect. Environmental Monitoring and Assessment, 193(4), pp.1–19.

Malherbe, J., Dieppois, B., Maluleke, P., Van Staden, M. and Pillay, D.L., 2016. South African droughts and decadal variability. Natural Hazards, 80(1), pp.657–681.

Manatsa, D. and Mukwada, G. 2012. Rainfall Mechanisms for the Dominant Rainfall Mode over Zimbabwe Relative to ENSO and/or IODZM. The Scientific World Journal, (2012) 926310, pp.1–16. doi:10.1100/2012/92631.

Marchane, A., Tramblay, Y., Hanich, L., Ruelland, D., & Jarlan, L. (2017). Climate change impacts on surface water resources in the Rheraya catchment (High Atlas, Morocco). Hydrological Sciences Journal, 62, 979 - 995.

Mason, S.J. (2001), El Niño, climate change, and Southern African climate. Environmetrics, 12, pp.327-345.

Mathivha, F.I., 2020. Drought in Luvuvhu River Catchment-South Africa: Assessment, Characterisation and Prediction (Doctoral dissertation). Department of Hydrology and Water Resources, University of Venda. http://hdl.handle.net/11602/1522.

Mango, L.M., Melesse, A.M., McClain, M.E., Gann, D. and Setegn, S., 2011. Land use and climate change impacts on the hydrology of the upper Mara River Basin, Kenya: results of a modeling study to support better resource management. Hydrology and Earth System Sciences, 15(7), pp.2245–2258.

Mazibuko, S.M., Mukwada, G. and Moeletsi, M.E., 2021. Assessing the frequency of drought/flood severity in the Luvuvhu River catchment, Limpopo Province, South Africa. Water SA, 47(2), pp.172-184.

Mao, D. and Cherkauer, K.A., 2009. Impacts of land-use change on hydrologic responses in the Great Lakes region. Journal of Hydrology, 374(1-2), pp.71–82.

Marais, D., Fischer, T., Kotze, D., Haasbroek, B., Govender, M., Pugin, J. and Horn, A., 2021. Economic valuation of the averted degradation of the Vyeboom Wetland in the Theewaterskloof Dam catchment, South Africa. Water SA, 47(1), pp.24-34.

Mbokodo, I., Bopape, M.-J., Chikoore, H., Engelbrecht, F., and Nethengwe, N., 2020. Heatwaves in the future warmer climate of South Africa. Atmosphere, 11(7), pp.1–18.

McKee, T.B., Doesken, N.J., Kleist, J., 1993. The relationship of drought frequency and duration to timescales. In: Proceedings of the 8th Conference on Applied Climatology. American Meteorological Society, pp.179–183.

Meko, D.M. (1985) Temporal and spatial variability of drought in Morocco. In: Proceedings of Conference on Drought, Water Management and Food Production, 21(24), pp.55–82.

Melgarejo, A.E., Ordoñez, P., Nieto, R., Peña-Ortiz, C., García-Herrera, R. and Gimeno, L., 2021. Mechanisms for severe drought occurrence in the Balsas River basin (Mexico). Atmosphere, 12(3), pp.116

Mendez, M., Maathuis, B., Hein-Griggs, D. and Alvarado-Gamboa, L.F., 2020. Performance evaluation of bias correction methods for climate change monthly precipitation projections over Costa Rica. Water, 12(2), pp.1–34.

Meque, A. and Abiodun, B.J. 2015. Simulating the link between ENSO and summer drought in Southern Africa using regional climate models. Climate Dynamics, 44(7), pp.1881–1900.

Midgley, G.F., Chapman, R.A., Hewitson, B., Johnston, P., De Wit, M., Ziervogel, G., Mukheibir, P., Van Niekerk, L., Tadross, M., Van Wilgen, B.W. and Kgope, B. 2005. A status quo, vulnerability and adaptation assessment of the physical and socio-economic effects of climate change in the Western Cape. Report to the Western Cape Government, Cape Town, South Africa. CSIR Report No. ENV-S-C 2005-073, Stellenbosch. pp.1–171.

Misra, V. 2003. The influence of Pacific SST variability on the precipitation over southern Africa. Journal of Climate, 16(14), pp.2408–2418.

Mishra, A.K. and Singh, V.P. 2010. A review of drought concepts. Journal of Hydrology, 391(1-2), pp. 202–216.

Mishra, V., Kumar, R., Shah, H.L., Samaniego, L., Eisner, S., & Yang, T. 2017. Multimodel assessment of sensitivity and uncertainty of evapotranspiration and a proxy for available water resources under climate change. Climatic Change, 141, 451-465.

Mitchell, T.D., Jones, P.D., 2005. An improved method of constructing a database of monthly climate observations and associated high- resolution grids. International Journal of Climatology 25, pp.693–712.

Monteith, J.L. (1965) Evaporation and environment. In: The state and movement of water in living organisms. Symposium of the Society Experimental Biology. New York: Academic Press, 19, pp.205–234.

Moriasi, D.N., Arnold, J.G., Van Liew, M.W., Bingner, R.L., Harmel, R.D. and Veith, T.L., 2007. Model evaluation guidelines for systematic quantification of accuracy in watershed simulations. Transactions of the ASABE, 50(3), pp.885–900.

Mtilatila, L., Bronstert, A., Bürger, G. and Vormoor, K., 2020. Meteorological and hydrological drought assessment in Lake Malawi and Shire River basins (1970–2013). Hydrological Sciences Journal, 65(16), pp.2750–2764.

Munoth, P. and Goyal, R., 2020. Impacts of land use land cover change on runoff and sediment yield of Upper Tapi River Sub-Basin, India. International Journal of River Basin Management, 18(2), pp.177–189.

Mutema, M., Jewitt, G., Chivenge, P., Kusangaya, S. and Chaplot, V., 2016. Spatial scale impact on daily surface water and sediment fluxes in Thukela River, South Africa. Physics and Chemistry of the Earth, Parts A/B/C, 92, pp.34–43.

Ncube, M. and Taigbenu, A.E. 2005. The impact of land cover and land use on hydrological response in the Olifants Catchment. In: Proceedings of special Colloquium Water Research Showcase, pp.51–54. Universities of Johannesburg, Pretoria and the Witwatersrand.

Nalbantis, I. and Tsakiris, G., 2009. Assessment of hydrological drought revisited. Water Resources Management, 23(5), pp.881–897.

Naik, M., and Abiodun, B.J., 2016. Potential impacts of forestation on future climate change in Southern Africa. International Journal of Climatology. 36 (14), pp.4560–4576. doi.org/10.1002/joc.4652.

Naik, M., and Abiodun, B.J., 2020. Projected changes in drought characteristics over the Western Cape, South Africa. Meteorological Applications, 27(1), pp.1–4.

Ndiritu, J., 2009. A comparison of automatic and manual calibration using the Pitman model. Physics and Chemistry of the Earth, Parts A/B/C, 34(13-16), pp.729-740.

NDMC. 2021. National Drought Mitigation Centre. School of Natural Resources. Available online: https://drought.unl.edu/. Accessed on 17 August 2021.

Neitsch, S.L., Arnold, J.G., and Srinivasan, R., 2002. Pesticide's fate and transport predicted by the soil and water assessment tool (SWAT). Atrazine, Metolachlor Trifluralin Sugar Creek Watershed: Report, 3, pp.1–100.

Neitsch, S.L., Arnold, J.G., Kiniry, J.R., Williams, J.R. and King, K.W., 2005. SWAT theoretical documentation version 2005. Soil and Water Research Laboratory, ARS, Temple Texas, USA, pp.1–494.

Neitsch, S.L., Williams, J., Arnold, J., Kiniry, J. 2009. Soil and Water Assessment Tool Theoretical Documentation Version; Technical Report No. 406; Texas Water Resources Institute: College Station, TX, USA.

Nguvava, M., & Abiodun, B., & Otieno, F., 2019. Projecting drought characteristics over East African basins at specific global warming levels. Atmospheric Research. 228, pp.1–14.

Nikulin, G., Lennard, C., Dosio, A., Kjellström, E., Chen, Y., Hänsler, A., Kupiainen, M., Laprise, R., Mariotti, L., Maule, C.F., van Meijgaard, E., Panitz, H.-J., Scinocca, J.F. and Somot, S. (2018) The effects of 1.5 and 2 degrees of global warming on Africa in the CORDEX ensemble. Environmental Research Letters, 13(6), pp.1–11.

Nigam, S. 2003. Teleconnections. In: J.R. Holton, J. Pyle and J.A. Curry (Eds.). Encyclopaedia of Atmospheric Sciences, Academic Press, Number 5, pp.2243–2269.

Ntale, H.K. and Gan, T.Y., 2003. Drought indices and their application to East Africa. International Journal of Climatology: A Journal of the Royal Meteorological Society, 23(11), pp.1335–1357.

Odoulami, R.C., Wolski, P. and New, M., 2021. A SOM-based analysis of the drivers of the 2015–2017 Western Cape drought in South Africa. International Journal of Climatology, 41, pp.1518–1530.

Oguntunde, P.G., Friesen, J., van de Giesen, N., Savenije, H.H.G., 2006. Hydroclimatology of the Volta River Basin in West Africa: Trends and variability from 1901 to 2002. Physics Chemistry of Earth, Parts A/B/C 31, pp.1180–1188.

Oki, T., Blyth, E.M., Berbery, E.H. and Alcaraz-Segura, D. 2013. Land use and land cover changes and their impacts on hydroclimate, ecosystems and society. Springer, Dordrecht. Climate Science for Serving Society, pp.185–203.

Otto, F.E., Wolski, P., Lehner, F., Tebaldi, C., Van Oldenborgh, G.J., Hogesteeger, S., Singh, R., Holden, P., Fučkar, N.S., Odoulami, R.C. and New, M., 2018. Anthropogenic influence on the drivers of the Western Cape drought 2015–2017. Environmental Research Letters, 13(12), p.124010.

Palmer, W.C., 1965. Meteorological drought, Weather Bureau, 30, pp.1–59. US Department of Commerce. Washington D.C. United States of America.

Pandey, V., Dhaubanjar, S., Bharati, L., & Thapa, B.R. 2019. Hydrological response of Chamelia watershed in Mahakali Basin to climate change. The Science of the total environment, 650 Pt 1, 365-383.

Páscoa, P., Russo, A., Gouveia, C.M., Soares, P.M., Cardoso, R.M., Careto, J.A. and Ribeiro, A.F., 2021. A high-resolution view of the recent drought trends over the Iberian Peninsula. Weather and Climate Extremes, 32, pp.1–9.

Pechlivanidis, I.G., Jackson, B.M., Mcintyre, N.R. and Wheater, H.S., 2011. Catchment scale hydrological modelling: a review of model types, calibration approaches and uncertainty analysis methods in the context of recent developments in technology and applications. Global NEST Journal, 13(3), pp.193–214.

Pegram, G. and Baleta, H., 2014. Water in the Western Cape economy. Progress report to the Water Research Commission, Project, K5–2075, pp.1–98.

Philippon, N., Rouault, M., Richard, Y. and Favre, A. (2012), The influence of ENSO on winter rainfall in South Africa. Int. J. Climatol., 32: 2333-2347. doi.org/10.1002/joc.3403.

Pinto, I., Jack, C., Lennard, C., Tilmes, S. and Odoulami, R.C., 2020. Africa's climate response to solar radiation management with stratospheric aerosol. Geophysical Research Letters, 47(2), pp.1–20.

Preston, I.R. & Le Maitre, David & Blignaut, James & Louw, Lynette & Palmer, C.G. (2018). Impact of invasive alien plants on water provision in selected catchments. Water South Africa. 44. 719. 10.4314/wsa.v44i4.20.

Price, K. 2011. Effects of watershed topography, soils, land use, and climate on baseflow hydrology in humid regions: A review, Progress Physical Geography, 635(35), pp.465-492.

Querner, EP and Zanen, M 2013, Modelling water quantity and quality using SWAT : a case study in the Limpopo River basin, South Africa. Alterra-report, no. 2405, Wageningen, Alterra. <https://edepot.wur.nl/250348>

Refsgaard, J.C., 1997. Parameterisation, calibration and validation of distributed hydrological models. Journal of Hydrology, 198(1:4), pp.69–97.

Riahi, K., Rao, S., Krey, V., Cho, C., Chirkov, V., Fischer, G., Kindermann, G., Nakicenovic, N., and Rafaj, P., 2011. RCP 8.5 – A scenario of comparatively high greenhouse gas emissions. Climate Change, 109, pp.33–57.

Roads, J.O., S.-C. Chen, A. Guetter, and K. Georgakakos. 1994. Large-scale aspects of the United States hydrologic cycle. Bulletin of the American Meteorological Society, 75, pp.1589–1610.

Roads, J. and Betts, A., 2000. NCEP–NCAR and ECMWF reanalysis surface water and energy budgets for the Mississippi River basin. Journal of Hydrometeorology, 1(1), pp.88-94.

Rostorfer, D., Mitler, D. and Ledbetter, K., 2015. Creating Shared Value Through Corporate Social Investment: Managing Water-Related Risk and Opportunity Through Coca-Cola's Replenish Africa Initiative. Master of Science Thesis in Natural Resources and Environment at the University of Michigan, pp.1–328.

Rosenberg, E.A., Keys, P.W., Booth, D.B., Hartley, D., Burkey, J., Steinemann, A.C. and Lettenmaier, D.P., 2010. Precipitation extremes and the impacts of climate change on stormwater infrastructure in Washington State. Climatic Change, 102(1), pp.319-349.

Roux, 2018. Agricultural water file: Farming for a drier future. WWF South Africa.

Pascale, S., Kapnick, S.B., Delworth, T.L. and Cooke, W.F. 2020. Increasing risk of another Cape Town “Day Zero” drought in the 21st century. Proceedings of the National Academy of Sciences, 117(47), pp. 29495–29503.

Pomposi, C., Funk, C., Shukla, S., Harrison, L. and Magadzire, T. 2018. Distinguishing southern Africa precipitation response by strength of El Niño events and implications for decision-making. Environmental Research Letters, 13(7), p.074015.

Reason, C.J.C., 2001. Subtropical Indian Ocean SST dipole events and southern African rainfall. Geophysical Research Letters, 28(11), pp.2225–2227.

Reason, C.J.C., Rouault, M., Melice, J.L. and Jagadheesha, D., 2002. Interannual winter rainfall variability in SW South Africa and large-scale ocean–atmosphere interactions. Meteorology and Atmospheric Physics, 80(1), pp.19–29.

Reason, C.J.C. and Rouault, M. 2002. ENSO-like decadal variability and South African rainfall. Geophysical Research Letters, 29(13), pp.1–4.

Reason, C.J.C. and Jagadheesha, D. 2005. A model investigation of recent ENSO impacts over southern Africa. Meteorology and Atmospheric Physics, 89(1), pp.181–205.

Reason, C.J.C. and Rouault, M. 2005. Links between the Antarctic Oscillation and winter rainfall over western South Africa. Geophysical Research Letters, 32(7), pp. 1-4.

Richard, Y., Trzaska, S., Roucou, P. and Rouault, M. 2000. Modification of the Southern African rainfall variability/El Niño southern oscillation relationship. Climate Dynamics, 16(200), pp. 883–895.

River Health Programme (RHP). 2004. State-of-Rivers Report: Berg River System. Department of Water Affairs and Forestry. Pretoria.

Rocheta, E., Evans, J.P. and Sharma, A., 2014. Assessing atmospheric bias correction for dynamical consistency using potential vorticity. Environmental Research Letters, 9(12), pp.1–8.

Rodell, M. & Famiglietti, J.S. 2001. An analysis of terrestrial water storage variations in Illinois with implications for the Gravity Recovery and Climate Experiment (GRACE). Water Resource Research, 37(5), pp.1327–1340.

Rosenberg, E.A., Keys, P.W., Booth, D.B., Hartley, D., Burkey, J., Steinemann, A.C. and Lettenmaier, D.P., 2010. Precipitation extremes and the impacts of climate change on stormwater infrastructure in Washington State. Climatic Change, 102(1), pp.319-349.

Rossi, G., Vega, T. and Bonaccorso, B., 2007. Methods and tools for drought analysis and management. Springer Science & Business Media, 62, pp.1–399.

Rost, S., Gerten, D. and Heyder, U., 2008. Human alterations of the terrestrial water cycle through land management. Advances in Geosciences, 18, pp.43-50.

Rouault, M., Pohl, B. and Penven, P., 2010. Coastal oceanic climate change and variability from 1982 to 2009 around South Africa. African Journal of Marine Science, 32(2), pp.237-246.

Sadiq Khan, M., Ullah, S., Sun, T., Rehman, A.U. and Chen, L., 2020. Land-use/land-cover changes and its contribution to urban heat island: A case study of Islamabad, Pakistan. Sustainability, 12(9), pp.1–17.

Santhi, C., Arnold, J.G., Williams, J.R., Dugas, W.A., Srinivasan, R. and Hauck, L.M., 2001. Validation of the swat model on a large river basin with point and nonpoint sources 1. JAWRA Journal of the American Water Resources Association, 37(5), pp.1169–1188.

Santos, J.F., Pulido-Calvo, I. and Portela, M.M. 2010. Spatial and temporal variability of droughts in Portugal. Water Resources Research, 46(3), pp.1–13.

Schubert, S.D., Suarez, M.J., Pegion, P.J., Koster, R.D. and Bacmeister, J.T. 2004. Causes of long-term drought in the US Great Plains. Journal of Climate, 17(3), pp.485–503.

Schütte, S. and Schulze, R.E., 2017. Projected impacts of urbanisation on hydrological resource flows: A case study within the uMngeni Catchment, South Africa. Journal of Environmental Management, 196, pp.527–543.

Seibert, M., Merz, B. and Apel, H., 2017. Seasonal forecasting of hydrological drought in the Limpopo Basin: a comparison of statistical methods. Hydrology and Earth System Sciences, 21(3), pp.1611-1629.

Semenov MA, Barrow EM (2002). LARS-WG: a stochastic weather generator for use in climate impact studies (Version 3.0). http://www.rothamsted.bbsrc.ac.uk/masmodels/larswg.html. Accessed 14 June 2015.

Servat, E. and Dezetter, A. 1991. Selection of calibration objective functions in the context of rainfall-ronoff modelling in a Sudanese savannah area. Hydrological Sciences Journal, 36(4), pp.307–330.

Shafer, B.A. and Dezman, L.E., 1982, January. Development of surface water supply index (SWSI) to assess the severity of drought condition in snowpack runoff areas. Proceeding of the Western Snow Conference.

Shah, D., Shah, H.L., Dave, H.M. and Mishra, V. 2021. Contrasting influence of human activities on agricultural and hydrological droughts in India. Science of The Total Environment, 774, pp. 1–13.

Shannon, L.V. and Nelson, G. 1996. The Benguela: Large scale features and processes and system variability. In: The South Atlantic (pp. 163–210). Springer, Berlin, Heidelberg.

Sharma, T.C. and Panu, U.S., 2010. Analytical procedures for weekly hydrological droughts: A case of Canadian rivers. Hydrological Sciences Journal, 55(1), pp.79–92.

Sharma, T.C. and Panu, U.S., 2012. Prediction of hydrological drought durations based on Markov chains: Case of the Canadian prairies. Hydrological Sciences Journal, 57(4), pp.705–722.

Sheffield, J., Goteti, G., Wen, F. and Wood, E.F., 2004. A simulated soil moisture-based drought analysis for the United States. Journal of Geophysical Research: Atmospheres, 109(D24), pp.1-19.

Sheffield, J., Goteti, G. and Wood, E.F., 2006. Development of a 50-year high-resolution global dataset of meteorological forcing for land surface modelling. Journal of Climate, 19(13), pp.3088–3111.

Sheffield, J., Livneh, B. and Wood, E.F. 2012. Representation of terrestrial hydrology and large-scale drought of the continental United States from the North American Regional Reanalysis. Journal of Hydrometeorology, 13(3), pp.856–876.

Shrestha, M., Acharya, S.C. and Shrestha, P.K., 2017. Bias correction of climate models for hydrological modelling – are simple methods still useful? Meteorological Applications, 24(3), pp.531–539.

Shukla, S. and Wood, A.W., 2008. Use of a standardized runoff index for characterizing hydrologic drought. Geophysical Research Letters, 35(2), pp.1–7.

Simpson, I.R., Tilmes, S., Richter, J.H., Kravitz, B., MacMartin, D.G., Mills, M.J., Fasullo, J.T. and Pendergrass, A.G., 2019. The regional hydroclimate response to stratospheric sulfate geoengineering and the role of stratospheric heating. Journal of Geophysical Research: Atmospheres, 124(23), pp.12587-12616.

Simmons, D. L., and Reynolds, R. J. 1982. Effects of urbanization on base-flow of selected south-shore streams, Long Island, New York, Water Resources Bulletin, 18, pp.797–805.

Singh, H. and Najafi, M.R., 2020. Evaluation of gridded climate datasets over Canada using univariate and bivariate approaches: Implications for hydrological modelling. Journal of Hydrology, 584, p.124673.

Sitterson, J., Knightes, C., Parmar, R., Wolfe, K., Avant, B. and Muche, M., 2018. An overview of rainfall-runoff model types. International Congress on Environmental Modelling and Software, pp.1–10.

Skupin, A. and Agarwal, P. 2008. Self-Organizing Maps Applications in Geographic Information Science, pp.1–219. John Wiley & Sons.

Sousa, P.M., Blamey, R.C., Reason, C.J., Ramos, A.M. and Trigo, R.M., 2018. The ‘Day Zero’ Cape Town drought and the poleward migration of moisture corridors. Environmental Research Letters, 13(12), p.124025.

Srinivasulu, S., Jain, A. (2008). Rainfall-Runoff Modelling: Integrating Available Data and Modern Techniques. In R. J. Abrahart, et.al (Ed.), Principal Hydro Informatics, Springer-Verlaf Berlin Heidelberg, 68, pp.59–70.

Statistics South Africa, 2010. Water Management Areas in South Africa, National Accounts: Environmental Economic Accounts. Pretoria 0001.

Stehr, A., Debels, P., Romero, F. and Alcayaga, H., 2008. Hydrological modelling with SWAT under conditions of limited data availability: evaluation of results from a Chilean case study. Hydrological Sciences Journal, 53(3), pp.588–601.

Tallaksen, L. M. 1995. A review of baseflow recession analysis. Journal of Hydrology 165, pp.349-370.

Tarboton, D.G., 1997. A new method for the determination of flow directions and upslope areas in grid digital elevation models. Water Resource Research. 33, pp.309.

Taylor, K.E., Stouffer, R.J. and Meehl, G.A. 2012. An overview of CMIP5 and the experiment design. Bulletin of the American Meteorological Society, 93(4), pp. 485–498.

Teng, J., Potter, N.J., Chiew, F.H.S., Zhang, L., Wang, B., Vaze, J. and Evans, J.P., 2015. How does bias correction of regional climate model precipitation affect modelled runoff? Hydrology and Earth System Sciences, 19(2), pp.711–728.

Teuling, A.J., Seneviratne, S.I., Stöckli, R., Reichstein, M., Moors, E., Ciais, P., Luyssaert, S., Van Den Hurk, B., Ammann, C., Bernhofer, C. and Dellwik, E. 2010. Contrasting response of European forest and grassland energy exchange to heatwaves. Nature Geoscience, 3(10), pp. 722–727.

Teuling, A.J., Van Loon, A.F., Seneviratne, S.I., Lehner, I., Aubinet, M., Heinesch, B., Bernhofer, C., Grünwald, T., Prasse, H., and Spank, U., 2013. Evapotranspiration amplifies European summer drought. Geophysical Research Letters, 40, pp.2071-2075. doi:10.1002/grl.50495.

Teutschbein, C. and Seibert, J., 2010. Regional climate models for hydrological impact studies at the catchment scale: A review of recent modeling strategies. Geography Compass, 4(7), pp.834–860.

Teutschbein, C. and Seibert, J., 2012. Bias correction of regional climate model simulations for hydrological climate-change impact studies: Review and evaluation of different methods. Journal of Hydrology, 456, pp.12–29.

Thoithi, W., Blamey, R.C. and Reason, C.J. 2021. Dry Spells, Wet Days, and Their Trends Across Southern Africa During the Summer Rainy Season. Geophysical Research Letters, 48(5), p. e2020GL091041.

Thompson, S.A. 1999. Water use, management, and planning in the United States, Academic Press, Elsevier, pp.1–371.

Thompson, D.W. and Wallace, J.M., 2000. Annular modes in the extratropical circulation. Part I: Month-to-month variability. Journal of Climate, 13(5), pp.1000–1016.

Thornthwaite, C.W., 1948. An approach toward a rational classification of climate. Geographical Review, 38, pp.55–94.

TIPS. 2016. Trade and Industrial Policy Strategies (TIPS). The Real Economy Bulletin Provincial Review 2016: Trends, Developments and Data. Available at: https://www.tips.org.za/images/The_REB_Provincial_Review_2016_Main_Report_.pdf. Accessed on November 15, 2020.

Tiwari, V.M., Wahr, J. and Swenson, S., 2009. Dwindling groundwater resources in northern India, from satellite gravity observations. Geophysical Research Letters, 36(18), pp.1–5.

Tizora, P., Le Roux, A., Mans, G. and Cooper, A. 2016. Land use and land cover change in the Western Cape Province: quantification of changes & understanding of driving factors. In: Planning Africa 2016; Making Sense of the Future – Disruption and Reinvention, 3-6 July 2016, Sandton Convention Centre, Johannesburg.

Trambauer, P., Maskey, S., Werner, M., Pappenberger, F., Van Beek, L.P.H. and Uhlenbrook, S., 2014. Identification and simulation of space–time variability of past hydrological drought events in the Limpopo River basin, southern Africa. Hydrology and Earth System Sciences, 18(8), pp.2925–2942.

Turpie J. Clearing thirsty alien trees will yield water returns for Cape Town. Dly. Maverick. 2018. https://www.dailymaverick.co.za/article/2018-07-02-clearing-thirsty-alien-trees-willyield-water-returns-for-cape-town/ (accessed Jan 30, 2019).

Tyson, P.D. 1986. Climatic change and variability in southern Africa. Oxford University Press, USA.

Ujeneza, E.L. and Abiodun, B.J. 2015. Drought regimes in Southern Africa and how well GCMs simulate them. Climate Dynamics, 44(5), pp.1595–1609.

UNISDR. 2009. United Nations International Strategy for Disaster Reduction. Drought risk reduction framework and practices: Contributing to the implementation of the Hyogo Framework for Action, 2009(197).

Van der Walt, A.J. and Fitchett, J.M. 2020. Statistical classification of South African seasonal divisions on the basis of daily temperature data. South African Journal of Science, 116(9-10), pp. 1–15.

Van Heerden, J. and Taljaard, J.J. 1998. Africa and the surrounding waters. In: Meteorology of the Southern Hemisphere, American Meteorological Society, Boston, MA, pp. 141–174.

Van Loon, A.F. 2015. Hydrological drought explained. Wiley Interdisciplinary Reviews: Water, 2(4), pp. 359–392.

Van Loon, A.F., Gleeson, T., Clark, J., Van Dijk, A.I., Stahl, K., Hannaford, J., Di Baldassarre, G., Teuling, A.J., Tallaksen, L.M., Uijlenhoet, R. and Hannah, D.M. 2016. Drought in the Anthropocene. Nature Geoscience, 9(2), pp. 89–91.

Van Niekerk, A. and Joubert, S.J. 2011. Input variable selection for interpolating high-resolution climate surfaces for the Western Cape. Water SA, 37(3), pp.1–10.

Vasiliades, L., Loukas, A. and Liberis, N., 2011. A water balance derived drought index for Pinios River Basin, Greece. Water resources management, 25(4), pp.1087–1101.

Vema, V.K., Sudheer, K.P. and Chaubey, I., 2020. Uncertainty of hydrologic simulation, and its impact on the design and the effectiveness of water conservation structures. Stochastic Environmental Research and Risk Assessment, 34, pp.973–991.

Vernimmen, R.R.E., Hooijer, A., Aldrian, E. and Van Dijk, A.I.J.M., 2012. Evaluation and bias correction of satellite rainfall data for drought monitoring in Indonesia. Hydrology and Earth System Sciences, 16(1), pp.133–146.

Vicente-Serrano, S.M., Beguería, S. and López-Moreno, J.I., 2010. A multiscalar drought index sensitive to global warming: the standardized precipitation evapotranspiration index. Journal of climate, 23(7), pp.1696–1718.

Vicente-Serrano, S., López-Moreno, J., Beguería, S., Lorenzo-Lacruz, J., Azorin-Molina, C., and Morán-Tejeda, E., 2012. Accurate computation of a streamflow drought index. Journal of Hydrological Engineering, 17, pp.318-332. doi:10.1061/(ASCE)HE.1943-5584.0000433.

Vidal, J.P., Martin, E., Franchistéguy, L., Habets, F., Soubeyroux, J.M., Blanchard, M. and Baillon, M., 2010. Multilevel and multiscale drought reanalysis over France with the Safran-Isba-

Modcou hydrometeorological suite. Hydrology and Earth System Sciences, 14(3), pp.459-478. doi:10.5194/hess-14-459-2010.

Wada, Y., Van Beek, L.P., Wanders, N. and Bierkens, M.F. 2013. Human water consumption intensifies hydrological drought worldwide. Environmental Research Letters, 8(3), pp.1–15.

Wagner, P.D., Kumar, S. and Schneider, K., 2013. An assessment of land use change impacts on the water resources of the Mula and Mutha Rivers catchment upstream of Pune, India. Hydrology and Earth System Sciences, 17(6), pp.2233-2246.

Wang, R., Kalin, L., Kuang, W., and Tian, H. 2014. Individual and combined effects of land use/cover and climate change on Wolf Bay watershed streamflow in southern Alabama, Hydrological Processes. 28, pp.5530-5546.

Warburton, M.L., Schulze, R.E. and Jewitt, G.P., 2012. Hydrological impacts of land use change in three diverse South African catchments. Journal of Hydrology, 414, pp.118–135.

Welde, K. and Gebremariam, B., 2017. Effect of land use land cover dynamics on hydrological response of watershed: Case study of Tekeze Dam watershed, northern Ethiopia. International Soil and Water Conservation Research, 5(1), pp.1–16.

Wolski, P. 2018. How severe is Cape Town's 'Day Zero' drought? Significance, 15(2), pp. 24–27.

Wilby, R.L., Charles, S.P., Zorita, E., Timbal, B., Whetton, P. and Mearns, L.O., 2004. Guidelines for use of climate scenarios developed from statistical downscaling methods. Supporting material of the Intergovernmental Panel on Climate Change, available from the DDC of IPCC TGCIA, 27. IPCC Report. Available at www.ipcc-data.org/guidelines/dgmno2v1092004.pdf

Wilcke, R.A.I., Mendlik, T. and Gobiet, A., 2013. Multi-variable error correction of regional climate models. Climatic Change, 120(4), pp.871–887.

Wilks, D.S., 2010. Use of stochastic weather generators for precipitation downscaling. Wiley Interdisciplinary Reviews: Climate Change, 1(6), pp.898–907.

Wilhite, D.A. 2005. Drought and water crises: Science, technology, and management issues. CRC Press.

Wilhite, D.A. and Glantz, M.H. 1985. Understanding the drought phenomenon: The role of definitions. Water International, 10(3), pp.111–120.

Wilhite, D.A., Sivakumar, M.V. and Pulwarty, R., 2014. Managing drought risk in a changing climate: The role of national drought policy. Weather and Climate Extremes, 3, pp.4-13.

Willink, D., 2020. Spatio-temporal precipitation patterns: From teleconnections to improved long-term forecasts. University of Berlin (Germany), pp.1–24.

WIREs, 2015. Hydrological drought explained. Water, 2, pp.359-392. doi: 10.1002/wat2.1085

WMO. 2012. World Meteorological Organization. Standardized Precipitation Index User Guide, (WMO-No. 1090). World Meteorological Organization, Geneva, Switzerland.

Wolski, P. 2018. How severe is Cape Town's 'Day Zero' drought? Significance, 15(2), pp. 24–27.

Wood, A.W., Maurer, E.P., Kumar, A. and Lettenmaier, D.P., 2002. Long-range experimental hydrologic forecasting for the eastern United States. Journal of Geophysical Research: Atmospheres, 107(D20), pp.1-9.

Wu, H., Hayes, M.J., Wilhite, D.A. and Svoboda, M.D., 2005. The effect of the length of record on the standardized precipitation index calculation. International Journal of Climatology: A Journal of the Royal Meteorological Society, 25(4), pp.505-520.

Xu, C.Y. and Singh, V.P., 2004. Review on regional water resources assessment models under stationary and changing climate. Water resources management, 18(6), pp.591–612.

Yang, X., Zhang, M., He, X., Ren, L., Pan, M., Yu, X., Wei, Z. and Sheffield, J. 2020. Contrasting influences of human activities on hydrological drought regimes over China based on high-resolution simulations. Water Resources Research, 56(6), p. e2019WR025843.

Yen, H., Park, S., Arnold, J.G., Srinivasan, R., Chawanda, C.J., Wang, R., Feng, Q., Wu, J., Miao, C., Bieger, K. and Daggupati, P., 2019. IPEAT+: A Built-in optimization and automatic calibration tool of SWAT+. Water, 11(8), pp.1–17.

Yihdego, Y., Vaheddoost, B., and Al-Weshah, R. A. 2019. Drought indices and indicators revisited. Arabian Journal of Geosciences. doi.org/10.1007/s12517-019-4237-z.

Yihdego, Y., and Eslamian, S. 2017. Drought Management: Initiatives and Objectives. In Handbook of Drought and Water Scarcity, pp. 1-25. CRC Press, 2017.

Youpeng, X., Jintao, X., Jinjia, D., Ying, C., Yixing, Y., and Xingqi, Z., 2010. Impacts of urbanization on hydrology in the Yangtze River Delta, China. Water Science and Technology, 62(6), pp.1221–1229.

Zargar, A., Sadiq, R., Naser, B. and Khan, F.I. 2011. A review of drought indices. Environmental Reviews, 19(NA), pp.333–349.

Zhai, J., Su, B., Krysanova, V., Vetter, T., Gao, C. and Jiang, T., 2010. Spatial variation and trends in PDSI and SPI indices and their relation to streamflow in 10 large regions of China. Journal of Climate, 23(3), pp.649–663.

Zhang, Y-K., and Schilling, K. E. 2006. Increasing streamflow and baseflow in Mississippi River since the 1940 s: Effect of land use change, Journal of Hydrology, 324, pp.412-422.

Zhang, M., Liu, N., Harper, R., Li, Q., Liu, K., Wei, X., Ning, D., Hou, Y., and Liu, S. 2017. A global review on hydrological responses to forest change across multiple spatial scales: Importance of scale, climate, forest type and hydrological regime, Journal of Hydrology, 546, pp.44-59.

Zhang, L., Zhao, Y., Hein-Griggs, D., Janes, T., Tucker, S. and Ciborowski, J.J., 2020. Climate change projections of temperature and precipitation for the Great Lakes basin using the PRECIS regional climate model. Journal of Great Lakes Research, 46(2), pp.255–266.